1988

Photophysical And Photoelectrochemical Studies Of A Langmuir-blodgett Film Of A Porphyrin Dye

Harold Alfred Dick

NOTICE

The quality of this microform is heavily dependent upon the quality of the original thesis submitted for microfilming. Every effort has been made to ensure the highest quality of reproduction possible.

If pages are missing, contact the university which granted the degree.

Some pages may have indistinct print especially if the original pages were typed with a poor typewriter ribbon or if the university sent us an inferior photocopy.

Previously copyrighted materials (journal articles, published tests, etc.) are not filmed.

Reproduction in full or in part of this microform is governed by the Canadian Copyright Act, R.S.C. 1970, c. C-30.

AVIS

La qualité de cette microforme dépend grandement de la qualité de la thèse soumise au microfilmage. Nous avons tout fait pour assurer une qualité supérieure de reproduction.

S'il manque des pages, veuillez communiquer avec l'université qui a conféré le grade.

La qualité d'impression de certaines pages peut laisser à désirer, surtout si les pages originales ont été dactylographiées à l'aide d'un ruban usé ou si l'université nous a fait parvenir une photocopie de qualité inférieure.

Les documents qui font déjà l'objet d'un droit d'auteur (articles de revue, tests publiés, etc.) ne sont pas microfilmés.

La reproduction, même partielle, de cette microforme est soumise à la Loi canadienne sur le droit d'auteur, SRC 1970, c. C-30.

PHOTOPHYSICAL AND PHOTOELECTROCHEMICAL STUDIES OF A LANGMUIR-BLODGETT FILM OF A PORPHYRIN DYE

by

Harold Alfred Dick

Department of Chemistry

Submitted in partial fulfillment
of the requirements for the degree of
Doctor of Philosophy

Faculty of Graduate Studies
The University of Western Ontario
London, Ontario
July, 1988

ISBN 0-315-43296-9

ABSTRACT

Time-resolved fluorescence lifetime measurements of 5-(4-carboxyphenyl)-10,15,20-tritolylporphyrin (TTPa) with dioleoylphosphatidylcholine (DOPC) in mixed Langmuir-Blodgett (LB) films on quartz slides were performed at two different laboratories in an attempt to create a standard system for future monolayer fluorescence work. TTPa in the mixed LB film exhibited a simpler and longer decay profile than for a pure TTPa monolayer. At a DOPC/TTPa molar ratio of 50:1, the decay consisted primarily of one lifetime of 10.7 ± 0.2 ns. Simplification and lengthening of the lifetime was attributed to reduction of TTPa aggregate formation in the film. This effect is also seen in fluorescence and absorption spectra.

In addition the photoelectrochemistry of pure TTPa monolayers deposited on SnO_2 semiconductor slides was studied. Measurements included capacitance versus voltage; current versus voltage, light intensity, electrolyte pH, supersensitizer concentration, and wavelength of excitation. Mott-Schottky plots and current-voltage measurements indicated that the monolayer formed was not insulating but allowed electrolyte to pass through it. Anodic photocurrents of up to $2\mu A/cm^2$ were observed for a single monolayer at low electrolyte pH. The photocurrent was highly dependent on supersensitizer concentration at low pH and rather insensitive at high pH. It is postulated that direct injection of electrons from the first excited singlet state of the porphyrin is operative at high pH whereas trapping of the electron by surface states occurs at low pH.

Cathodic photocurrents were also seen for electrolytes containing only supporting electrolyte. This was attributed to reduction of adsorbed oxygen by the excited porphyrin.

ACKNOWLEDGMENTS

The making of this thesis included some interesting and helpful collaborations. In this connection I would like to thank Roger Leblanc, Gilles Picard, and Gaétan Munger from the Centre de recerche en photobiophysique a Trois-Rivières for having shared their expertise and hospitality. I would also like to thank John Turner and Art Nozik from the Solar Energy Research Institute in Golden Colorado for the use of their excellent photoelectrochemical equipment.

I would like to thank Aleksander Seimiarczuk for many uncomplaining hours spent assisting me in the photophysical experiments.

I would like to thank my supervisor James Bolton his encouragement and for making these collaborations possible, allowing me to choose my own course of work while making the best expert advice and equipment available.

Finally I would like to thank my wife for her support and enthusiasm for my every endeavor.

TABLE OF CONTENTS

	Page
CERTIFICATE OF EXAMINATION	ii
ABSTRACT	iii
ACKNOWLEDGMENTS	iv
TABLE OF CONTENTS	v
LIST OF TABLES	vii
LIST OF FIGURES	viii
LIST OF PHOTOGRAPHIC PLATES	x
CHAPTER 1 - INTRODUCTION	1
CHAPTER 2 - EXPERIMENTAL	
2.1 The Langmuir Trough	
2.2 The Subphase	
2.3 The Substrate	
2.4 Electrical Contacts	
2.5 Chemicals	
2.6 Monolayer Deposition and LB Film Production	
2.7 Fluorescence Techniques	
2.8 The Electrochemical Cell	
2.9 The Electrolyte	
2.10 Cell Illumination	
2.11 Photo-action Spectra	
2.12 Mott-Schottky Plots	
CHAPTER 3 - PHOTOPHYSICAL STUDIES	
3.1 Photophysics	
3.2 The Single Photon Counting Technique	
3.3 Monolayer Techniques	
3.4 Literature Review	
3.5 Results and Discussion	
CHAPTER 4 - PHOTOELECTROCHEMICAL STUDIES	
4.1 Electronic Energy in the Cell	
4.1.1 Electronic Energy in the Semiconductor Bulk	
4.1.2 " " near the Semiconductor Surface	
4.1.3 " " in the Interfacial Double Layers	
4.1.4 " " in the Dye Monolayer	
4.1.5 " " in the Electrolyte Bulk	
4.1.6 " " at the Metal Electrode	
4.2 Capacitance of the Cell	
4.3 pH Dependence of the Flatband Potential	
4.4 Theories of Current Production	
4.4.1 Dark Current	
4.4.2 Photocurrent	
4.5 Literature Review	
4.5.1 Elucidative Dye Sensitization Studies	
4.5.2 Porphyrin and Chlorophyll Studies	
4.5.3 Summary of the Literature Findings	
4.6 Experimental Results	
4.6.1 Monolayer Deposition	
4.6.2 Photo-action Spectrum	
4.6.3 Current-Voltage Curves	

4.6.4 Dependence of the Photocurrent on pH.....
4.6.5 Mott-Schottky Plots.....
4.6.6 Dependence of the Photocurrent on Irradiance.....
4.6.7 Dependence of the Photocurrent on Thiourea Concentration.....
4.6.8 Photocurrent Quantum Yield.....
4.6.9 Photocurrent Onset Voltage.....
4.7.10 Fluorescence Quenching.....
4.8 Discussion of the Results.....

CHAPTER 5 - CONCLUSIONS AND SUGGESTIONS FOR FURTHER RESEARCH.....
5.1 Summary of Observations.....
5.1.1 Photophysical Studies.....
5.1.2 Photoelectrochemical Studies.....
5.2 Conclusions.....
5.2.1 Photophysical Studies.....
5.2.2 Photoelectrochemical Studies.....
5.3 Suggestions for Further Research.....

REFERENCES.....

VITA.....

LIST OF TABLES

Table	Description	Page
3.1	Fluorescence Lifetime Measurements for Monolayer Films of TTPa	

LIST OF FIGURES

Figure	Description	Page
2.1	The Langmuir trough assembly	
2.2	The slide dipping assembly	
2.3	The photoelectrochemical cell	
2.4	Voltage application and current measurement circuits	
2.5	The experimental setup for photoelectrochemical measurements	
2.6	A block diagram of the photo-action spectral apparatus	
3.1	The single photon counting apparatus	
3.2	The surface pressure area isotherm of stearic acid	
3.3	Z and X layer deposition of Langmuir -Blodgett films	
3.4	The surface pressure area isotherm of a 50:1 DOPC/TTPa mixed monolayer	
3.5	The surface pressure area isotherm of a pure TTPa monolayer	
3.6	Absorption spectra of mixed LB films of DOPC and TTPa	
3.7	Optical absorption spectra of TTPa in methylene chloride, in a LB film of TTPa alone, and in a 50:1 DOPC/TTPa mixed monolayer	
3.8	Fluorescence excitation spectra of TTPa in methylene chloride, in an LB film of TTPa alone, and in a 50:1 DOPC/TTPa mixed monolayer	
3.9	Fluorescence emission spectra of TTPa in methylene chloride, in an LB film of TTPa alone, and in a 50:1 DOPC/TTPa mixed monolayer	
4.1	The dye sensitization scheme	
4.2	A schematic diagram of the photoelectrochemical cell	

4.3	Ohmic and Schottky barrier junctions: descriptions and current-voltage characteristics
4.4	A comparison of the distributions of the solvent sheath vibrations and the electronic states of the redox active electron
4.5	An energy level diagram of the semiconductor electrolyte interface
4.6	A comparison of the cell photo-action spectrum with absorption spectra
4.7	Current-voltage plots for the cell under conditions of oxygen and nitrogen bubbling
4.8	Current-voltage plots for two electrolyte conditions
4.9	Current-voltage plots under high and low pH conditions
4.10	Plots of light response vs. electrolyte pH under various electrolyte conditions
4.11	Plots of light response under various electrode and electrolyte conditions
4.12	Mott-Schottky plots of the cell under various pH conditions
4.13	Flatband potential variation with pH
4.14	Photocurrent vs. irradiance for two electrolyte conditions
4.15	Plots of light response of the cell vs. thiourea concentration at high and low pH
4.16	Onset of photocurrent vs. pH for two electrolyte conditions
4.17	A Shockley plot for a blank slide.
4.18	A fit to the low pH TU concentration dependence

LIST OF PHOTOGRAPHIC PLATES

Plate	Description	Page
2.1	A scanning electron micrograph of the surface of a blank SnO_2 slide.	

CHAPTER 1 INTRODUCTION

The direct use of solar energy offers probably the safest and most morally acceptable form of energy consumption being contemplated today. More solar energy impinges on this earth every hour than could be used by the most greedy and naive society.[1] It is limited in its utility however by its low energy density.[2] In order to make this a viable and competitive source of energy the efficiency of solar energy converters must be maximized and fabrication cost minimized. Direct conversion of sunlight to electricity seems to be the obvious choice since the number of energy wasteful conversion steps is minimized.

Conventional solar to electric converters or photovoltaic cells are usually fabricated from inorganic semiconductor crystals such as silicon. The physics behind these types of devices seems to be fairly well understood as evidenced by the fact that their conversion efficiency approaches the thermodynamic limit. However this type of cell is not in wide scale use since the cost of production is presently prohibitively high. Much research has gone into the reduction of this cost most notably the development of amorphous thin inorganic semiconductor films. The results here have been very encouraging.[3]

Another younger field of endeavor has arisen around the attempt to mimic the photoconversion process taking place in green plants.[4] The first step of this process is the absorption of light by carotenoid and antenna chlorophyll molecules located within the protein matrix of the thalykoid membrane of green leaves. These molecules are located sufficiently close together to permit energy transfer between them. The absorbed light energy therefore migrates throughout the matrix, probably by an exciton hopping mechanism, until it encounters a reaction center protein which spans the thylakoid membrane. It is then finally

transferred to a chlorophyll dimer located within the reaction center on the inner side of the thylakoid membrane; the photo-excited dimer then undergoes photoelectron transfer to a neighboring ubiqinone molecule located on the outer side of the membrane. An electronic charge is therefore produced across the membrane which stores electrical energy as in a capacitor and powers slower dark photosynthetic chemistry. The conversion efficiency of the primary electron transfer process has been estimated to be ~16%.[5]

In order to fabricate a device that will mimic this process effectively an understanding of the kinetic and thermodynamic parameters influencing the efficiency of this process is required. One approach has been the synthesis and study of donor-acceptor molecules in which intramolecular photoelectron transfer takes place from a donor moiety to an acceptor moiety.[6] Variation of parameters such as the redox potential difference between the donor and acceptor, the physical distance between them and the nature of the linking molecules has increased the understanding of this process. At present however only solution spectroscopic studies have been conducted to infer photoelectron transfer.

The system of study in this thesis consists of a Langmuir-Blodgett (LB) film of a surface-active porphyrin deposited either onto a quartz slide or onto a SnO_2 semiconductor. The semiconductor system is analogous to the reaction center in that photoelectron transfer can take place from the photo-excited porphyrin monolayer to the conduction band of the semiconductor. If this system is placed into an electrochemical cell the modified semiconductor acts as a photoelectrode. It is thus possible to measure directly the photoelectron transfer process by observing the current produced by light impinging on the electrode.

The thesis is divided into four chapters of which the introduction and the experimental detail comprise the first two. The third chapter describes a study of the time resolved fluorescence of pure porphyrin LB films and films in which the porphyrin is mixed with a second film forming molecule used to block the porphyrin molecules from each other. These films are deposited on quartz slides. The fourth chapter deals with the photoelectrochemistry of LB films of porphyrin deposited on SnO_2 semiconductor slides.

CHAPTER 2 EXPERIMENTAL

The time resolved fluorescence studies were performed in parallel at our laboratory (UWO) and at the Centre de Recherche en Photobiophysique at the Université du Québec á Trois-Rivières (UQTR) in an effort to produce a possible standard system for future time resolved fluorescence measurements. A 50:1 mixed Langmuir-Blodgett (LB) film of dioleoylphosphatidylcholine (DOPC) with 5-(4-carboxyphenyl)-10,15,20-tritolylporphyrin (TTPa) deposited onto a quartz slide was chosen to be tested by both laboratories. The following experimental section details for the most part only techniques used in our laboratory. Monolayer deposition and LB film formation techniques differed only slightly between the two laboratories; however the time resolved fluorescence measurement techniques varied considerably and are contrasted.

The photoelectrochemical measurements, except for the Mott-Schottky plots which were performed at the Solar Energy Research Institute in Golden Colorado, were performed only at our laboratory.

2.1 The Langmuir Trough

The Langmuir trough used for deposition of monolayers was built from a solid block of teflon. It is shown in Figure 2.1. The surface area taken up by the monolayer was controlled by a movable barrier consisting of a square iron rod wrapped in teflon which rode along the top of the sides of the trough oriented perpendicular to the length of the trough. Its movement was controlled by an undercarriage assembly consisting of a worm gear-driven set of forks attached to either end of the movable barrier. The worm gear was driven by a synchronously wound chopper motor (Ithaco Model 382) providing a wide range and excellent control of barrier speed. Square wave output from the chopper motor normally used as a reference signal for lock-in amplification provided

Figure 2.1 The Langmuir trough. It consists of a teflon trough (a) of 13 cm × 60 cm × 1 cm deep interior dimensions and 15 cm × 62 cm × 5 cm deep exterior dimensions. A hole (b) 8 cm × 11 cm × 2.5 cm deep is located below the slide deposition apparatus. The teflon trough is screw mounted onto a 2.5 cm thick aluminum base which rests on four leveling screws. A movable teflon barrier (c) rides along the top of the sides of the trough. It is propelled by two arms (d) attached to a worm gear (e) located underneath the base of the trough. The worm gear is powered by a synchronously wound chopper motor (f) via a reduction gear assembly (g). The surface pressure is monitored by a teflon float (i) of 0.6 cm × 11.1 cm × 0.1 cm dimensions. Seal is made to the sides of the trough by teflon tape (j) which is friction held in a vertical slit on either end of the float and clamped to the sides of the trough with a teflon clamp utilizing an alligator clip. The teflon float is attached to the lower arms of a torsion balance (k). The core from a linear transducer is hung from a horizontal arm of the balance and extends into the core of the transducer (l).

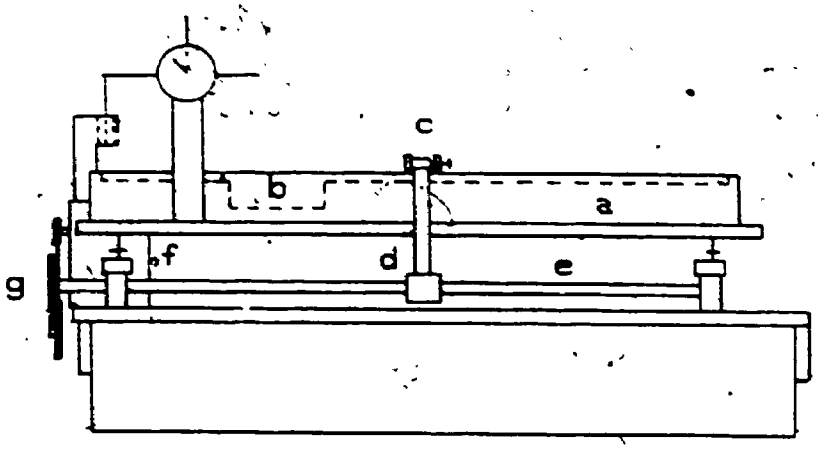
c
b
a
f
d
e
g

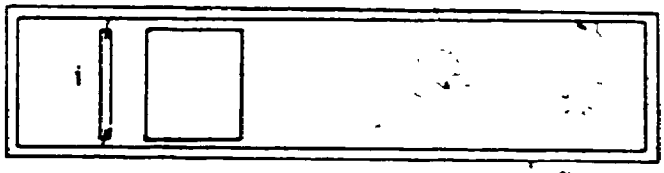
i

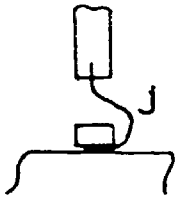
j

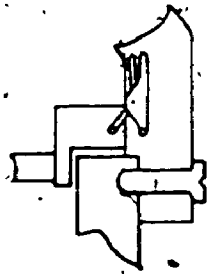

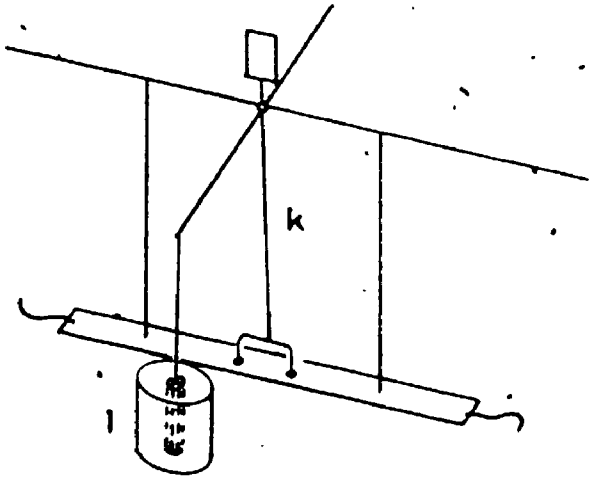
k
l

an external time base for a Nicolet digital oscilloscope (Model 206).

The surface pressure was monitored by a teflon float mounted to a torsion pendulum. The movable core from a linear transducer (Hewlett-Packard Model 7DCDT-050) was suspended from one arm of the torsion pendulum and extended into the transducer. Care was taken to ensure that the core did not touch the sides of the transducer. Thus a highly sensitive surface pressure-to-voltage converter was created. The signal was sent to the digital oscilloscope. This voltage plotted against the external time base produced a surface pressure area isotherm of the monolayer.

The entire assembly was enclosed in a Plexiglas dust cover with lids on one side to provide access for the user.

2.2 The Subphase

The subphase, unbuffered water, was purified as follows. House distilled water was passed through scale elimination, deionization, organic removal columns (D8921, D8922 SYBRON/Barnstead), distilled in a quartz bidistillation apparatus (Bi4, Englehart, Amersil Quartz Division) and then stored in Pyrex volumetric flasks fitted with inverted ground glass stoppers. The conductivity of the water was $\sim 10^{-6}\ \Omega^{-1}{}_{m}{}^{-1}$.

2.3 The Substrate

2.5 cm x 7.6 cm quartz slides obtained from Corning provided a substrate for LB films in photophysical studies. Before deposition they were cleaned by soaking for three days in concentrated chromic acid followed by 15 rinses with Barnstead filtered water and sonication for 15 min in 0.01 M NaOH (Fisher). This was followed by 10 rinses with filtered water, 5 rinses with triply distilled water and sonication for

15 min in the final rinse. The slides were then dried with prepurified nitrogen.

The substrate employed for photoelectrochemical studies was *n*-type Sb-doped SnO_2 obtained from Corning in polycrystalline form deposited on a glass sheet. This was subsequently cut into 2.5 cm by 5 cm slides. The sheet resistance of the slides was rated at 10 Ω/ by Corning. The SnO_2 film was estimated by scanning electron microscopy (SEM) to have a thickness of a few hundred Angstroms. SEM also revealed surface texture of ~100 nm^2 dimensions. A micrograph of the SnO_2 surface is given in Plate 2.1. The slides were cleaned either by soaking in chromic acid for 48 hrs or by sonication in chromic acid for one hour. Either cleaning method was followed by copious rinsing and sonication in bidistilled water. Surface cleanliness as measured by quality of monolayer deposition turned out to be the same using either cleaning technique.

2.4 Electrical Contacts

Electrical contact was made to the SnO_2 slide by gluing a thin metal wire to the uncovered portion of the slide with silver paste. To ensure that ohmic contact was established between the wire and the slide a current-voltage plot taken for the slide with two such leads attached was verified to be linear within the current ranges employed in the photoelectrochemical experiments.

2.5 Chemicals

The TTPa was synthesized by the method of Little *et al.*[7] The mono-acid compound (TTPa) was separated on a 2.5 cm x 50 cm silica gel column with 1% methanol in chloroform as an elutant. The TTPa fraction produced a single spot on a TLC slide using 5% methanol in chloroform. Its identity was confirmed by mass spectroscopy, and UV-visible absorption

Plate 2.1 A scanning electron micrograph of the surface of a blank SnO_2 slide.

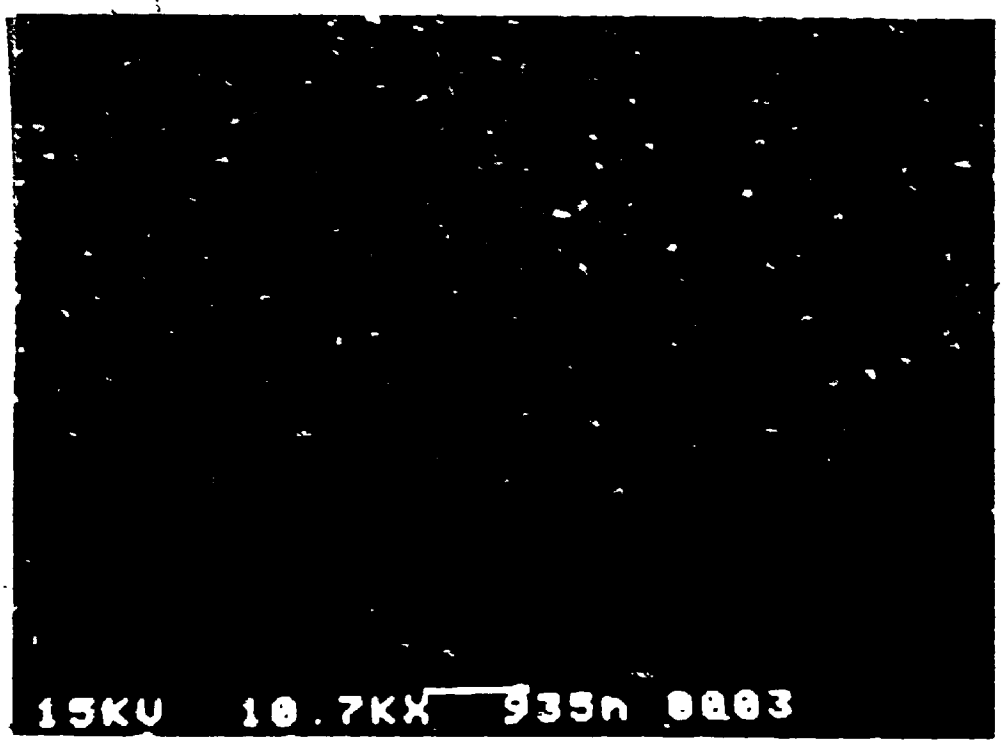
15KV 10.7KX 933n 0003

and fluorescence spectroscopy. The extinction coefficients in chloroform were found to be: λ_{max} (nm) [ϵ ($M^{-1}cm^{-1}$)]: 646.5 [4.75 x 10^3], 590 [5.27 x 10^3], 552 [8.96 x 10^3], 516.5 [1.73 x 10^4], 420 [4.49 x 10^5]. Since the absorption of TTPa in chloroform follows Beer's law to the solubility limit, its concentration can be determined by colorimetry. The DOPC obtained from Sigma was weighed on a micro-balance before being dissolved in chloroform. The two solutions were mixed in the desired proportion using Pressure Lok syringes (Precision Sampling Corp.). Fisher spectral grade chloroform was used as solvent throughout.

2.6 Monolayer Deposition and LB Film Production

The solution was deposited on the subphase (20 ± 2°C) with a syringe maintaining a minimum of 3 s between drops. Compression of the monolayer was begun 1 min after the end of deposition at a rate of 5.5 x 10^{17} $Å^2 min^{-1}$. The film was compressed until a surface pressure of 20 mN m^{-1} was reached at which point the slide was dipped in and out of the water at a rate of 2.0 cm min^{-1}. This was accomplished by a slide dipping assembly powered by a gear motor which was situated above the trough near the teflon float. The assembly is shown in Figure 2.2. During transfer of the monolayer the surface pressure was maintained at 20 mN m^{-1} by continual reduction of the surface area. The quality of the deposition was determined by the ratio of the area lost on the water surface at constant surface pressure to that taken up by the monolayer on the substrate. Only slides exhibiting a deposition ratio of 1.0 ± 0.1 were accepted for photophysical studies. Deposition ratios for LB films deposited on the SnO_2 slides tended to be higher than unity. Ratios of 1.1 ± 0.3 were accepted for study.

Figure 2.2 The slide dipping assembly. A brass reel powered through a rubber o-ring gear assembly by a gear motor raises and lowers the slide holder by two strings.

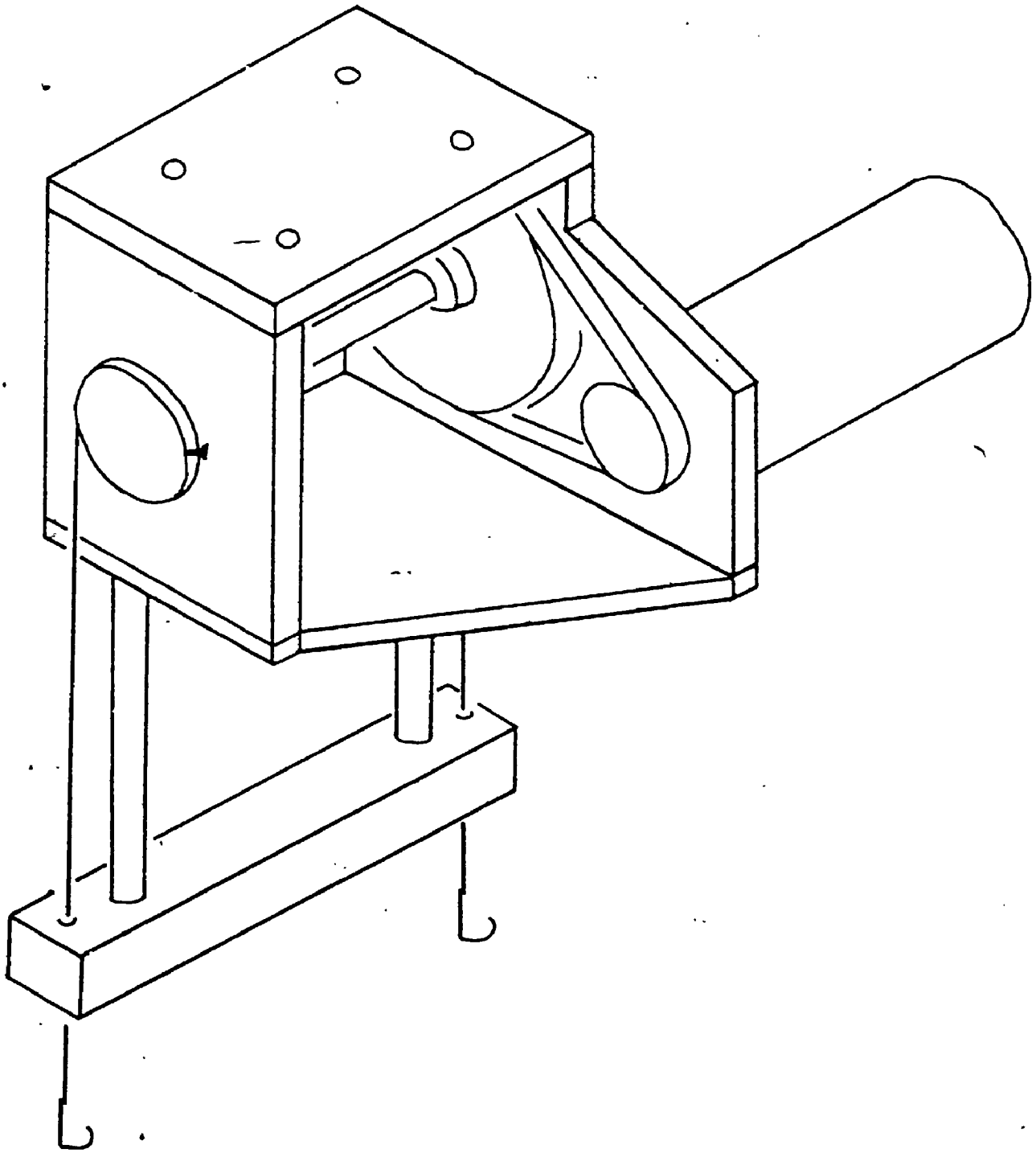

2.7 Fluorescence Techniques

Fluorescence measurements were performed within 24 hrs to one week after deposition. Both laboratories used PRA International Model 3000 fluorescence lifetime single photon counting (SPC) equipment. During measurement the monolayers were exposed to room air. Differing modifications of the equipment between the two laboratories are as follows.

The UWO laboratory generated excitation light by a cavity dumped dye laser (7210 Coherent) synchronously pumped by a mode-locked argon-ion laser (CR-53 HD Coherent). Rhodamine 6G was used as the lasing dye. The laser light (15 ps pulse width, 590 nm) was focused through a linear polarizer onto the sample with an intensity of 10^8 photons/flash at a repetition rate of 1 MHz. Sample fluorescence was focused through a 620 nm cut-off filter and a monochromator tuned to 650 nm. Data were analyzed using a statistical reconvolution program designed at UWO.[8]

The UQTR laboratory generated excitation light by a nitrogen flash lamp (4 ns pulse width, 10^6 photons/flash, 30 kHz rep. rate). The light passed through a monochromator set at 420 nm. Fluorescence was collected through a 630 nm cut-off filter by an ellipsoidal mirror focused on the photomultiplier tube. Data were analyzed using a PRA statistical reconvolution program.

Absorption spectra were measured on a Hewlett-Packard 8450A diode array spectrophotometer. Fluorescence spectra were taken on a Spex Fluorolog 2 spectrofluorometer.

2.8 The Electrochemical Cell

The electrochemical cell shown in Figure 2.3 consisted of a solid block of Plexiglas into which a 3.5 cm x 1.5 cm hole was drilled horizontally. The hole was sealed by sandwiching a rubber O-ring between

Figure 2.3 The photoelectrochemical cell (a) Ag/AgCl reference electrode (b) Plexiglas cell body (c) platinum grid counter electrode (d) teflon stir bar (e) pH electrode (f) Plexiglas slide holder (g) Luggin capillary (h) silver paste (i) semiconductor slide

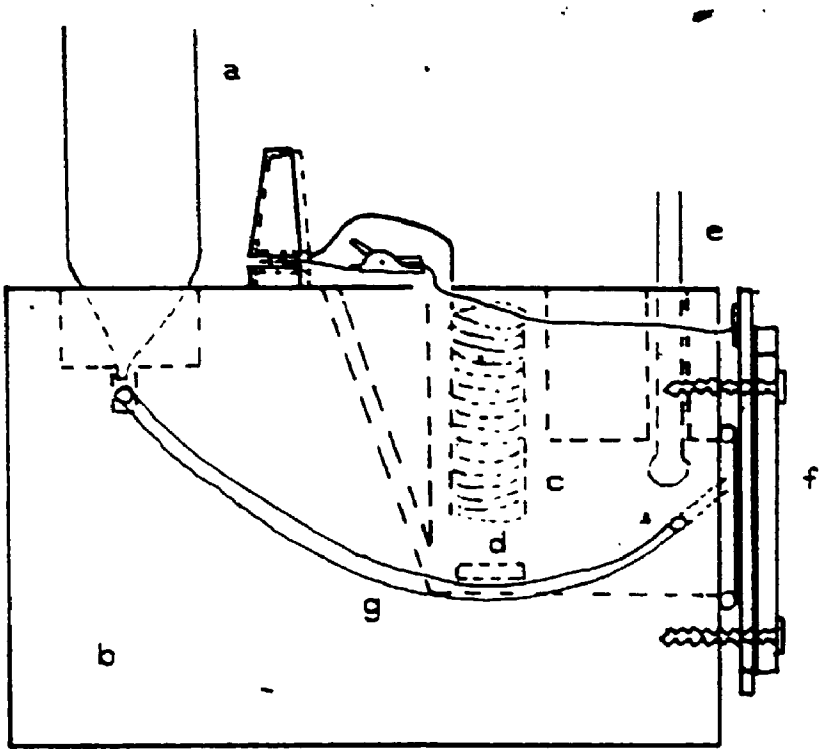
a
e
c
f
d
g
b

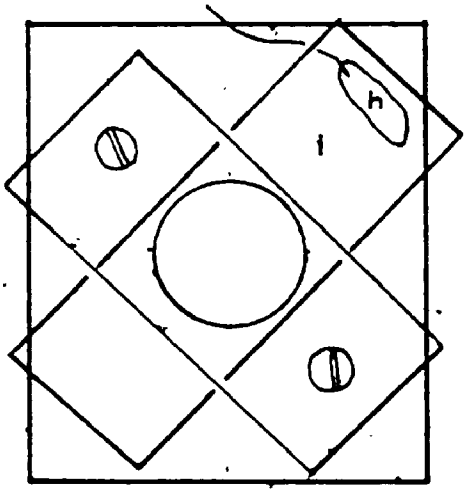
h
i

the block and the monolayer-bearing slide. Other holes were drilled through the block into the compartment to provide access for the counter electrode, a pH electrode and a Luggin capillary which led to a Ag/AgCl reference electrode. The photoactive area of the slide was 3.3 cm^2.

The cell was usually used in the two-electrode configuration in which the Ag/AgCl reference electrode doubled as the counter electrode. The electrical circuit used in applying voltage across the cell and measuring its current is shown in Figure 2.4. Cell voltage was applied by a EG&G PARC Universal Programmer (Model 175). The voltage across a monitoring resistor gave a measure of the current flowing through the cell. The voltage across the cell was calculated by subtracting the resistor voltage from the applied voltage. Current voltage plots were scanned at a rate of 1.25 mV/sec. The monitoring resistor voltage was recorded by a Nicolet Digital Oscilloscope (Model 206) and then analyzed by a Hewlett-Packard 9816 micro-computer. Point-by-point subtraction of the monitoring resistor voltage for current-voltage plots was done using a home-made program on the computer.

The measurement for Mott-Schottky plots required the use of a three-electrode configuration under potentiostatic control. Here a platinum grid counter electrode was employed. A Luggin capillary whose end was placed close to the SnO_2 electrode provided electrical contact to the Ag/AgCl reference electrode. The validity of the two electrode detection procedure was checked occasionally by comparing results obtained using either configuration. They were consistently identical to within the reproducibility of the results on any one system.

The electrical scheme for application of cell potential and measurement of the current in the three-electrode configuration is shown in Figure 2.4. Current voltage plots in this configuration employed a

Figure 2.4 The upper circuit is used to monitor the cell voltage and current in the two electrode configuration. Voltage V is applied to the cell. The current is converted into voltage V by the resistor R.

The lower circuit incorporates the potentiostat for measurement in three electrode configuration. Current is driven through the cell between the working electrode (1) and the counter electrode (2) by the potentiostat untill the voltage between the reference electrode (3) and the working electrode matches the applied voltage V.

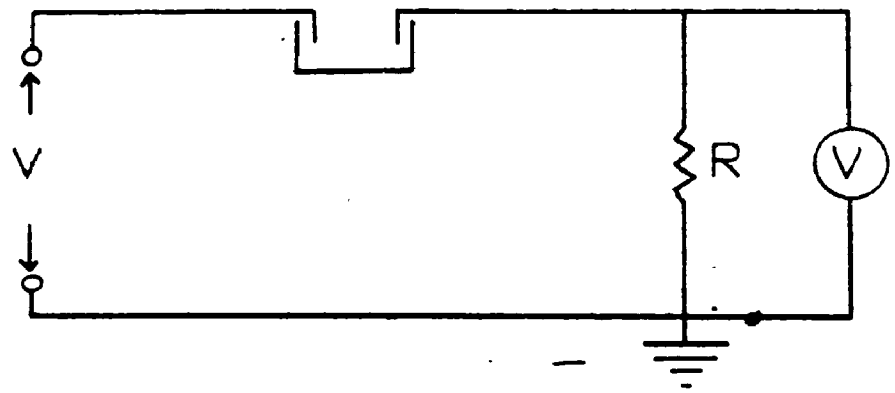
V
R
V

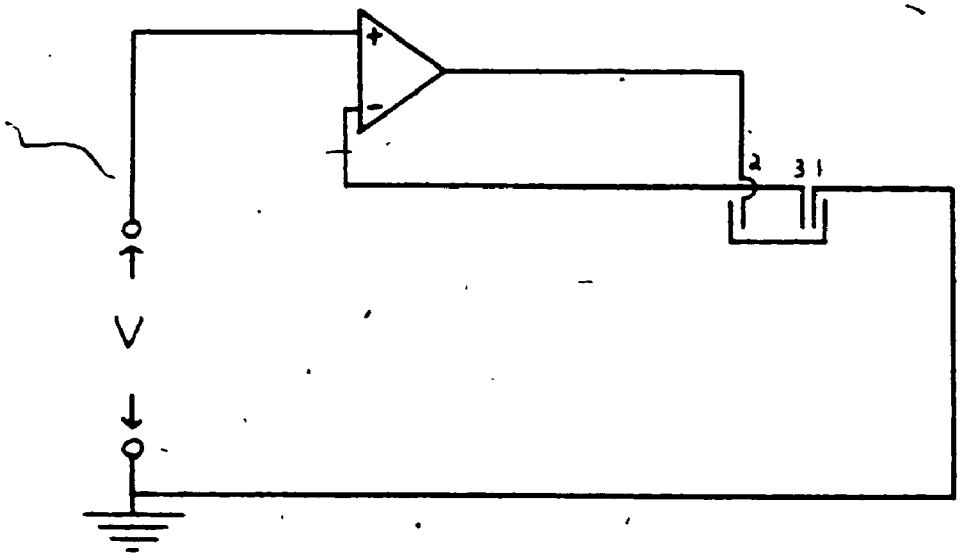
+
-
2
3
1
V

Figure 3.4 Surface pressure area isotherm of a 50:1 DOPC/TTPa mixed monolayer. Subphase, unbuffered water at 20 ± 2°C,

Figure 2.5 The photoelectrochemical measurement assembly. (a) tungsten light source (b) neutral density filters (c) black plexiglass blind (d) radiometer detector (e) electrochemical cell (f) optical rail (g) swiveling support (h) magnetic stirrer

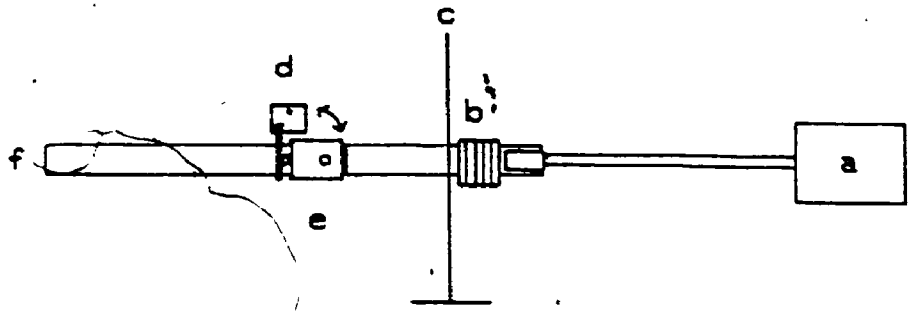
c
d
b
f
a
e

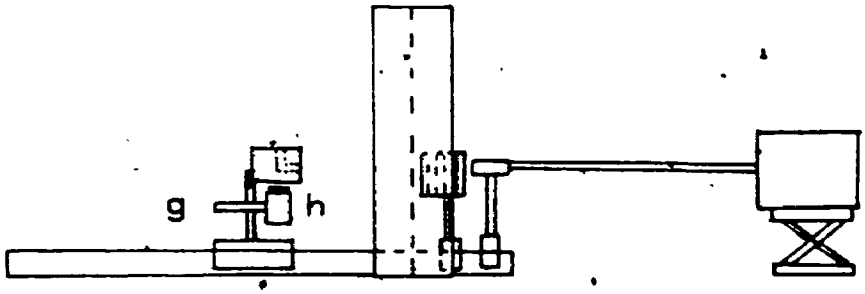
g
h

Figure 2.6 Block diagram of the apparatus used for taking action spectra. Lamp light is chopped and then passed through monochromator (MONO) to the electrochemical cell. The cell signal as well as a reference signal from the chopper is sent to a lock-in amplifier. The amplified signal is sent to a digital oscilloscope and then a computer.

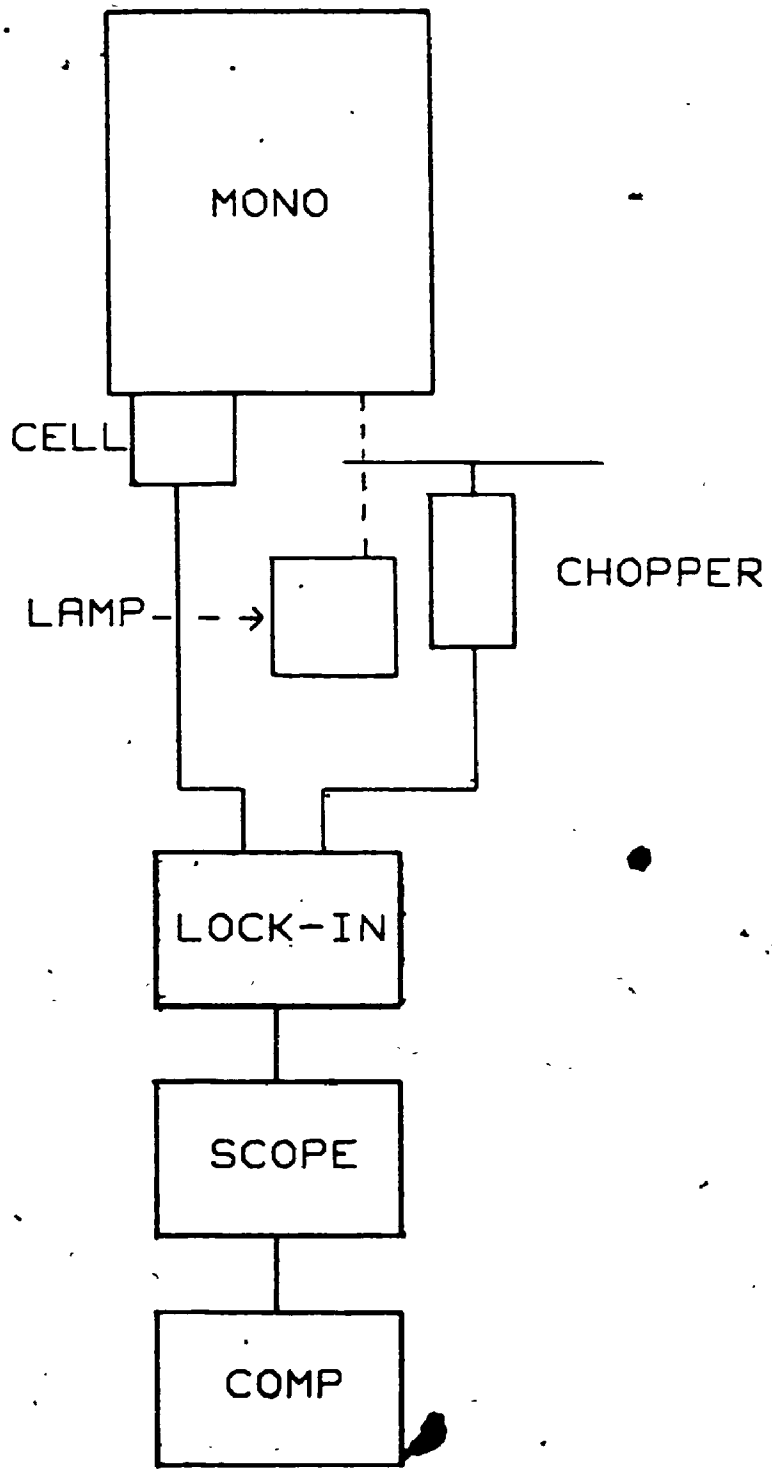
MONO
CELL
CHOPPER
LAMP
LOCK-IN
SCOPE
COMP

an Ithaco Dynatrac 391 lock-in voltmeter the signal of which was sent to the Nicolet Digital Oscilloscope. The spectra are therefore action spectra of the photovoltage, however they were taken at a light intensity where the photovoltage increases approximately linearly with the light intensity and hence are proportional to photocurrent action spectra. The spectra were scanned slowly with respect to the reciprocal time constant of the lock-in voltmeter and in both directions to ensure that no distortion of the spectra occurred. A home made phototransistor, light chopper assembly was attached to the axle of the spectrometer wavelength meter providing an external time base for the scope.

Incident light intensity at each wavelength was determined by replacing the electrochemical cell with the radiometer detector. The radiometer output in units of W m^{-2} was converted to units of photons s^{-1} cm^{-2} by a homemade computer program. The cell photoresponse was then divided by this value at each wavelength.

2.12 Mott-Schottky Plots

Mott-Schottky plots were performed at the Solar Energy Research Institute in Golden Colorado. In this experiment the voltage applied to the cell in three electrode configuration is the sum of a dc voltage provided by a EG&G PARC Universal Programmer Model 175 and an ac voltage provided by a Hewlett-Packard 3325a Synthesizer/Function Generator. The voltage summing was performed in a Princton Applied Research Potentiostat/Galvanostat Model 173. The current response of the cell was converted into a voltage by the measuring resistor in the potentiostat. The in and out-of-phase components of this voltage were measured with a Princton Applied Research Lock-in Analyzer Model 5204. To obtain data for the Mott-Schottky plots the dc component of the applied voltage was varied between -.05 and .5 V w.r.t. the Ag/AgCl reference electrode in

steps of 50 mV keeping the rms voltage of the ac component at 6.81 mV and the frequency at 1 kHz. The out-of-phase response of the cell current was measured for each step after equilibrium had been established in the cell. The applied ac voltage was then divided by the out-of-phase response to give the out-of-phase impedance which was inverted and squared using an IBM personal computer.

CHAPTER 3 PHOTOPHYSICAL STUDIES

This portion of the thesis describes an experiment to control the degree of aggregation of TTPa molecules in LB films deposited on quartz slides with a view to producing a standard monolayer system for the measurement of monolayer fluorescence lifetimes. Such a measurement is desirable as it is a direct measure of the deactivation kinetics of the excited state in the absence of electron injection into the substrate. Comparison of such a system with a system involving deactivation by electron trapping by a conduction band orbital of a semiconductor would aid understanding of the kinetics of the electron injection step. It is desirable to adjust the environment of the excited dye in such a way as to maximize its fluorescence lifetime so that this deactivation pathway does not compete with photoelectron injection.

A few attempts have been made to make this measurement for LB films. However experience has shown that these can be very difficult to reproduce. One of the reasons for this is that the concentration of molecules in this environment is sufficiently high to produce extensive aggregation of the dye molecules resulting in a highly inhomogeneous environment for the molecules. The fluorescence decay profile is therefore likely to have many components reflecting many different degrees of fluorescence quenching. Indeed it is now thought that for such type of system the components of the fluorescence profile will be spread into a continuous distribution of lifetimes.[9]

One way to reduce the aggregation is to mix the molecules with other nonphotoactive surface active molecules in a mixed monolayer. Here the nonphotoactive molecules act as blockers separating the dye molecules from each other. Since aggregation of absorbing dyes is reflected in shifts of their absorption spectra, generally red shifts,

the effectiveness of the blocker can be tested. For example a 100:1 mixed monolayer of DOPC and TTPa shows only monomeric absorption similar to that found in dilute methylene chloride whereas the same mixture using stearic acid in place of DOPC produces only aggregate spectra.

By using this technique a standard system was produced in which only one lifetime predominated whose value was close to that found in dilute methylene chloride. This system was extensively tested at two laboratories, and proposed as a standard for future monolayer fluorescence work. The system consists of a mixed LB film (50:1 molar ratio) of dioleoylphosphatidylcholine (DOPC) and 5-(4-carboxyphenyl)-10,15,20-tritolylporphyrin (TTPa) deposited from a Langmuir trough onto quartz slides.

3.1 Photophysics

Absorption of an excitation photon by a fluorophor consists of electron excitation from the ground S_o state to some other excited vibronic state. In condensed media this is followed by internal conversion to the zero point vibrational energy level of the first excited singlet state within ~1ps.[10] Depletion of this state is accomplished either by fluorescence (k_f), internal conversion (k_{ic}) to the ground state or intersystem crossing (k_{isc}) to the triplet state. The rate of these depletion processes can be summed into a total rate constant

$$k_T = k_f + k_{ic} + k_{isc} \qquad (3.1)$$

The time evolution for the excited S_1 state after an instantaneous excitation pulse is

$$\frac{-d[S_1]}{dt} = k_T[S_1] \qquad (3.2)$$

This describes exponential decay with a lifetime $\tau = 1/k_T$.

Fluorophors embedded in a monolayer may aggregate into dimers or larger clusters. The fluorescence of such aggregates is often highly quenched compared to the monomer species. The fluorescence of the monomer may be quenched by these aggregates also if the absorption band of the aggregate overlaps with the fluorescence band of the monomer allowing energy transfer to take place from the monomer to the aggregate in competition with monomer fluorescence. The new rate constant for the depletion of the excited state will be

$$k_T' = k_f + k_{ic} + k_{isc} + k_q \quad (3.3)$$

where k_q is the rate constant for the energy transfer process. The new fluorescence lifetime will be the reciprocal of the new rate constant. Since k_q may vary depending on the quenching environment a highly variable lifetime $1/k_T'$ is expected. It is therefore desirable to reduce the population of aggregate species in the monolayer, which is done in this study by dilution of the fluorophor with a blocking molecule.

3.2 The Single Photon Counting Technique

At present three methods for the measurement of fluorescence lifetimes are popular: the phase shift fluorimetry method,[11] pulsed laser flash photolysis which makes use of a streak camera as a detection source,[12] and the single photon counting method.[13] The last has been found to be probably the most effective and convenient technique for this measurement.

A block diagram of the SPC apparatus is shown in Figure 3.1. A pulse emitted from the light source, in this case a synchronously pumped dye laser powered by a mode locked argon ion laser, impinges on the fluorescent sample as well as triggering the start of a linear capacitor

Figure 3.1 The single photon counting apparatus. Laser light impinges on the sample. Sample fluorescence is passed through a monochromator (MONO) and detected by a photomultiplyer tube (PMT). The PMT signal is passed through a discriminator (DISC) to a time to amplitude converter (TAC). The laser light impinges on a second PMT whose signal is passed through a DISC to the TAC. The TAC signal is converted to a digital signal by an analogue-to-digital converter (ADC). The digitized signal is sent to a multichannel analyzer (MCA) and analyzed on a computer.

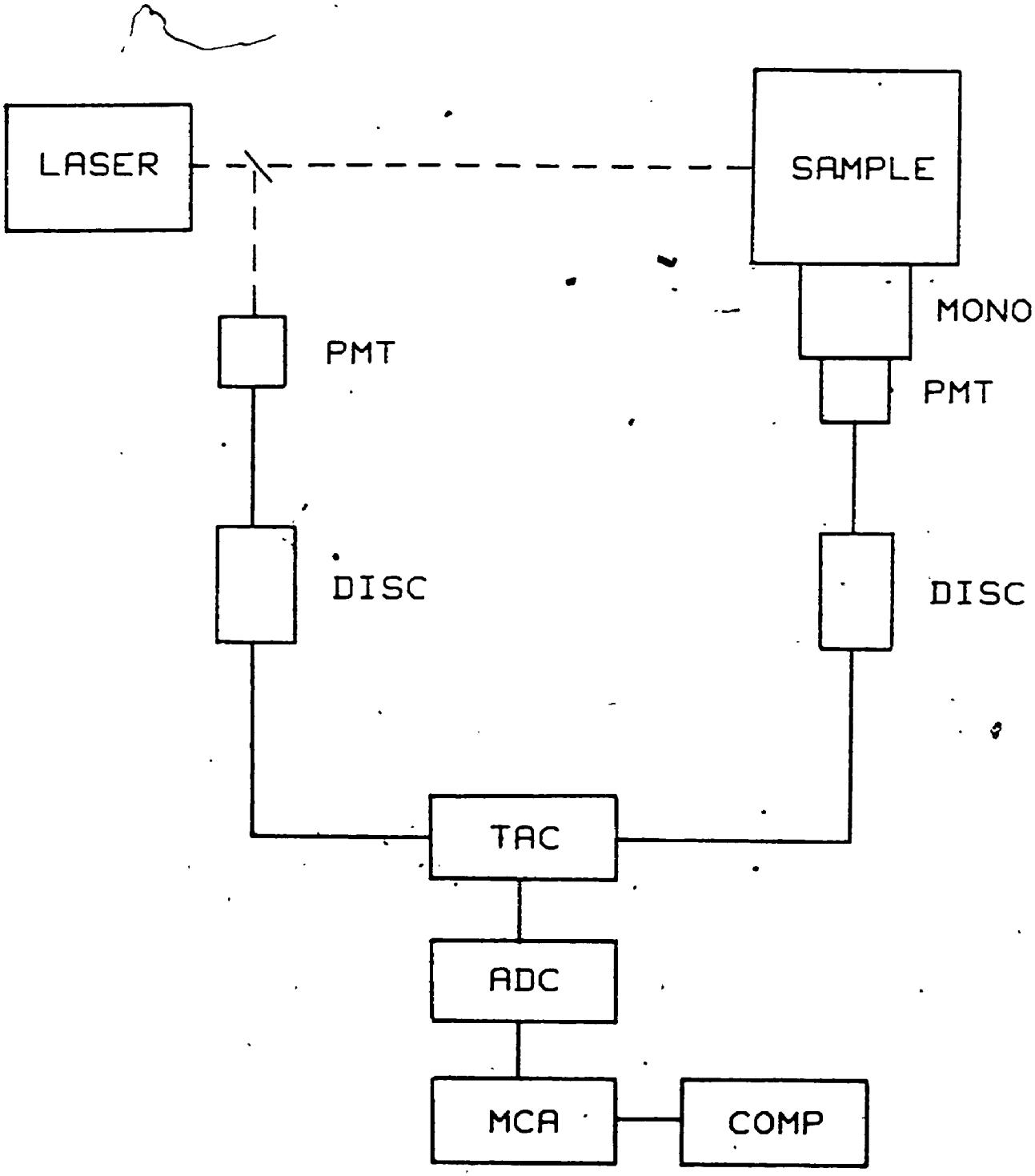
LASER
SAMPLE
MONO
PMT
PMT
DISC
DISC
TAC
ADC
MCA
COMP

charging in a time-to-amplitude converter (TAC). The first fluorescent photon emitted from the sample is converted into an electrical impulse by a photomultiplyer tube which stops the capacitor charging. The TAC converter then emits a voltage signal whose amplitude is proportional to the capacitor charge. This amplitude is converted into a channel number by an analogue-to-digital converter. Each signal is stored as a point in a channel determined by the TAC voltage. In this way a histogram of first emitted photons as a function of time develops. An assumption in this technique is that the time evolution of the probability of emission of a single photon by a fluorophor is identical to the fluorescence decay profile of a large ensemble of fluorophors.

The observed signal is the convolution of the profile of the excitation pulse and the sample fluorescence decay. In order to obtain the sample decay from the observed signal the excitation profile is first measured alone using a light scatterer. This profile is then convoluted iteratively with a computer-generated trial sample decay whose initial parameters are chosen by the experimenter. In each iteration the synthesized convolution is compared to the real signal. The difference between the two is minimized using reduced χ^2 statistics within approximately 10 itterative cycles.[14]

3.3 Monolayer Techniques

Some water-insoluble compounds when spread onto a water surface will form a single oriented monolayer on the surface. In order for a monolayer to be formed the compound must bear both a hydrophobic and a hydrophilic portion. An example would be stearic acid whose hydrophilic portion is the carboxylic acid group. This portion is oriented into the water whereas the hydrophobic alkane chain points out of the water. Monolayers exhibit surface pressure which is a resistance to compression

along the two dimensions of the interface. This may be measured by a float in contact with the monolayer and attached to a torsion pendulum. Surface pressure is measured in millinewtons per length of float in meters.

The apparatus usually employed for the production of monolayers is shown in Figure 2.1. The trough is first filled to the brim with water. A monolayer is then spread on the surface as a solution with some volatile, water immiscible compound such as chloroform. After the solvent has been allowed to evaporate the surface area of the trough is varied using a movable barrier which rides along the top of the sides of the trough. The surface pressure measured by the float-torsion pendulum assembly is plotted against the surface area. This plot made at constant water temperature is called a surface pressure area isotherm. A typical fatty acid isotherm is shown in Figure 3.2.[15] The sudden increase in surface pressure at some point along the curve is associated with the point at which the molecules are packed together as in vapor condensation.

In 1917 Irving Langmuir and Katherine Blodgett published a technique for the removal of a monolayer from the water surface to a solid substrate.[16] This removal is accomplished by first compressing the monolayer to some specified surface pressure and then dipping the substrate, such as a microscope slide, in and out of the water keeping the surface pressure constant. As the slide is dipped a meniscus is formed whose direction depends on whether the substrate surface is hydrophilic or hydrophobic. The monolayer is transferred to the slide via this meniscus as shown in Figure 3.3. Monolayers that transfer only on the downward dip are said to form X layers, those that only deposit on withdrawal Z layers and those that deposit on either form Y layers.[17]

Figure 3.2 Surface pressure area isotherm of stearic acid at 25°C subphase temperature.

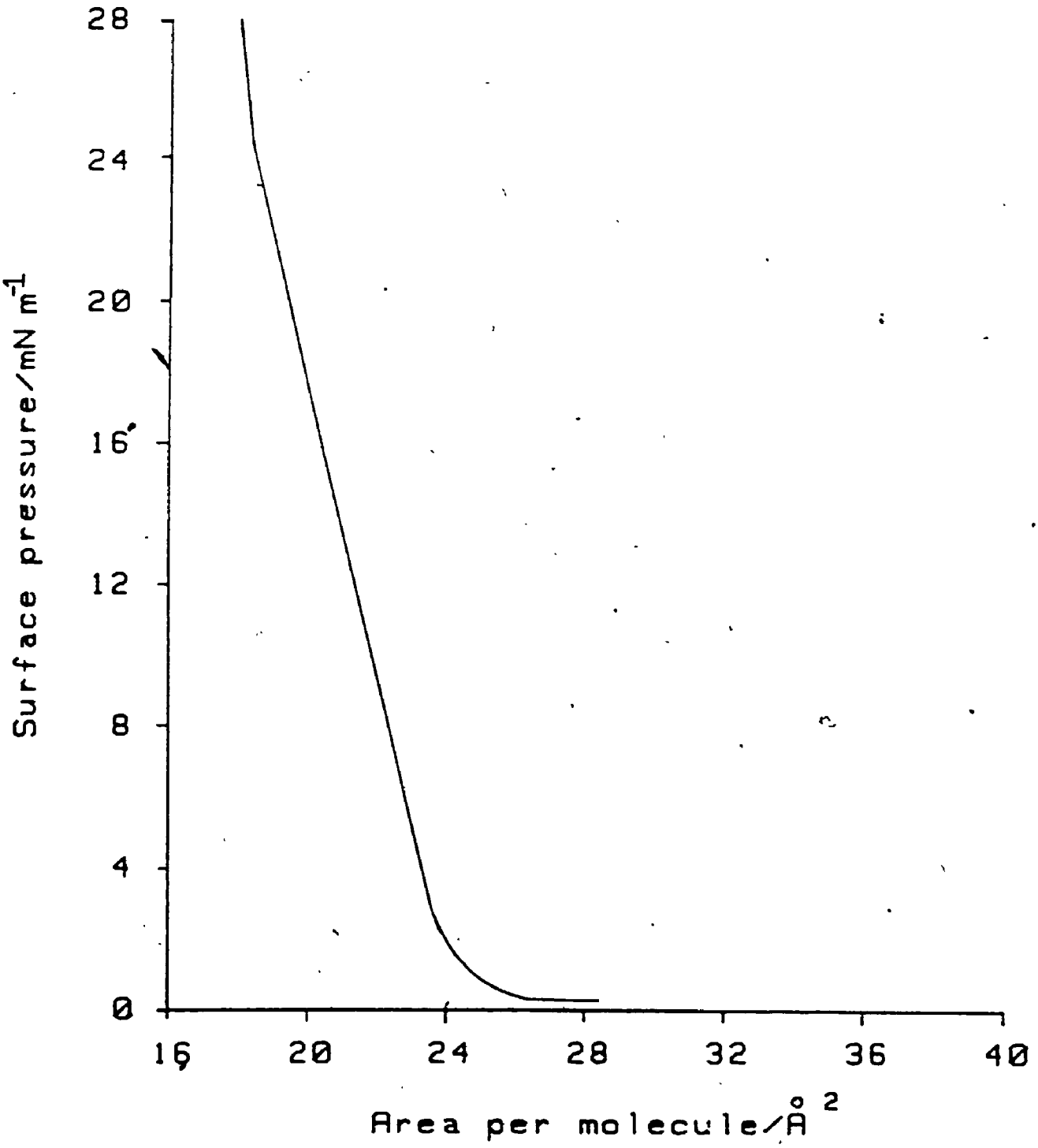
28
24
20
16
12
8
4
0
Surface pressure/mN m-1
16
20
24
28
32
36
40
Area per molecule/Å2

Figure 3.3 (a) Z layer deposition on withdrawal of a hydrophylic substrate. (b) X layer deposition on insertion of a hydrophobic substrate. Circles represent the hydrophylic portion of the surfactant molecule. Sticks represent the hydrophobic portion.

a

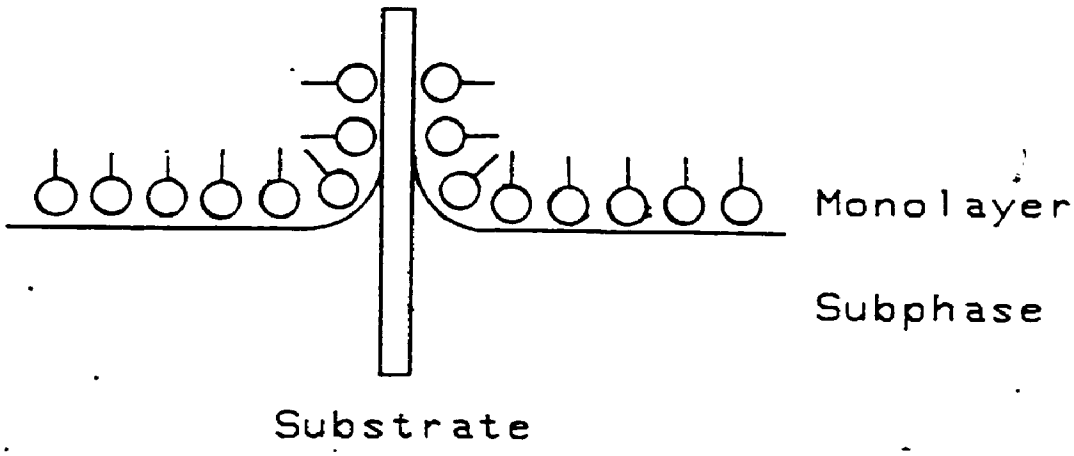
Monolayer
Subphase
Substrate

b

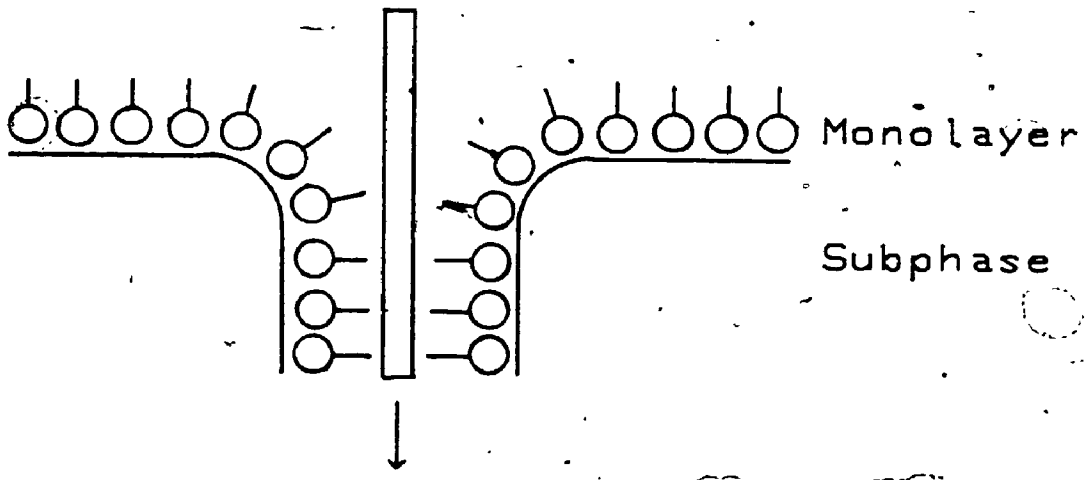
Substrate
Monolayer
Subphase

3.4 Literature Review

One of the motivations for attempting to produce a standard is that only a few attempts have been made to make this measurement. The following is a review of all the attempts to date found by the author.

Picard *et al.* have measured the fluorescence lifetime of chlorophyll *a* in pure and mixed LB films with DOPC using both the SPC technique and picosecond spectroscopy using a streak camera and a mode locked Nd^{3+}/YAG laser emitting a 40 ps pulse.[18] Fluorescence decays of pure monolayers were shorter than the resolution limit of both techniques and therefore were estimated to be less than 10 ps. 100:1 DOPC/chlorophyll *a* mixed monolayers exhibited two components of 4.9 and 2.3 ns by the SPC technique and a single component of 3.3 ns by the picosecond technique. The differences between the two measurements were attributed to the large difference in incident photon flux between the two techniques. (800 photons/Chl *a* for the picosecond technique and 10^{-7} photons/Chl *a* for the single photon counting technique).

Agrawal *et al.* measured the fluorescence lifetime of chlorophyll *a* in mixed monolayers with DOPC at the nitrogen-water interface.[19] They were able to fit their data to a single lifetime component of 5.5 ± 0.3 ns for a chlorophyll *a* mole fraction of 0.0084. This reduced to 1.0 ± 0.1 ns for a mole fraction of 0.08. Fluorescence excitation spectra taken at this interface indicated that monomeric chlorophyll *a* was the primary fluorescent specie.

The same group published a 3.8 ns lifetime for chlorophyll *b* mixed monolayers at low concentration.[20] Stern-Volmer type plots for the two types of chlorophyll indicated that dynamic, diffusional quenching predominated in the former and static quenching in the later. No explanation for this apparent difference was offered.

Bardwell & Bolton reported a 10 ns lifetime for monomeric TTPa in pure LB films.[21] By controlling the subphase pH and thus the protonation of the carboxylic acid group they were able to select the packing arrangement of the film. Comparison of fluorescence excitation and emission spectra with that of solution spectra indicated that at low subphase pH a small fraction of monomeric form resident in the pure monolayer could be transferred to the LB film.

Recently Bohorquez *et al.* have measured lifetimes for monolayers of DOPC to which a pyrene probe was attached.[22] Fluorescence excitation spectra of mixed monolayers with unattached DOPC taken at the nitrogen water interface indicated the presence of pyrene excimer emission. The lifetime components of this emission were fitted by equations developed by Birks *et al.*[23] for transient excimer fluorescence. Comparison of fitting parameters to those used for pyrene in solution indicated considerable steric hindrance to excimer formation in the monolayer.

3.5 Results and Discussion

The surface pressure area isotherms of a 50:1 DOPC/TTPa monolayer and a pure TTPa monolayer are shown in Figures 3.4 and 3.5 respectively. The DOPC/TTPa isotherm is essentially identical to that of pure DOPC which would be expected since the TTPa concentration in the monolayer is low. The observed molecular area at 20 mN m^{-1} surface pressure and 20°C subphase temperature is 72 ± 1 $Å^2$ $molecule^{-1}$ for the mixture, 71 ± 1 $Å^2$ $molecule^{-1}$ for pure DOPC, and 79 ± 1 $Å^2$ for pure TTPa. The area per molecule in the mixed monolayer agrees with the weighted average of the areas taken up by molecules in the pure monolayers which constitute the mixture indicating that ideal mixing occurs in the mixed monolayer. This might be expected since DOPC monolayers have been shown to be in a quasi-liquid state at 20 mN m^{-1}. The molecules are therefore not packed

Figure 3.4 Surface pressure area isotherm of a 50:1 DOPC/TTPa mixed monolayer. Subphase, unbuffered water at 20 ± 2°C,

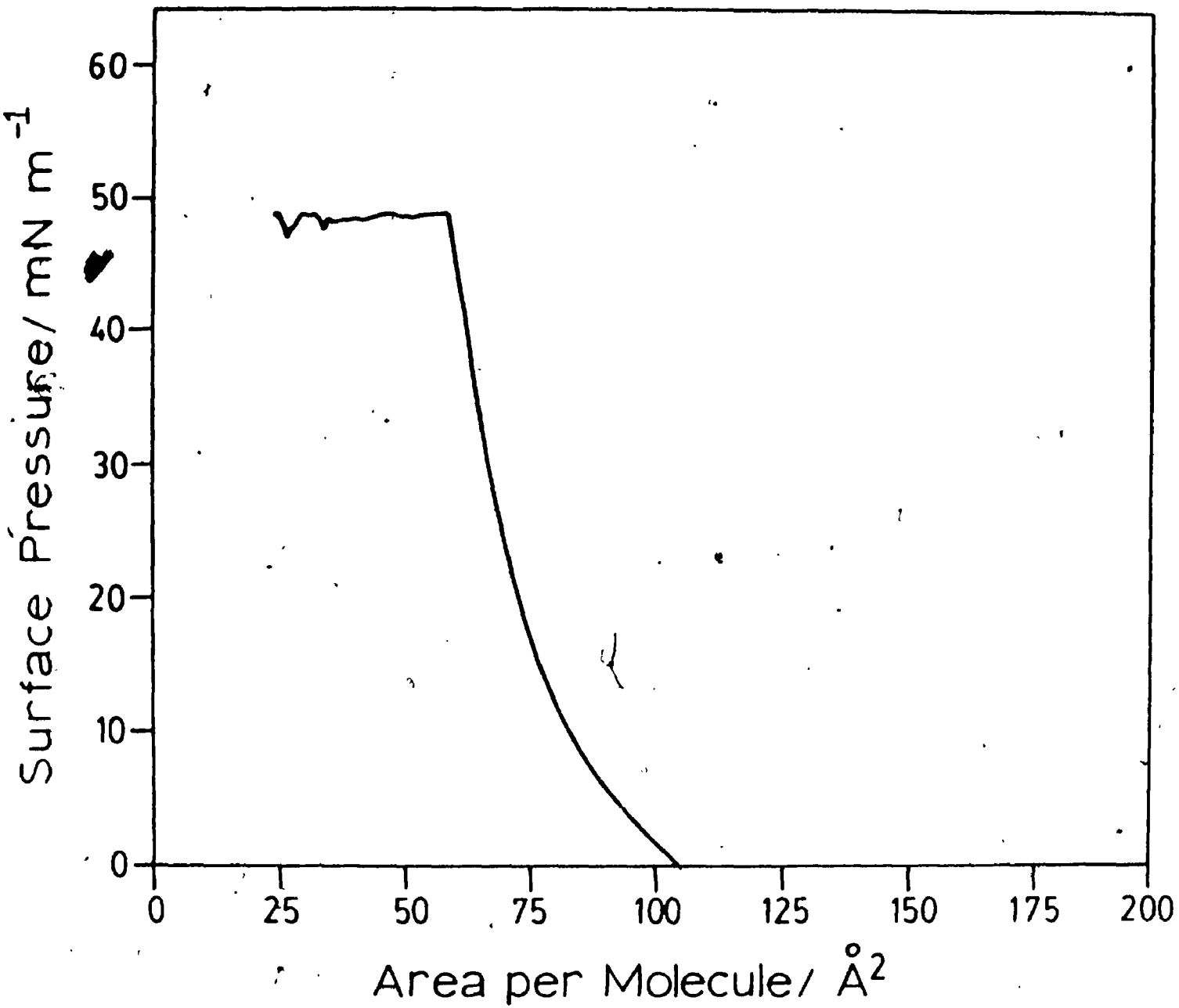
Surface Pressure/ mN m^{-1}
60
50
40
30
20
10
0
0
25
50
75
100
125
150
175
200
Area per Molecule/ Å^2

Figure 3.5 Surface pressure area isotherm of a pure TTPa monolayer. Subphase, unbuffered water at 20 ± 2°C.

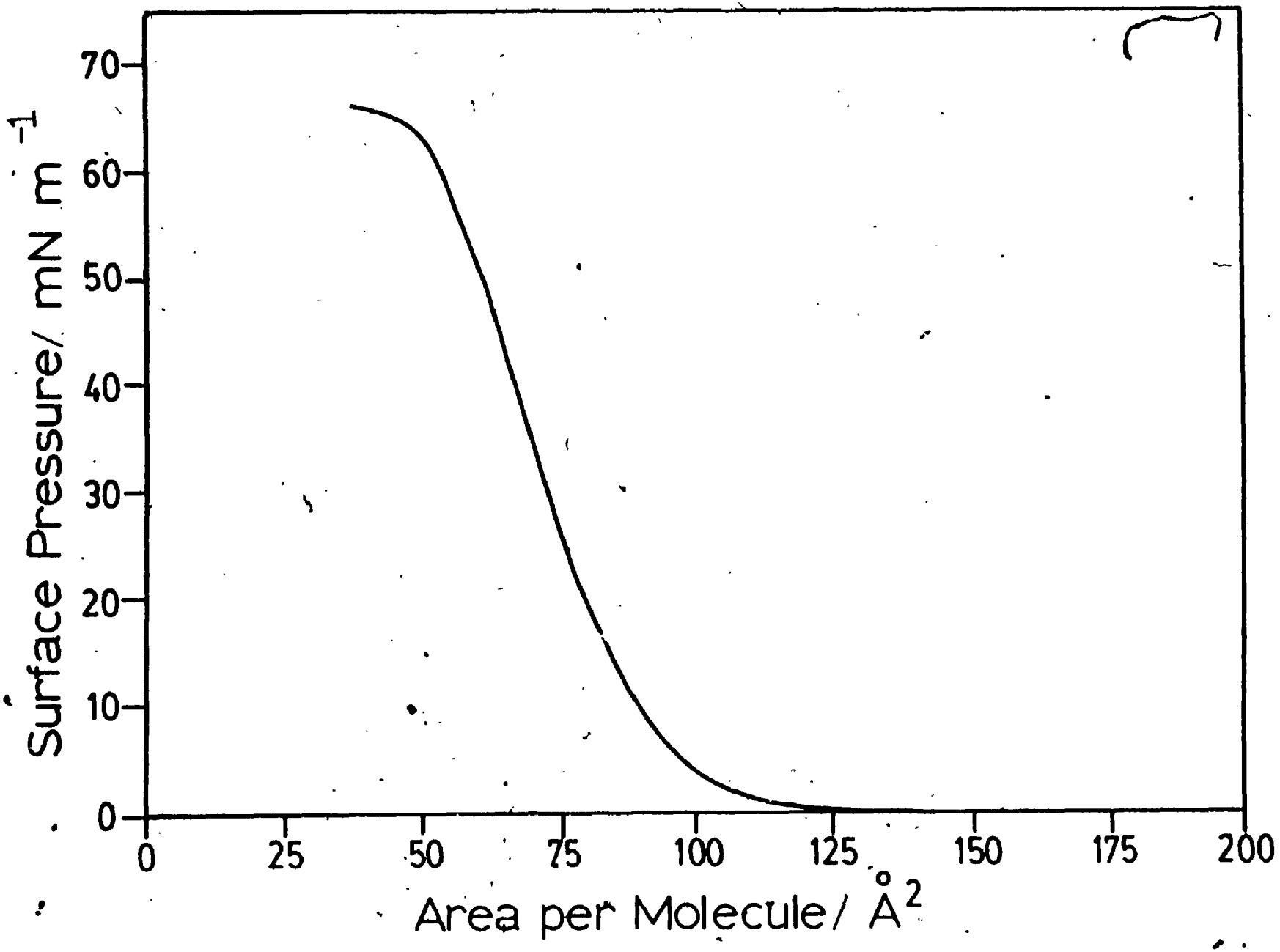
Surface Pressure/ mN m^{-1}
70
60
50
40
30
20
10
0
0
25
50
75
100
125
150
175
200
Area per Molecule/ Å^2

into arrays but are free to move encouraging good mixing.[24]

Further proof of the uniform dilution of the TTPa by the DOPC is given by the absorption spectra of the LB films. Figure 3.6 shows a series of spectra for LB films whose mixing ratios vary from 100 DOPC per TTPa to 0. At low TTPa concentration the 420 nm absorption varies linearly with concentration. As the concentration increases a red shifting of the peak occurs which has been associated with aggregate formation.[21] It therefore seems likely that the low concentration species is monomeric. The pure TTPa LB film exhibits a 420 nm shoulder which is present for films deposited from low pH subphases. This has been associated with a monomeric subpopulation. This hypothesis was tested by comparing the absorption spectra with that of dilute TTPa in solution. Figure 3.7 compares the absorption spectrum of a film of TTPa alone and a film of the TTPa/DOPC mixture with that of TTPa in methylene chloride (10^{-6} M). The red shifted aggregate peak earlier reported for the TTPa film[21] is entirely absent from the spectrum of the mixed film suggesting the predominance of the same monomeric form as found in dilute solution. The fluorescence excitation and emission spectra in Figures 3.8 and 3.9 support this hypothesis in a similar fashion. In both cases the spectra of the mixed film agree closely with the solution spectra and differ from the spectrum of the TTPa film shown here and reported previously.[21]

The dilution effect is also seen in the fluorescence decay profiles. The values of the lifetime components of the 50:1 mixed film, the pure film, and TTPa in dilute solution are given in Table 3.1. The pure film exhibits at least three lifetimes all of which are shorter than the lifetime of TTPa in solution whereas 93% of the signal is made up of a long lifetime component in the mixed film which is 1.5 ns longer

Figure 3.6 Absorption spectra of mixed LB films of DOPC and TTPa. (a) pure TTPa film, (b) 1:1.16 DOPC/TTPa, (c) 1.13:1, (d) 2.2:1, (e) 3.1:1, (f) 4.32:1, (g) 10:1, (h) 20:1, (i) 50:1.

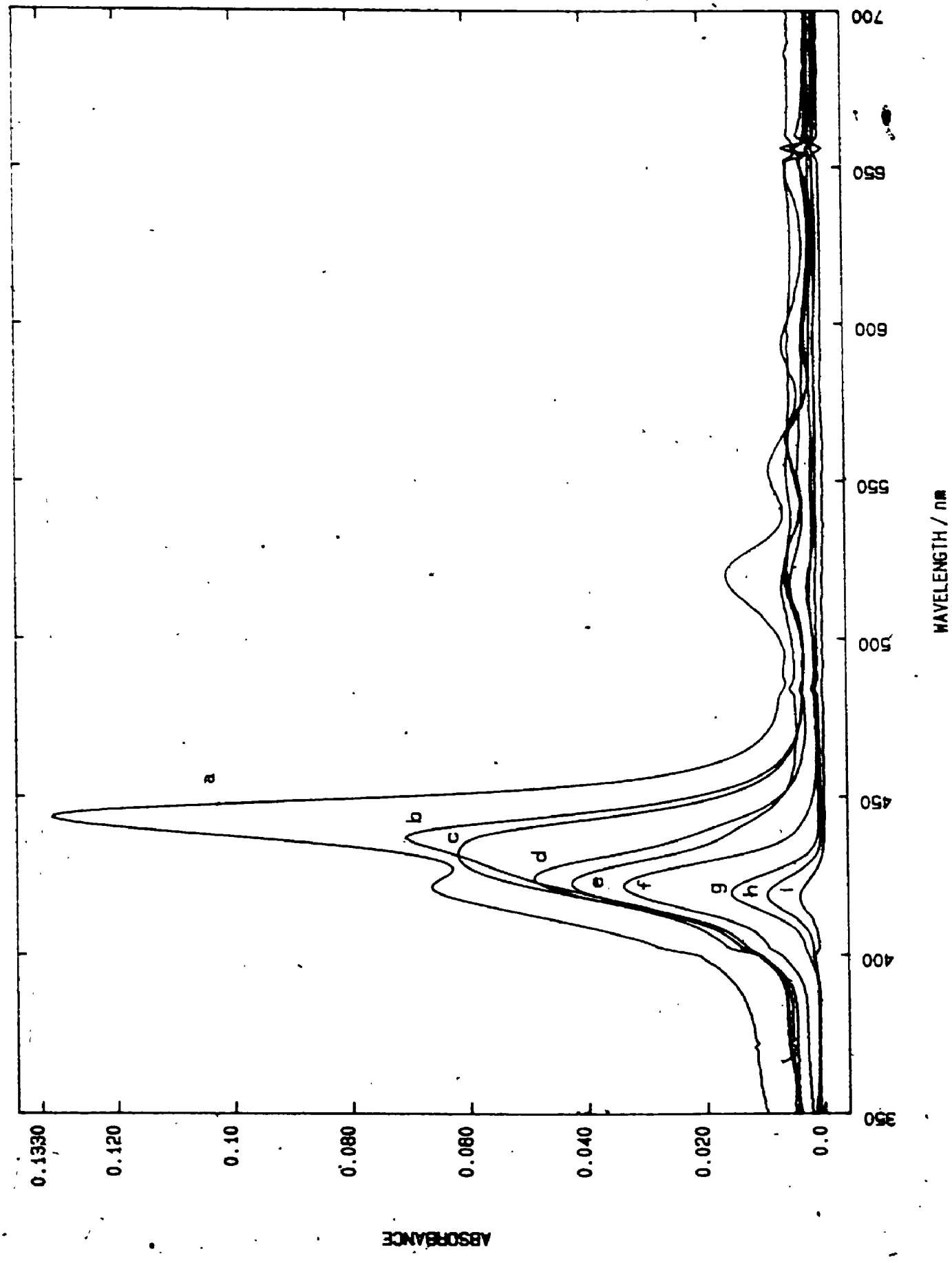
ABSORBANCE
0.1330
0.120
0.10
0.080
0.080
0.040
0.020
0.0
350
400
450
500
550
600
650
700
WAVELENGTH / nm
a
b
c
d
e
f
g
h
i

Figure 3.7 Optical absorption spectra of TTPa in methylene chloride (10^{-6}) (- —), in a LB film of TTPa alone (- - -), and in a 50:1 DOPC/TTPa mixed film (——).

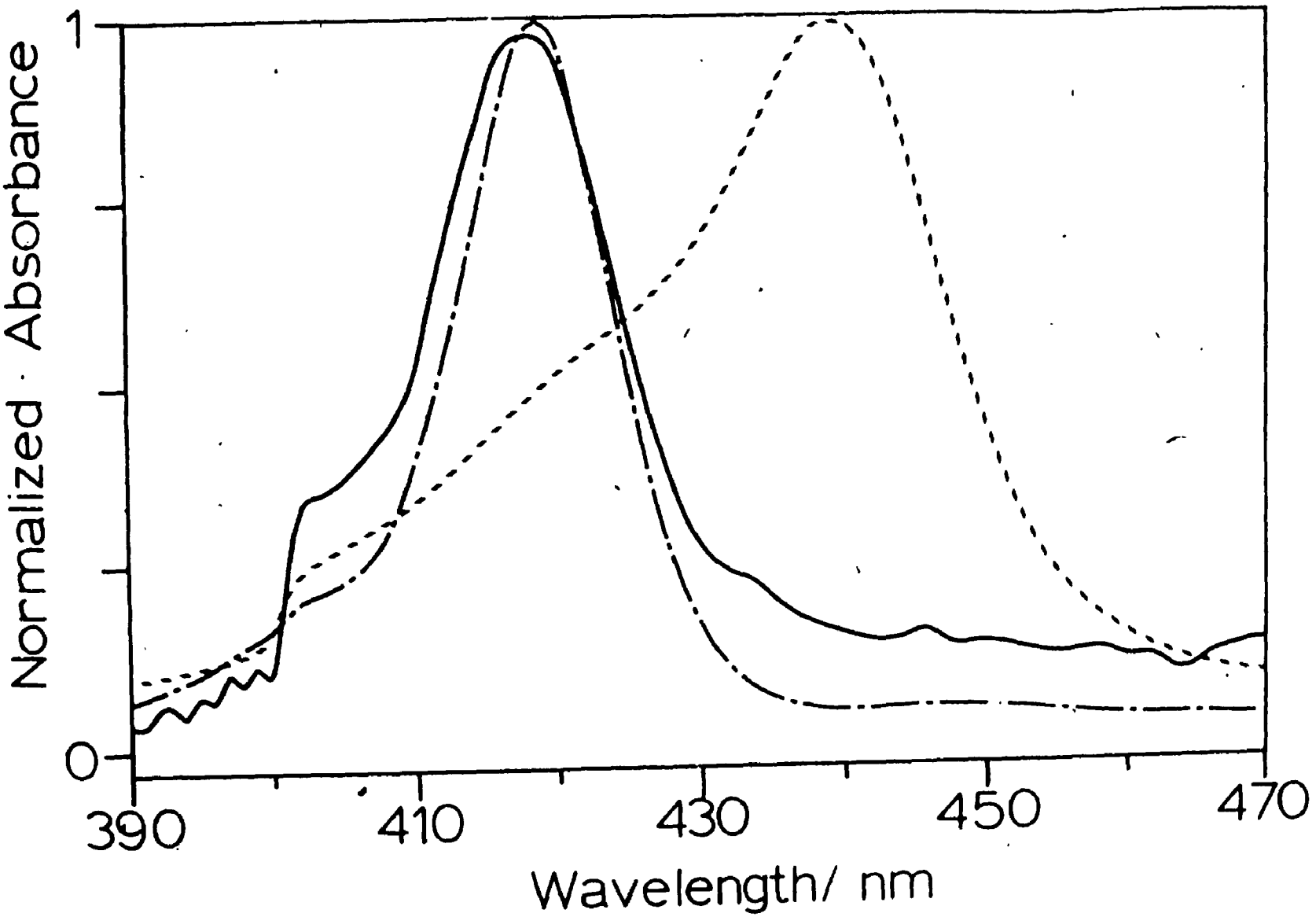
Normalized · Absorbance
1
0
390
410
430
450
470
Wavelength/ nm

Figure 3.8 Fluorescence excitation spectra of TTPa in methylene chloride (10^{-6}M) (- —), in an LB film of TTPa alone (- - -), and in a 50:1 DOPC/TTPa mixed film (——); λ_{em} = 650 nm.

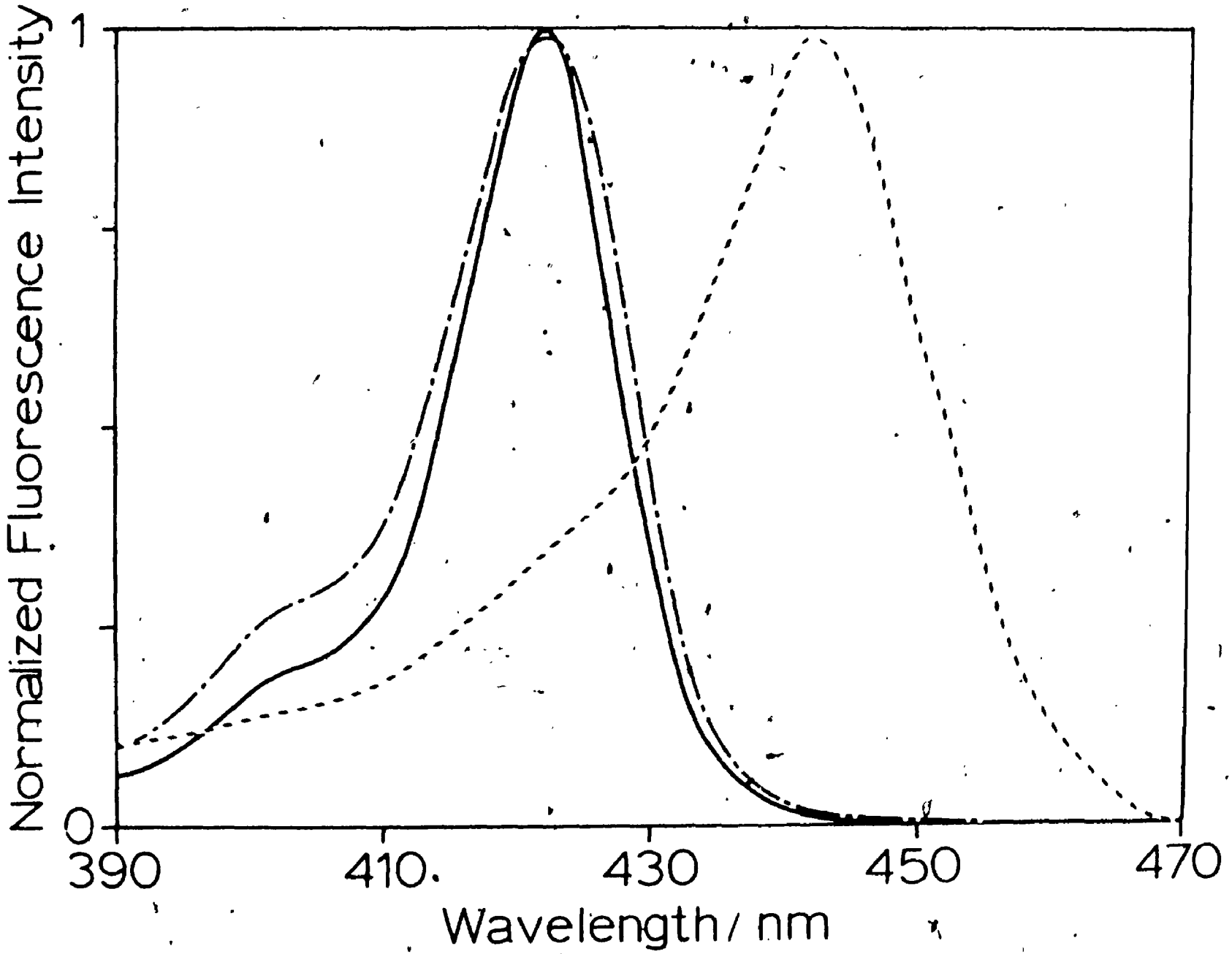
Normalized Fluorescence Intensity
1
0
390
410.
430
450
470
Wavelength / nm

Figure 3.9 Fluorescence emission spectra of TTPa in methylene chloride (10^{-6}M) (- —), in an LB film of TTPa alone (- - -), and in a 50:1 DOPC/TTPa mixed film (——); λ_{ex} = 420 nm.

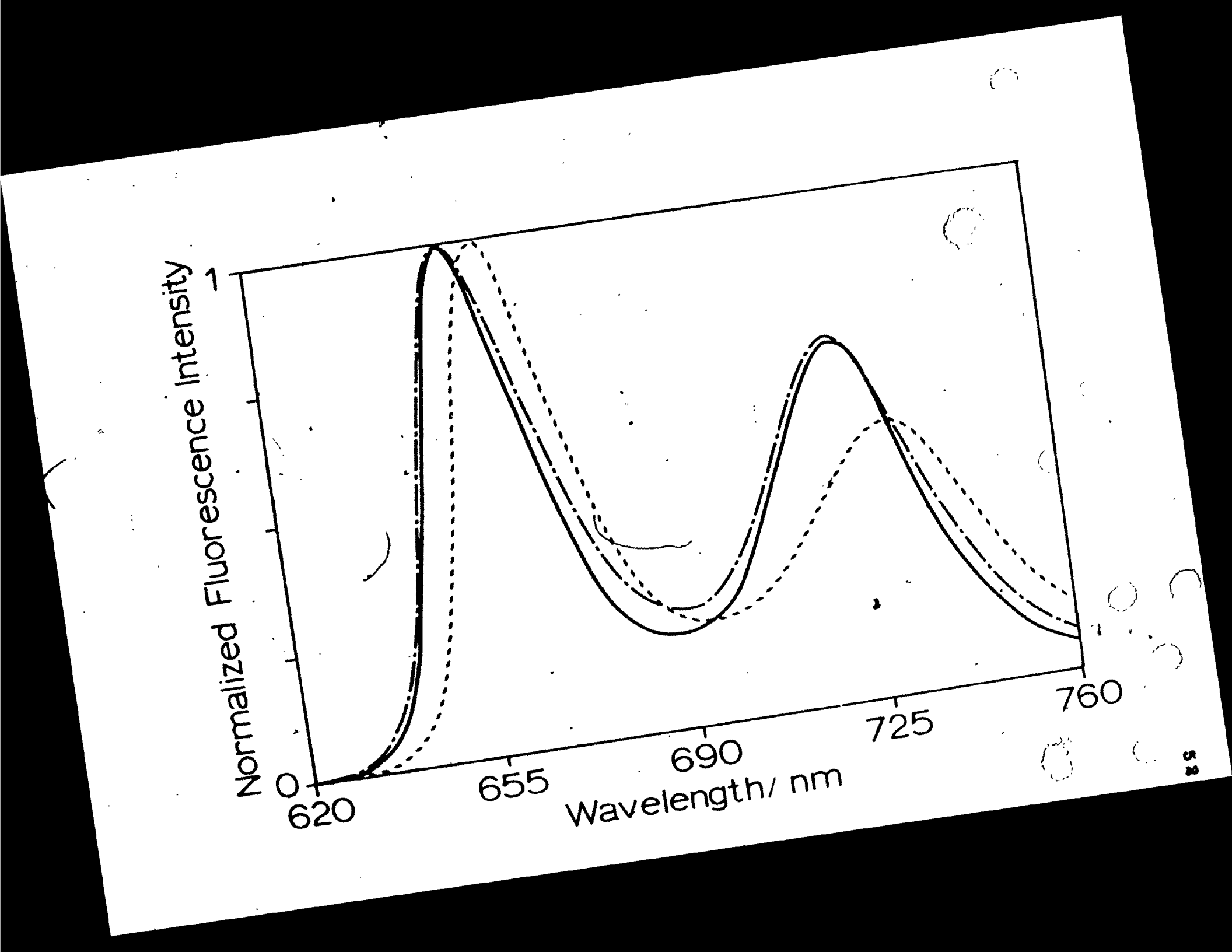
Normalized Fluorescence Intensity
1
0
620
655
690
725
760
Wavelength/ nm

Table 3.1 Fluorescence lifetime measurements for monolayer films of TTPa.

System	τ_1/ns	A_1(%)[a]	τ_2/ns	A_2(%)[a]	τ_3/ns	A_3(%)[a]	number of measurements
50:1, DOPC/TTPa, mixed LB film	2.2 σ ±0.9	7 σ ±2	10.7 σ ±0.2	93 σ ±2			24
pure TTPa LB film	0.73 σ ±0.05	50 σ ±17	1.3 σ ±0.01	18 σ ±29	2.8 σ ±0.2	32 σ ±13	3
TTPa in CH_2Cl_2	9.2 ±0.1						-

a Amplitudes normalized to 100.

than that of solution. We suspect that the short component may be due to an aggregate specie since its value matches that of one of the components in the decay profile of the pure monolayer in which at least two aggregate species have been postulated to exist.[21] Since the component was only 7% of the total signal it would not show up in the absorption or fluorescence spectra. The slight shortening of the solution lifetime compared to that of the diluted LB film may be due to a heavy atom effect. That is, the chlorine atom in the solvent molecule may be acting to promote intersystem crossing in competition with fluorescence.

The mean value of the long component of the 50:1 mixed film was found to be 10.7 ns with a standard deviation of 0.2 ns. Since we found this lifetime to be highly reproducible both within and between our two laboratories, we have proposed this system as a standard for future testing of time-resolved fluorescence of monolayer systems. Agreement between the two laboratories was found to be within 0.05 ns. The standard deviation in 24 measurements on the same sample was 0.2 ns. These measurements spanned the period of one week with no noticeable trend in the results indicating the chemical stability of the system with respect to the photophysics. The standard deviation in the measurement of 8 different samples was 0.1 ns. At a 50:1 DOPC/TTPa molar ratio the change in the long component value as a function of mixing ratio was 1.25×10^{-2} ns/ratio point. Hence, an error of 8 ratio points is acceptable before a change in the long component value is seen.

CHAPTER 4 PHOTOELECTROCHEMICAL STUDIES

In the previous section we considered the deactivation processes of energy transfer to aggregate porphyrin species that resulted in a quenching of the excited state of the porphyrin embedded in an LB film. The substrate was thought to play little or no role in this. If we replace the glass substrate with the semiconductor SnO_2 chosen so that there is the possibility of isoenergetic electron-transfer to the semiconductor to act as a deactivation pathway, we find that the fluorescence is partially quenched. The following section studies this pathway by considering the characteristics of the photocurrent produced in a cell in which the photoactive electrode is a semiconductor bearing a single TTPa monolayer.

The reasons for choosing a semiconductor in an electrochemical cell are pragmatic. In order to study the current due to photoelectron injection conductive contacts must be made to the LB film. The contacts must be made such that an electric field is seen across the film resulting in unidirectional electron flow. One way to do this would be to sandwich the film between two metal contacts by first depositing it onto a metal surface using the LB method and then evaporating a second metal layer on top.[25] This method suffers from two disadvantages. The first is that the electric field exists solely due to the insulating ability of the film. The film must therefore be made perfect since any holes would create short circuits in the system. This has proven extremely difficult to do. The film must not only be physically perfect but also chemically pure. Impurities such as oxygen from the air have been known to act as dopants rendering measurements irreproducible. In fact some recent measurements under ultra-high vacuum conditions have called into question the basic assumption that electron transfer of the

type generally assumed is taking place at all in these sandwich cells.[26]

The second problem is that the metal contacts have been found to be excellent energy transfer quenchers of the dye excited state.[27] This might be expected since the absorption spectrum of the metal extends across the entire visible spectrum and therefore overlaps well with the dye fluorescence profile. Studies of multilayer sandwich cells have shown that at least three to four monolayers are needed to produce appreciable photocurrent.[28] Here the middle monolayers find themselves separated from the metal sufficiently for photo-ionization to compete with deactivation by energy transfer to the metal. The problem in this scheme is that since the photo-ionizer is spatially separated from the metal the electrons must tunnel through the relatively insulating ground state dye molecules before being injected into the metal. These sandwich cells therefore tend to have high resistivities that set a low ceiling on the photocurrent, sufficiently low in many cases to make detection difficult.[28]

Photocurrent may be produced by electron injection from a photoexcited dye located at a semiconductor-electrolyte interface. This technique called dye sensitization evolved from the need to produce a photo-electrode stable to oxidation by water.[29] Wide bandgap oxide semiconductor electrodes met this requirement but required ultraviolet light to produce photocurrent. Photocurrent in a conventional semiconductor electrode is produced by electron hole pair production in or within a diffusion length of the space charge layer. This involves bandgap excitation. The width of the bandgap for oxide semiconductors stabilizes it chemically but also precludes excitation by visible light. The semiconductor may be sensitized to visible wavelengths by location of a dye at the surface either by adsorption from solution, evaporation

from a solvent, or deposition of a monolayer. It is required that either the excited or ground state energy of the dye overlap with a semiconductor band. Thus when the dye is excited by visible light it may either donate an electron to the conduction band or a hole to the valence band. Except for transient photocurrents a second reductant, called a supersensitizer, is needed to rereduce the photo-oxidized dye or reoxidize the photo-reduced dye.[30] This supersensitizer takes the place of the second metal contact. A supersensitizer need not always be added to the electrolyte since occasionally the conductive medium itself performs this function as in the case of dye sensitized water splitting.[31]

A monolayer in the dye sensitization scheme does not suffer from the problems associated with a sandwich cell and can produce substantial photocurrent. A single monolayer is thin enough to allow electron tunneling. Furthermore the spacing between molecules may be large enough to allow ion penetration to the electrode. In either case the resistance of the monolayer will be low allowing higher current to pass. In this case also an insulating layer is not required for electric field production since the semiconductor-electrolyte junction itself produces a field. In fact, most dye sensitization work has been carried out using electrolyte soluble dyes where only those dye molecules that are within a few Å of the electrode contribute to the photocurrent production. In an n-type semiconductor in depletion mode a positive space charge forms just below the surface irrespective of the presence of the monolayer or adsorbed dye. This space charge produces an electric field which oxidizes the photoexcited dye. Energy transfer is precluded for wide bandgap semiconductors since their absorption bands are much higher in energy than the fluorescence profile of the dye. The electrolyte also

provides a much better electrical contact to the electrode. Rather than being sandwiched between two solid phases the dye covering the electrode surface is accessible and can be affected by changes in electrolyte composition that can be controlled by the experimenter. Impurities can be controlled more easily. Furthermore the energetics of the electron-transfer process can be studied by varying the redox potential of the supersensitizer. This sensitization scheme is shown in Figure 4.1.

The following discussion is divided into four sections. First there is a theoretical section in which the energetics of current carriers in each of the phases and boundaries in the dye sensitization scheme is considered. This section will include the basic theory of current production and capacitance for such systems. This is followed by a literature review in which previous research studies in this field will be discussed. Only papers that are very close in nature to this study or presenting pertinent concepts will be discussed. The results of this study will then be presented and compared to the previous findings.

4.1 Electronic Energy in the Cell

The photoelectrochemical experiments were conducted on a cell of the following general configuration.:

metal|semiconductor|dye monolayer|aqueous electrolyte|metal

In order to understand the behavior of this type of cell we must follow the energetics of the charge carriers through all of the five phases. We shall then be able to make predictions about the behavior of the cell as a whole. Before we begin some terminology needs to be made clear, specifically that concerning the electrochemical potential of an electron. In a solid phase this can be shown to be the Fermi energy, the

Figure 4.1 The dye sensitization scheme. Absorption of a photon ($h\nu$) by the dye excites an electron from the ground state (S_o) to the first excited singlet state (S_1). This is followed by isoenergetic electron transfer to the conduction band (c) of the semiconductor. The oxidized dye is rereduced by a supersensitizer (Sp) in solution.

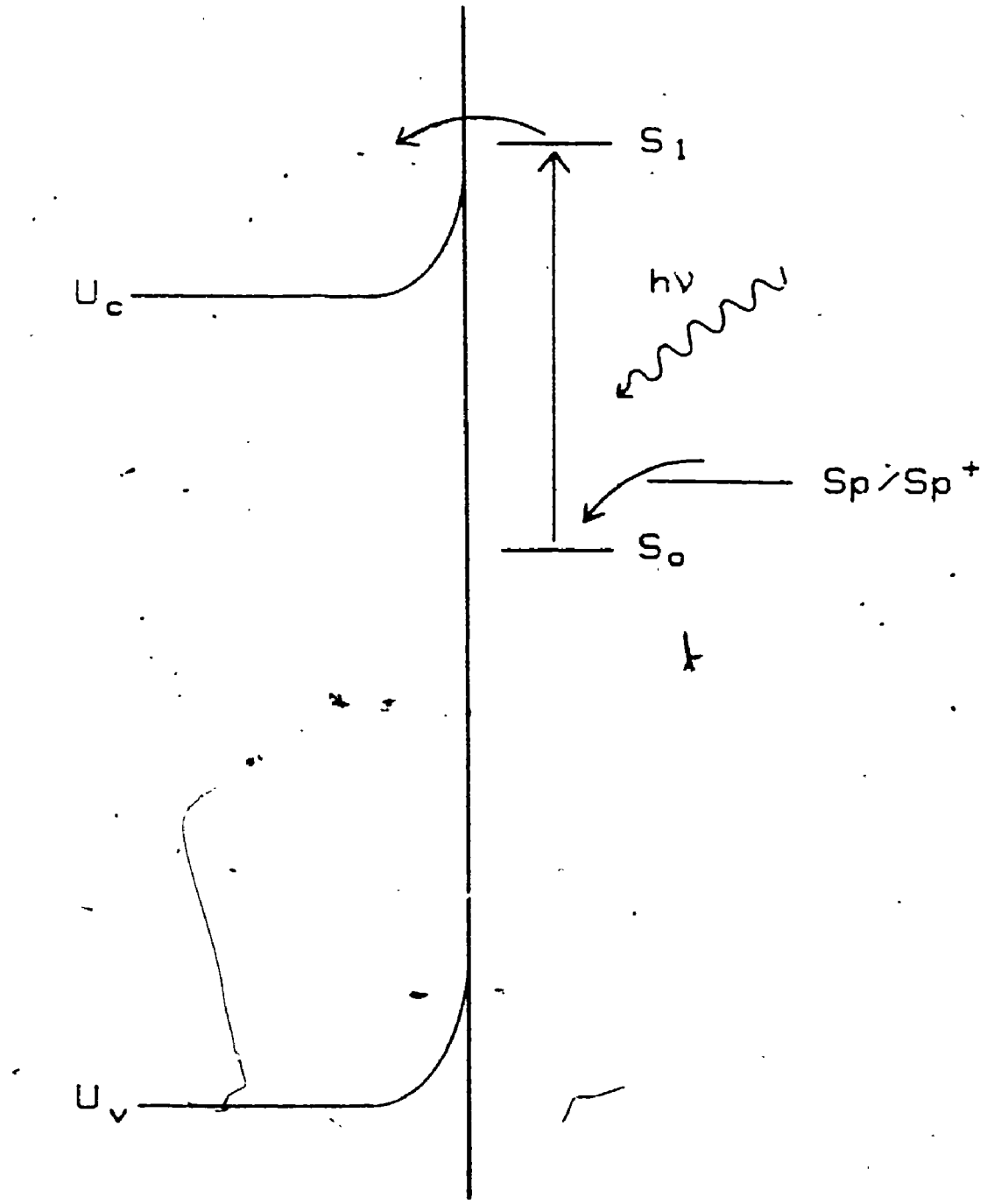
S1
hν
Sp/Sp+
So
Uc
Uv
Semiconductor
Dye
Electrolyte

energy at which the probability of finding an electronic orbital filled is 1/2. The probability that electronic bands or orbitals of energy lower than the Fermi energy will be filled approaches unity within approximately 1 kT approaches zero in the same interval for bands or orbitals higher. The Fermi energy in a metal is therefore identical to the negative of its work function. The electrochemical potential of an electron resident in a redox couple in solution is the redox potential of the couple. In a solid the electrochemical potential is measured with respect to vacuum whereas solution redox potentials are referenced to the standard hydrogen electrode. These two can be related by determining the Fermi level of an electron in the platinum of the standard hydrogen electrode. Theoretical and experimental determinations agree quite well and place it at 4.44 eV below vacuum.[32]

At equilibrium the electrochemical potential of an electron in all phases of the electrochemical cell must be identical to maintain zero net current. Therefore when a number of phases of different electrochemical potential are brought into electrical contact current flows from phases of higher electrochemical potential to phases of lower until the electrochemical potentials of all phases are the same. This builds up charge within certain phases. Potential applied to the leads of the cell destroys the equilibrium to which the cell responds by producing current.

A picture of the energetics of an electron throughout the entire cell is given in Figure 4.2 and may referred to by the reader in the succeeding sections.

4.1.1 Electronic Energy in the Semiconductor Bulk

The Fermi energy U_f of an electron in the bulk of a non-degenerate

Figure 4.2 An energy level diagram of the photoelectrochemical cell. Here voltage V_{cell} is applied to the cell.

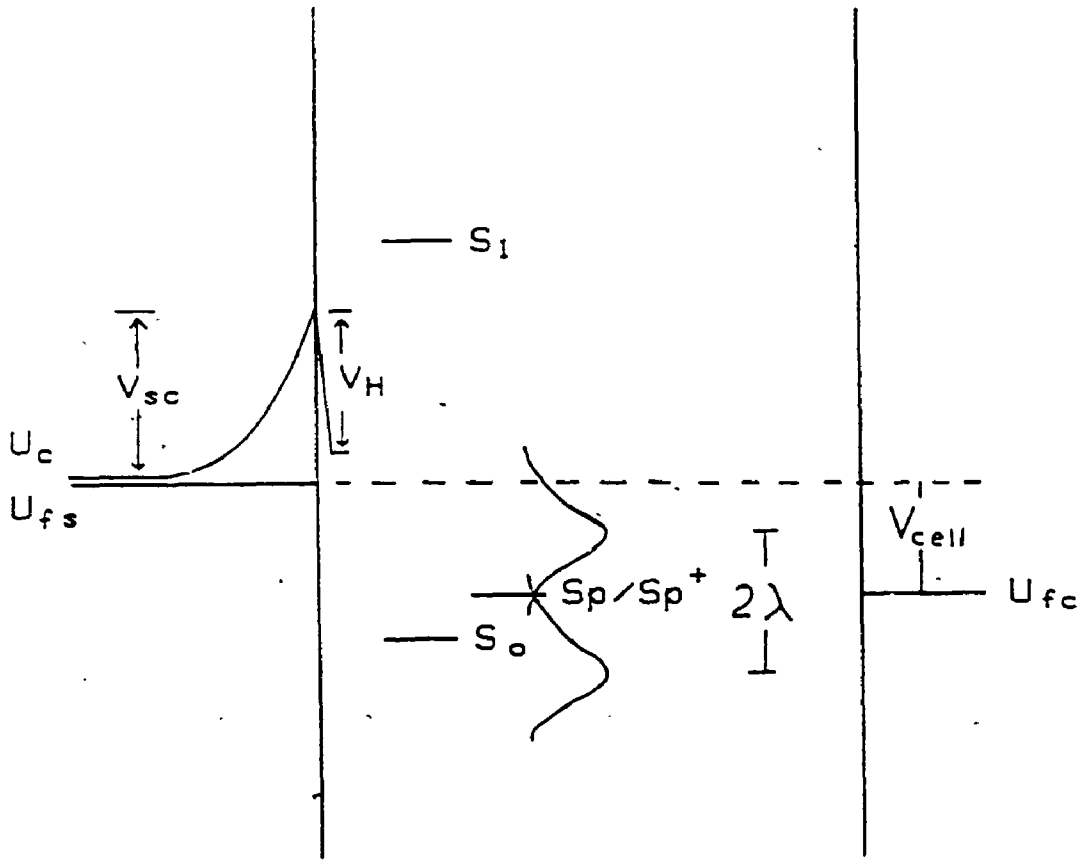
S1
Vsc
VH
Uc
Ufs
Vcell
Sp/Sp+
2λ
Ufc
So
Semiconductor
Dye
Electrolyte
Electrode

semiconductor obeying Boltzmann statistics is given by[33]

$$U_f = U_C + kT\ln(n_o/N_c) \qquad (4.1)$$

where U_f is the Fermi energy of the electron, U_C is the energy of the conduction band edge, k is the Boltzman constant, n_o is the density of free electrons in the conduction band in the bulk and N_C is the effective density of states at the conduction band edge. Similarly the Fermi level for holes is given by

$$U_f = U_v - kT\ln(p_o/N_v) \qquad (4.2)$$

where U_v is the energy of the valence band edge, p_o is the density of holes in the valence band in the bulk and N_v is the effective density of states at the valence band edge.

In an intrinsic (non-doped) semiconductor the Fermi level is located near the midpoint of the bandgap. n-Doping causes U_f to rise to a level between the discrete donor level of the dopants and the conduction band edge. In a highly n-doped degenerate semiconductor the Fermi level may be located within the conduction band causing it to behave like a metal.

Equation 4.1 indicates that the Fermi level depends on the electron density in the conduction band. If a source or sink for electrons such as a metal lead is attached to the semiconductor and a voltage is applied, the Fermi level will shift accordingly to maintain equilibrium.

4.1.2 Electronic Energy near the Semiconductor Surface

A region of localized charge exists at the surface of the semiconductor. If the semiconductor is located in a vacuum a space charge may exist because of surface states, called Tamm states, that are formed by the disruption of the repetitive lattice.[33] These states are

located within the band gap and act to trap charge. If, for example, the surface states trap electrons from the conduction band a negative charge builds up at the surface that is compensated by a positive space charge near the surface. The extent to which the space charge extends into the interior of the semiconductor depends on the conductivity of the semiconductor, which in turn depends on the doping level of the material. Highly doped materials bear a relatively thin space charge layer.

The voltage variation with position in the space charge layer may be evaluated for an intrinsic semiconductor by solving the Poisson equation for charge in that region[34]

$$\frac{d^2\phi_x}{dx^2} = \frac{-\rho_x}{\epsilon\epsilon_o} \tag{4.3}$$

where ϕ_x is the potential at a distance x away from the surface measured with respect to the potential at the surface. ρ_x is the charge at x, ϵ is the dielectric constant and ϵ_o is the permittivity of free space. For an intrinsic semiconductor

$$\rho_x = q(p_x - n_x) \tag{4.4}$$

$$= q[p^o{}_x\exp(-q\phi_x/kT) - n^o{}_x\exp(q\phi_x/kT)]$$

where p^o and n^o are the acceptor and donor densities in the semiconductor bulk. By substituting 4.4 into 4.3

$$\frac{d^2\phi}{dx^2} = \frac{8\pi qn^o}{\epsilon\epsilon_o\sinh(q\phi_x/kT)} \tag{4.5}$$

Integrating ϕ twice and approximating sinhx = x gives the form

$$\phi_x = \phi_s e^{-kx} \tag{4.6}$$

where ϕ_s is the potential at the surface. k^{-1} called the Debye length is given by

$$k^{-1} = \left[\frac{8\pi n^o q^2}{\epsilon_o \epsilon kT}\right]^{-1/2} \tag{4.7}$$

and is a measure of the thickness of the region. The thickness of the space charge reqion can be seen to vary inversely as the square root of the free carrier density. The expression for an extrinsic semiconductor is essentially the same and produces a similar though more complicated dependence.

When an n-type semiconductor is brought into contact with a metal of work function greater than that of the semiconductor (lower Fermi energy) electrons flow from the semiconductor to the metal. This produces a positive charge at the semiconductor surface and a negative charge at the metal surface. Since the conductivity of the metal is high the negative charge all appears at the surface, whereas the positive charge is spread throughout the space charge region of the semiconductor. There is therefore a potential rise in the interfacial region which rises abruptly on the metal side and more gradually on the semiconductor side. This potential rise represents a barrier to electron flow as shown in Figure 4.3. When an external potential is applied across this interface, the change is seen across the semiconductor space charge layer since the conductivity of this phase is lower than the metal. The size of the semiconductor side of the barrier is therefore potential dependent but invariant on the metal side. Electrons flowing from the metal to the semiconductor always experience a

Figure 4.3 (a) A Schottky barrier junction between a semiconductor with Fermi level U_F and a metal of work function wf. (a1) Before contact. (a2) After contact. (a3) The current voltage plot of a Schottky barrier. (b) An ohmic contact. (b1) Before contact. (b2) After contact. (b3) The current voltage plot of an ohmic contact.

a1

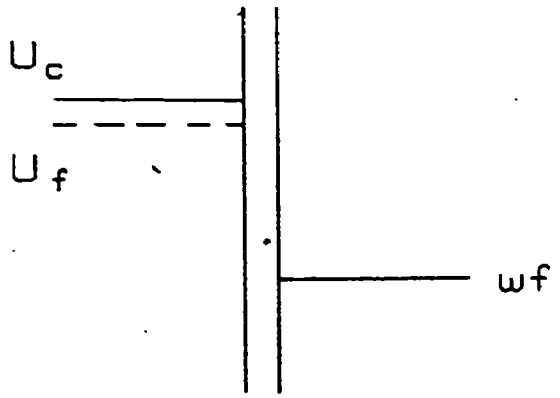

b1

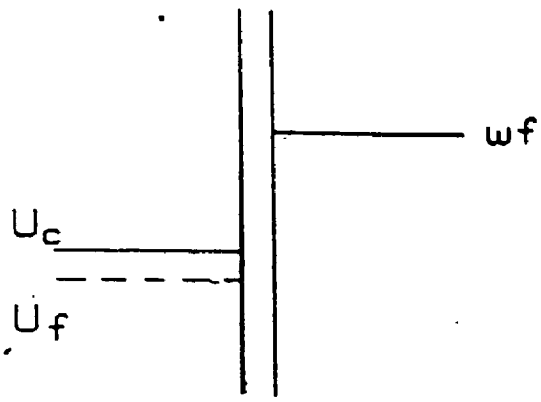

a2

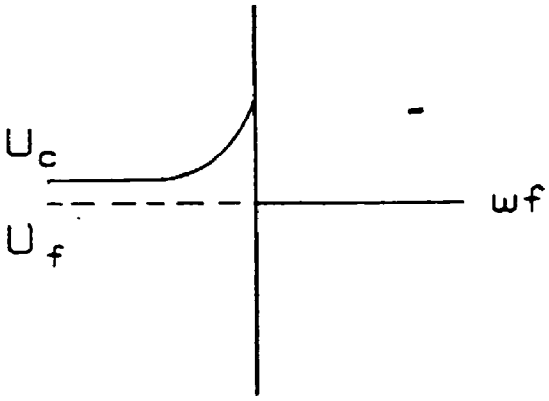

b2

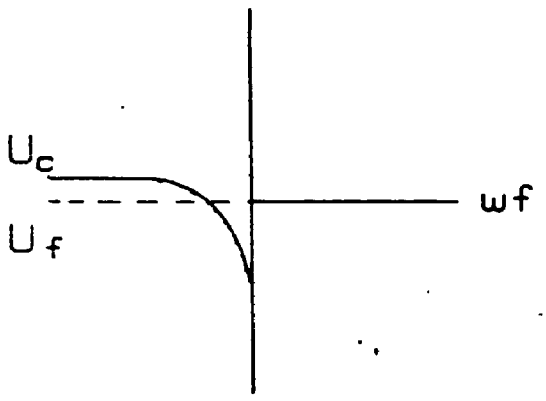

a3

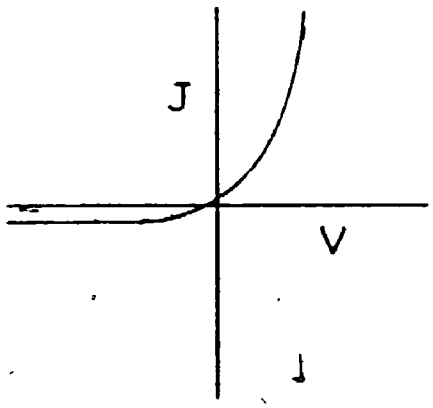

b3

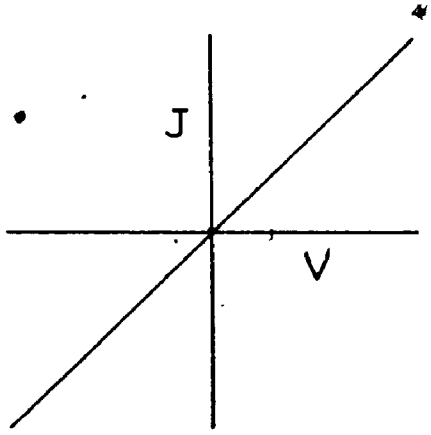

considerable barrier to flow whereas the barrier to electron flow from the semiconductor to the metal may be reduced by an applied potential. The contact therefore becomes rectifying allowing substantial current to pass only from the semiconductor to the metal. If the work function of the metal is less than that of the semiconductor, there is no barrier to electron flow and the contact is said to be ohmic. Figure 4.3 illustrates the current-voltage dependence for the two cases.

The semiconductor electrolyte junction behaves in a manner identical to that of the semiconductor metal junction provided that the electrolyte is sufficiently concentrated so that its conductivity is much greater than that of the semiconductor.[35] In this case the work function is replaced by the redox potential of the dominant redox couple and the charge carriers in the electrolyte phase are solvated ions. Surface states may exist at either the semiconductor electrolyte or semiconductor metal junction due to Tamm states or adsorption of impurities. If the surface state density is high enough, equilibrium will be established with the surface states rather than with free carriers in the semiconductor leading to Fermi level pinning in the space charge region.[36]

The metal lead attached to the semiconductor is chosen so that an ohmic contact is formed since the junction of interest is that between the semiconductor and the electrolyte.

4.1.3 Electronic Energy in the Interfacial Double Layers

When a semiconductor is immersed in solution its surface charge may attract ions of opposite sign thus forming a space charge on the electrolyte side of the junction.[37] Such a space charge may form even without a surface charge since the surface is the site of disruption of

the geometry of solvation forces acting on the ions in solution.

Two distinct regions of charge exist in electrolyte solutions of medium to low concentrations. The Helmholtz region begins at the surface and extends to the distance of closest approach of solvated ions. This distance of closest approach forms a plane called the outer Helmholtz plane. The second region is the diffuse Gouy-Chapman region. It begins at the outer Helmholtz plane and extends into the solution bulk. By reasoning similar to that for the semiconductor space charge region this space charge potential can be shown to fall off exponentially with distance from the surface. In a sufficiently concentrated electrolyte the region disappears and all the charge is located at the outer Helmholtz plane. In this case any voltage drop across the solution is located in the Helmholtz region and is linear in this region.

The electrochemical potential of a redox active electron, as given by the redox potential of the couple in which it resides, will depend in this region on the size and the sign of this space charge and will therefore not, in general, be identical with that of the bulk solution. If all the charge resides in the Helmholtz region, the redox potential will coincide with that of bulk solution since solvated ions cannot exist within it.

4.1.4 Electronic Energy in the Dye Monolayer

Whether or not the dye orbital responsible for the photoinjection is located inside or outside the Helmholtz region is determined by the method of dye attachment. In most cases it seems to be located outside. Electrolyte soluble dyes remain outside the Helmholtz plane. If an LB film is deposited, the results can vary depending on whether or not the molecule is oriented in such a way that the dye group is directed toward the surface.[38] If the dye group is oriented away from the surface then

the rest of the molecule may be large enough to place it outside of the Helmholtz plane. The oxidation potential of the first excited singlet state (S_1) of a photoelectron injecting dye is estimated by adding the singlet excitation energy to the oxidation potential of the ground state as determined experimentally. This potential must be sufficiently large that the energy of an electron in the excited state of the dye is greater than the conduction band edge allowing for isoenergetic electron transfer into the conduction band.

4.1.5 Electronic Energy in the Electrolyte Bulk

The redox potential of a sufficiently dilute redox couple $A^{n-}/A^{(n+1)-}$ in solution is given by

$$E_{redox} = E^{o}_{redox} - \frac{kT}{e} \ln \frac{[A^{n-}]}{[A^{(n+1)-}]} \qquad (4.8)$$

where E^{o}_{redox} is the standard redox potential of the couple and A^{n-} and $A^{(n+1)-}$ are the oxidized and reduced forms of the couple. The redox potential may be thought of as an energy level that the electron may occupy or vacate. This energy level is not indifferent to the presence of the electron as in the case of the semiconductor or metal but shifts down or up depending on whether the electron is present in it or not. The removal or addition of an electron to the redox level represents a change in ion charge to which the solvent molecules that make up the sheath surrounding the ion respond by reorienting to compensate for the charge. Polarization of the environment surrounding the redox active electronic orbital depends on whether the electron is present or not and hence also the energy of the orbital. The energy shift due to a single electron removal or addition is 2λ where λ is called the reorganization energy.[46] The energy of the oxidizing agent is therefore greater

than that of the reducing agent by 2λ with the redox potential located half way in between.[39] λ may vary between 0.2 and 1 eV for redox couples in solution. It is usually less for adsorbed species since the solvent only interacts with one side of the couple.

A further perturbation of the the redox level is caused by thermal fluctuations of the polarization of the solvent sheath. These fluctuations produce a Gaussian shaped distribution of electronic energy levels centered about the reduction and oxidation potentials as can be seen by the following considerations. Let us assume that the solvent deformations that produce polarization follow parabolic energetics. That is, the energy of the deforming bond increases quadratically with deformation distance from equilibrium. Marcus has shown that the energy of a large population of such deformers also follows these energetics. With this assumption it can be shown that the Gibbs energy ΔG required to increase the electronic energy to a level E from E_r, the energy of the reducing agent, is

$$\Delta G = (E - E_r)^2/4\lambda \qquad (4.9)$$

The equilibrium Boltzmann distribution (P_e) of the thermal energy fluctuations produces a Gaussian distribution in the electronic energy levels. (see Figure 4.4)

$$P_e = \exp(-\Delta G/kT) = \exp[-(E - E_r)^2/4\lambda kT] \qquad (4.10)$$

This energy level distribution is not analogous to a semiconductor band in that it consists of temporal fluctuations of discrete levels whereas electronic energy levels in a semiconductor band exist simultaneously. Figure 4.4 shows the distribution of thermal fluctuations of the solvent cage and the electronic states of the redox

Figure 4.4 (a) Distribution of vibrational states of the solvent sheath. (b) Distribution of electronic states of the redox active electron.

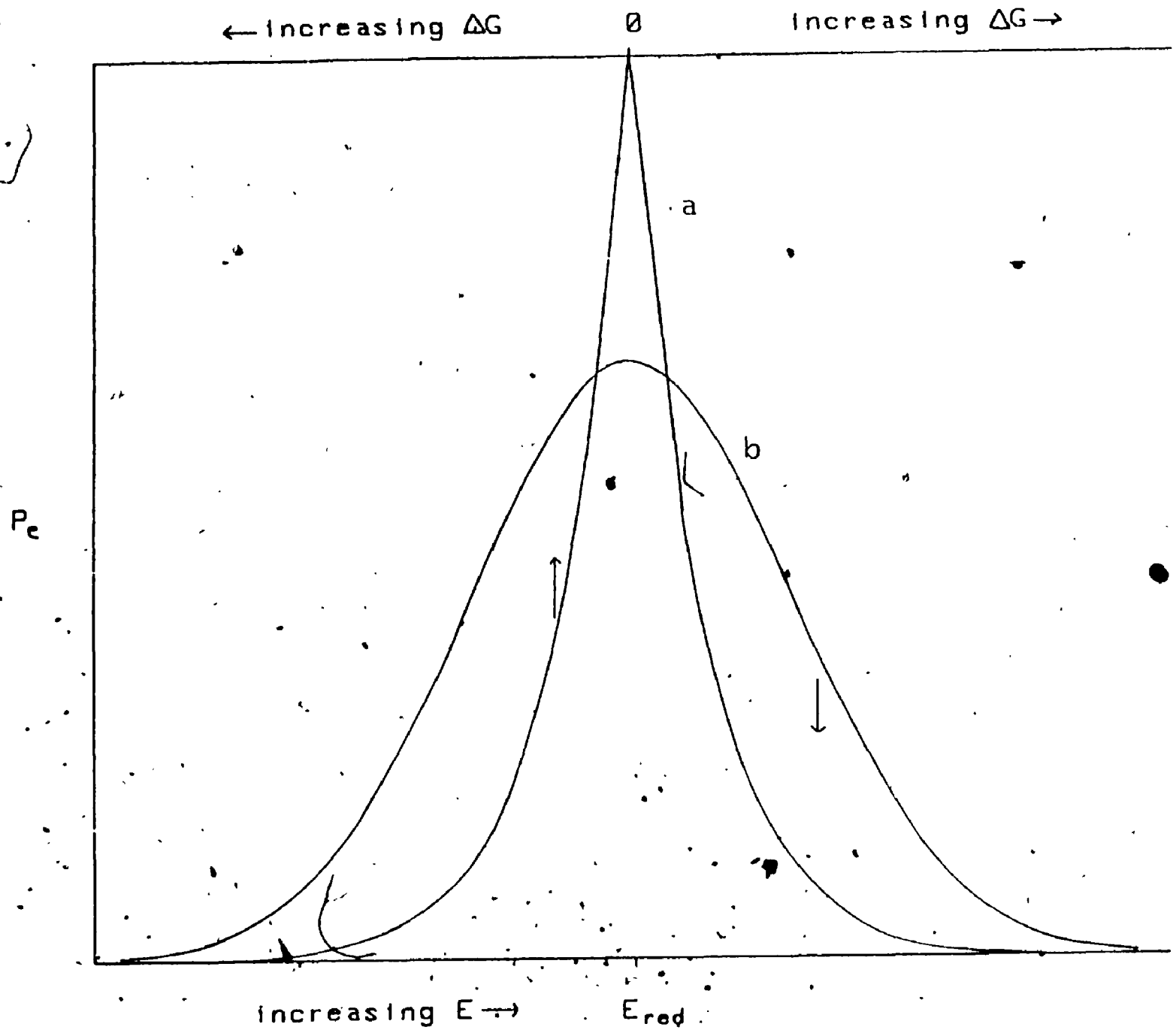
← increasing ΔG
0
increasing ΔG →
a
b
P_c
increasing E →
E_{red}

active electron.

4.1.6 Electronic Energy at the Metal Electrode

The solution side of the electrolyte metal junction will be identical to that for the semiconductor electrolyte junction. Since the metal conductivity is high, any charge that develops in it will be confined to the surface. Therefore any potential drop must be located in the Helmholtz region.

Provided that the semiconductor conductivity is low enough compared with the conductivity of the other phases and junctions, changes in applied potential will be seen entirely across its space-charge layer. The voltage changes across the two space charge regions in the electrolyte would then remain invariant with change in applied potential. This may be accomplished by using electrolyte solutions of sufficient concentration.

4.2 Capacitance of the Cell

One electrical characteristic of any electrochemical cell is its capacitance defined as[40]

$$C = \partial Q / \partial V \qquad (4.11)$$

where Q is the charge that develops on either of the two metal leads connected to the cell when the potential difference between them is V. This capacitance is actually the reciprocal sum of all the individual capacitances of phases and boundaries containing a potential drop. In our electrochemical cell the capacitance associated with bulk phases can be neglected, since the potential drop through these regions is small compared to the boundaries. Since the junctions are successive with respect to electron flow their reciprocal capacitances add in series.

$$1/C_T = 1/C_1 + 1/C_2 + \ldots \qquad (4.12)$$

Clearly if one of the capacitances is much smaller than the rest its will dominate the sum and

$$1/C_T \sim 1/C_{smallest} \qquad (4.13)$$

To develop an expectation for how the total capacitance of the cell should behave we must consider each junction separately and add up their capacitances. Our aim is to adjust the parameters of the cell in such a way as to simplify the final expression for the total capacitance as much as possible. We begin at the left side of the cell.

The first boundary encountered is the metal semiconductor boundary. This boundary will exhibit negligible reciprocal capacitance if the metal is chosen such that the contact is ohmic, since there will be little voltage drop across this boundary.

The next junction encountered is that between the semiconductor and the electrolyte. This includes the semiconductor space charge layer, the Helmholtz layer and the Gouy layer. The Gouy layer can be eliminated by using electrolyte solutions of sufficient concentration such that the voltage drop is restricted to the Helmholtz and space charge layers. The boundary capacitance can be further simplified if it can be assumed that the Helmholtz reciprocal capacitance is small either because of the thinness of the layer or because the potential drop across the region is invariant with change in the applied potential. The capacitance of this layer may be estimated by comparing it to a parallel plate capacitor the capacitance of which is given by

$$C = A\epsilon\epsilon_0/d \qquad (4.14)$$

where A is the area of the plate, d is the distance between the plates, ϵ is the dielectric constant of the insulating medium and ϵ_o is the permittivity of free space. For a Helmholtz region 3 Å thick assuming a dielectric constant of 5

$$C/A = 5(8.85\times10^{12}\ Fm^{-1})/3\times10^{-10}\ m \qquad (4.15)$$

$$\simeq 10^{-5}\ F/cm^2$$

In many cases the space charge capacitance is much less than this. Then the total capacitance of the interface is simply that of the space charge in the semiconductor.

The space charge capacitance for an n-type semiconductor may be determined by again solving the Poisson equation for that region.

$$\frac{d\phi^2}{dx^2} = \frac{-\rho}{\epsilon\epsilon_o} \qquad (4.16)$$

For an n-doped semiconductor where the applied potential is adjusted so that the space charge is depleted creating N_{sc} positive charges

$$d^2\phi_x/dx^2 = -(N_{sc}q/\epsilon\epsilon_o)[\exp(-q\phi_x/kT) - 1] \qquad (4.17)$$

Here the density of holes is small compared to the density of electrons and is therefore neglected. Integrating and applying Gauss's law

$$C_{sc} = (q\epsilon\epsilon_o N_{sc}A^2/2)^{1/2}(V - V_{fb} - kT/q)^{-1/2} \qquad (4.18)$$

$$1/C_{sc}^2 = (2/q\epsilon\epsilon_o N_{sc}A^2)(V - V_{fb} - kT/q) \qquad (4.19)$$

where we have set $\phi_{x=0}$ equal to V_{fb}, the applied potential at which the space charge potential is zero, and equated ϕ with the applied potential V taking into account that ϕ is measured with respect to the

semiconductor bulk and V with respect to a reference electrode. A is the area of the electrode and is generally eliminated from the equation so that capacitance is measured per area of electrode in contact with electrolyte. The final equation, equation 4.19, called the Mott-Schottky relation predicts that the inverse square of the capacitance should vary linearly with the applied voltage in the depletion region.

The final junction is that between the electrolyte and the counter electrode. Since this electrode is a metal the total voltage drop is across the Helmholtz layer. Its capacitance may sometimes be discounted for the same reason as above. Also if the counter electrode area is made large compared to that of the semiconductor electrode its reciprocal capacitance will be negligibly small.

The above considerations suggest that in some cases the cell may be designed so that the total capacitance is simply that of the semiconductor space charge. For these cases the intercept of a Mott-Schottky plot of the cell capacitance determines the flatband potential and the slope determines the donor density of the semiconductor.

4.3 pH dependence of the Flatband Potential

Many semiconductor surfaces contain acidic or basic groups and maintain equilibria with the electrolyte of the type shown[41]

$$S + H^+ \rightleftharpoons SH^+ \qquad (4.20)$$

$$SO^- + H^+ \rightleftharpoons SOH \qquad (4.21)$$

where SOH, SO^-, SH^+, and S, are the protonated and deprotonated surface acidic and basic groups respectively. Taking the activity of these to be unity the Nernst equations for these equilibria are

$$E_i = E_i^{\circ} + (2.303RT/F)\log[H^+] \qquad (4.22)$$

$$= E_i^{\circ} - 0.059pH \qquad (4.23)$$

If there is no other adsorption of charged ions the Helmholtz potential depends on these equilibria and the orientation of molecular dipoles at the surface. There will be a certain pH at which the surface charge will be canceled by the acidic and basic groups. This point is called the point of zero charge (PZC). Therefore the Helmholtz potential is only due to oriented dipoles at the PZC and will have a potential drop of no more than 20 mV.

For systems bearing surface acidic and basic groups the flatband potential has been shown experimentally to follow the same pH relation as 4.23[42]

$$E_{fb} = E^{\circ}_{fb} - 0.059pH \qquad (4.24)$$

where E_{fb} is the flatband potential measured with respect to a reference electrode. Neglecting the potential due to oriented dipoles the Helmholtz potential at a certain electrolyte pH is the difference between the flatband potential at that pH and at the PZC. The intercept of a Mott-Schottky plot increases roughly 60 mV per pH unit for these systems. Since the slope of the plot depends only on the semiconductor composition the plot should consist of parallel lines for solutions that differ only in their pH.

4.4 Theories of Current Production

A number of different theories for current production at metal and semiconductor electrodes have been developed. The two most widely used theories were developed by Marcus[43] for metal electrodes and by Gerischer[44] for more general use. The theories turn out to be similar and yield equivalent results.

4.4.1 Dark Current

The expression for dark current that Marcus developed for electron injection from a one-equivalent redox couple into a metal electrode is

$$J = FZc_r\exp(-\Delta G^*/kT) \tag{4.25}$$

where F is Faraday's constant, Z is a transmission factor which takes into account tunneling probability, c_r is the surface concentration of the reducing agent, and ΔG^* is the Gibbs free energy of activation required to inject the electron. Since electron injection is isoenergetic and faster than molecular movement the reducing agent and its surrounding solvent sheath must reorient to the point at which the orbital containing the electron is at the same energy as the lowest unoccupied orbital of the metal which is located just above the Fermi level U_f. By the fluctuating energy model introduced earlier, the Gibbs energy required to accomplish this is

$$\Delta G^* = (U_f - E_r)^2/4\lambda \tag{4.26}$$

At equilibrium the Fermi energy must equal the redox potential. Since we are dealing with a metal electrode, any applied overpotential η causing a departure from equilibrium appears across the Helmholtz layer which separates the metal surface from the reducing agent. Therefore

$$U_f - E_r = E_{redox} - E_r - \eta q \tag{4.27}$$

Substitution of equation 4.27 and 4.26 into equation 4.25 leads to an expression for the anodic current in terms of the overpotential. An equivalent expression for cathodic current can be derived. If these two are added, the total current is

$$J = J_o[\exp(\tfrac{1}{2}\eta q/kT) - \exp(-\tfrac{1}{2}\eta q/kT)] \tag{4.28}$$

This is the Tafel equation which has been proven experimentally for many systems. An assumption leading to this expression is that the reorganization energy λ is much larger than the overpotential. If this is not true a curved Tafel plot ($\ln J$ vs. η) is expected even at large η. This has been seen for redox couples such as the ferro, ferricyanide couple.[45] A second assumption is that all the significant electron transfer takes place into the lowest unoccupied molecular orbital of the metal or oxidizing agent.

The Gerischer model considers isoenergetic electron transfer at all energy levels in the formulation of a general expression for electron injection and then later assumes a narrow electron transfer region. His expression for electron injection into the conduction band of a semiconductor is

$$J_a = Fc\int_{-\infty}^{\infty} k(E)N_{un}(U)\overline{D_{red}}(E)dE \qquad (4.29)$$

where c is the concentration of donors, k(E) is a transmission coefficient, $N_{un}(U)$ is the density of unoccupied states in the electrode at energy U, and $D_{red}(E)$ is the density of donor states at energy E. In a non-degenerate semiconductor N_{un} would be N_c', the density of states in the conduction band assuming that very few are occupied. In a degenerately doped semiconductor this may not be so. This case will be discussed separately. By substitution of equation 4.10 for $D_{red}(E)$ the expression becomes

$$J_a = Fc/(\pi kT\lambda)^{\frac{1}{2}}\int_{U_{cs}}^{\infty} k(E)N_c'\exp[-(E - E_{redox}-\lambda)^2/4kT\lambda]dE \qquad (4.30)$$

where $E_r = E_{redox} + \lambda$. Here constants have been included before the integral to normalize the distribution. The integral begins at U_{cs}, the conduction band edge at the surface, since $N_{un} = 0$ in the band gap. This integral cannot be solved analytically and the assumption is therefore made that most of the electron transfer takes place within 1 kT of the bottom of the conduction band due to the small overlap between the donor distribution and the band. The distribution is taken to be constant over this range. The expression then becomes

$$J_a = Fc/(\pi kT\lambda)^{1/2}\int_{U_{cs}}^{U_{cs}+kT} k(U_{cs})N_c \exp[-(U_{cs} - E_{redox} - \lambda)^2/4kT\lambda]dE \qquad (4.31)$$

$$= Fc(kT/\pi\lambda)^{1/2}k(U_{cs})N_c\exp[-(U_{cs} - E_{redox} - \lambda)^2/4kT\lambda] \qquad (4.32)$$

The equivalent expression for cathodic current due to electron donation from the conduction band to an oxidizing agent is

$$J_c = Fc(kT/\pi\lambda)^{1/2}k(U_{cs})n_s\exp[-(U_{cs} - E_{redox} + \lambda)^2/4kT\lambda] \qquad (4.33)$$

where n_s is the density of electrons at the surface and depends on the surface potential

$$n_s = n_o\exp[-q(U_{cs} - U_{cb})/kT] \qquad (4.34)$$

where U_{cb} is the conduction band edge in the bulk. n_o is the electron density in the bulk.

Equivalent expressions for the valence band processes can be obtained. For an n-type semiconductor the current due to these processes will be small because of the low minority carrier density p_o and the low overlap between the D and the valence band. The current will then be due

to conduction band processes and is given by

$$J_T = J_c - J_a \tag{4.35}$$

$$= Fc(kT/\pi\lambda)^{1/2}k(U_{cs})n_s\exp[-(U_{cs} - E_{redox} + \lambda)^2/4kT\lambda] -$$

$$Fc(kT/\pi\lambda)^{1/2}k(U_{cs})N_c\exp[-(U_{cs} - E_{redox} - \lambda)^2/4kT\lambda]$$

Since, for a semiconductor, shifts in the applied potential are seen in the space charge layer and not at the surface, $U_{cs} - E_{red}$ will remain constant. The only potential-dependent term in the above expression is n_s. Substituting equation 4.34 for n_s and equation 4.1 for n_o we obtain

$$J_T = J_1\exp(-qV_s/kT) - J_2 \tag{4.36}$$

where we have set V_s equal to $(U_{cs} - U_{cb})/q$. This is similar to the Shockley equation usually used to describe the current-voltage dependence at a Schottky barrier. It differs from the Shockley equation in that since the cathodic and anodic electron transfer processes are not the same, J_2 is not identical to J_1. It is also found experimentally that currents due to flaws are much larger than the equilibrium exchange current predicted by the Shockley equation. These are generally added to J_2 producing a useful semi-empirical equation.

Many of the experiments cited in the following sections utilized degenerately n-doped semiconductor electrodes. For these cases a number of new factors are present. Firstly, Boltzmann statistics no longer hold since the Fermi level is often located within the conduction band. This has two effects on the current. The size of n_s can no longer be predicted exactly by equations 4.1 and 4.34, and $N_{un} \neq N_c$, since a sizable number of conduction band states are now occupied. The departure of n_o behavior from that of equation 4.1 is not great for the degenerate

case and since N_c' is still expected to be much greater than n_o the overall conditions are close to that of the non-degenerate case. These effects may contribute to a modest change in shape of the current-voltage plot.

A more important effect arises from the thinness of the space charge layer.[46] For doping levels of 10^{20} cm^{-3} and V_s = 1 V the space charge is approximately 30 Å thick. This is thin enough to permit tunneling through the space charge barrier. In this case total rectification is not seen. The voltage dependence turns out to be exponential in the blocking region through the transmission coefficient k(E)

$$J \sim k(E) \sim \exp[(-E_a^{\circ} - \beta F\eta)/2.3RT]\exp(-x/x_o) \qquad (4.37)$$

where β is the transfer coefficient, η is the overpotential, x is the thickness of the blocking region and E_a° and x_o are constants. This equation, developed by Schultze and Vetter for thin oxide films, relates tunneling current to overvoltage and barrier thickness.[47] It can be seen then that sufficiently thin barriers behave like metal electrodes showing little rectification.

4.4.2 Photocurrent

The expression for photocurrent is similar to that for dark current given by equation 4.31 except that E_{redox} is changed to E^*_{redox}. The expression for anodic current J_{la} due to conduction band processes is

$$J_{la} = Fzc/(\pi\lambda kT)^{1/2}\int_{U_{cs}}^{\infty} k(E)N_c \exp[-(E - E^*_{redox} - \lambda)^2/4kT\lambda] \qquad (4.38)$$

The approximation made earlier that the overlap between D and the conduction band is small can no longer be made and therefore quantitative predictions of the size of the photocurrent cannot be made. However it does predict that the photocurrent should be potential independent since the overlap between N_c and D is. Cathodic photocurrent will be negligible if the dye is chosen such that only the excited state electron energy overlaps with the conduction band.

4.5 Literature Review

The following literature review is divided into two sections. The first section deals with recent studies of dye sensitization systems that have been of particular value in elucidating the mechanism. The second section includes porphyrin and chlorophyll sensitization systems only. This review is not exhaustive and the reader is referred to more complete reviews by Honda[48] and Memming.[49]

All the results reported in both sections are of cells of the type

Electrode|Dye|Electrolyte|Counter Electrode

4.5.1. Elucidative Dye Sensitization Studies

Honda *et al.* investigated the effect of semiconductor doping on the quantum yield of photocurrent production for the system[50]

Electrode: SnO_2, doping range: 10^{18} - 10^{21} cm^{-3}

Dye: Rose Bengal, Rhodamine B; both adsorbed from electrolyte solution

Electrolyte: $NaClO_4$ as supporting electrolyte, H_2Q as supersensitizer, acetonitrile as solvent

Counter Electrode: Pt

They found that the photocurrent for lightly doped SnO_2 was much more dependent on H_2Q concentration than for highly doped SnO_2. They also

found that a photocurrent quantum yield vs. doping density plot rose to a maximum at a doping level of 4×10^{20} cm^{-3}. The maximum photocurrent quantum yield for Rose Bengal was approximately unity at a doping of 4×10^{20} cm^{-3}. Using these results a quantum yield for energy transfer to the semiconductor of 0.3 was obtained for Rhodamine B and 0 for Rose Bengal. They postulated the following mechanism:

$$D + h\nu \xrightarrow{k_1} D^*$$

$$D^* \xrightarrow{k_2} D$$

$$D^* \xrightarrow{k_3} D^+ + e_{cb}^-$$

$$D^+ + e_{cb}^- \xrightarrow{k_4} D$$

$$D^+ + R \xrightarrow{k_5} D + R^+$$

Doping was thought mainly to effect k_3 and k_4. In the lightly doped case recombination via surface states (k_2) competes effectively with electron removal to the bulk via the space charge electric field (k_3). Since k_2 is larger than k_5 the supersensitizer can't compete in rereduction of the dye. Those electrons that are separated are prevented from recombining with the oxidized dye by the relatively thick surface barrier. In the highly doped case the space charge electric field is much stronger owing to its thinness. The electron is therefore swept away from the surface. It can however recombine with the oxidized dye by tunneling back through the thin surface barrier (k_4). In this case the supersensitizer competes with the tunneling process in reduction of the dye. Therefore the photocurrent quantum yield depends strongly on the concentration of the supersensitizer for this case. At supersensitizer

concentrations higher than 10^{-2} M the quantum yield decreases. This was thought to be due to deactivation of the dye excited state by the supersensitizer by direct photoreduction. This would be reasonable if the reduced dye would have a lower electron injection probability.

A second factor controlling the dye sensitization photocurrent quantum yield is the pH of the electrolyte. A number of studies of this dependence have been performed. In general it appears that only systems whose flatband potentials vary with the pH exhibit photocurrent dependence on pH. For example CdS, in which there is no equilibrium between adsorbed and solution protons, exhibits neither flatband potential nor dye sensitization photocurrent quantum yield dependence on pH. Dependent systems generally vary logarithmically with the pH with some exceptions.[49,51,52]

Watanabe *et al.* have developed a theoretical expression for the pH dependence.[53] They reasoned that the electric field at the location of the dye would depend on the Helmholtz potential drop ($\Delta\phi$). They therefore postulated an ordinary electrochemical rate equation for photoelectron injection i_{inj}.

$$i_{inj} \propto \exp\left[\frac{\alpha F \eta}{RT}\right] \tag{4.39}$$

where $$\eta = \text{const.} + \Delta\phi \tag{4.40}$$

and α is the transfer coefficient

Since $\Delta\phi$ is dependent on pH

$$\Delta\phi = \text{const.} - \frac{2.3RT}{F}\text{pH} \tag{4.41}$$

then $$\log i_{inj} = \text{const.}' - \alpha\text{pH} \tag{4.42}$$

This predicts the observed exponential dependence on pH. Using this method the authors obtained transfer coefficient values of 0.26-0.40 for sensitized TiO_2 and ZnO electrodes.

Frippiat *et al.* performed time resolved laser flash induced photovoltage measurements on the following system.:[54]

Electrode: highly n-doped SnO_2

Dye: Rhodamine B adsorbed from electrolyte solution

Electrolyte: H_2Q and $LiNO_3$, N_2 bubbled, acetate buffer in aqueous solution

For 10^{-2} M H_2Q concentrations they noticed that the photovoltage response could be divided into three parts. For sufficiently anodic prepolarizations the initial fast voltage rise, due to direct electron injection into the conduction band, was followed by a slower charging which they attributed to capture of the electron by surface states followed by electron tunneling into the conduction band. At low prepolarization this slow charging competed with discharging via back tunneling. Dependence of this slow charging on H_2Q concentration indicated that the reduced surface state was competing with the H_2Q in reduction of the oxidized dye. Thus two possible electron injection routes were postulated for this system, one via surface states and another via direct injection. The extent to which the slow charging contributed to the total photovoltage rise varied depending on which spot on the surface of the electrode was illuminated indicating that the density of surface states was nonuniform across the surface. This inhomogeneity could be eliminated by prepolarization of the electrode at +200 mV. After such a prepolarization the slow response at different illuminated spots was uniform and large. This was attributed to O_2 chemisorption under anodic bias leading to the production of a uniformly

large number of surface states.

Fromhertz & Arden reported sequential energy and electron transfer in a bilayer system.[55] A docosylamine bilayer was deposited on Indium-Tin Oxide by depositing two monolayers using the LB technique. Coumarin dye was incorporated into the outer monolayer and cyanine into the inner. The cyanine dye absorption profile overlap with the fluorescence profile of the coumarin could be controlled through the pH dependence of the position of the fluorescence profile of the coumarin. Therefore a device was realized whose photocurrent was dependent on pH. In order to see the dependence strictly due to the coumarin acid equilibrium, the variation in photocurrent with Helmholtz potential had to be removed. To accomplish this the photocurrent was measured for each pH at a potential such that the conduction band bending remained constant. Under these conditions a titration curve for the photocurrent was seen whose pK_a matched that of the coumarin dye. The same system excluding the dye showed no such behavior. Furthermore the action spectrum of the photocurrent matched the coumarin dye absorption spectrum.

In an earlier study Fromhertz & Arden reported the photocurrent due to sensitization by cyanine alone embedded in a docosylamine bilayer.[56] Capacitance studies on the system indicated that the bilayer was neither fully insulating nor entirely porous but rather contained holes. These holes, defined as areas of the electrode that were in direct contact with the electrolyte, were thought to exist due to surface roughness of the electrode.

Thiourea was found to be a supersensitizer for the dye. By simultaneous measurement of the fluorescence, absorption, and photocurrent Fromhertz & Arden were able to monitor the chemical state of the dye during operation. Since there was neither suppression of

bleaching or fluorescence of the dye by the supersensitizer during operation they concluded that the supersensitization effect was neither rereduction of the oxidized dye nor reductive quenching of the excited state. They therefore concluded that the thiourea must be competing with recombination to S_o from an intermediate D^+e^- state composed of a reduced surface state oxidized dye pair. With these assumptions they were able to fit the photocurrent to a Stern-Volmer type expression in thiourea concentration.

4.5.2 Porphyrin and Chlorophyll Studies

Bulkowski *et al.* have reported some photoelectrochemical measurements on the cell:[57]

Electrode: SnO_2 highly n-doped with Sb

Dye: meso-tetra(α,α,α,α-o-aminophenyl)porphyrin deposited with stearic acid as a single mixed monolayer

Electrolyte: aqueous H_2Q, KCl, deaereated with N_2

Counter Electrode: Pt

They reported anodic photocurrent on illumination with visible light which decreased rapidly with time if no reducing agent was present in solution. Addition of H_2Q stabilized the current for a period of hours. By pretreatment of the SnO_2 surface they were able to orient the porphyrin head group toward or away from the surface. Photocurrent increased by a factor of 10 for cells in which the porphyrin head group was oriented away from the surface.

Chandrasekaran *et al.* have reported the photoelectrochemistry of the cell:[58]

Electrode: Low n-doped SnO_2

Dye: hexadecyltetraminophenylporphyrin, one or more monolayers

Electrolyte: aqueous KCl, TEA, DMA, DIPEA, H_2Q, p-dimethoxybenzene

Counter Electrode: Pt foil

They observed no photocurrent without the presence of one of the supersenitizers. This as well as flash photolysis results that indicated the presence of long lived transients for both glass and SnO_2 suggested the following mechanism for current production:

$$D + h\nu \longrightarrow D^*$$

$$D^* + R \longrightarrow D^- + R^+$$

$$D^- \longrightarrow D + e_{cb}^-$$

where D is the dye and R the supersensitizer. In contrast to the usual conclusions regarding this type of system, direct de-excitation of the excited state by the substrate was thought to be less important than photoreduction of the dye by a supersensitizer.

Umezawa *et al.* have reported anodic photocurrents for surface active porphyrins deposited from solution onto Pt by evaporation.[59] These measurements proved to be irreproducible due to loss of the dye from the surface.

Breddells *et al.* studied a series of metallated porphyrins deposited on to SnO_2 by solution evaporation.[60] They reported anodic photocurrent that was dependent on the film thickness rising to a maximum at a thickness of 50 Å and then remaining constant. The photocurrent increased with increasing hydroquinone concentration until 10^{-2} M. No correlation was found between the quantum yield of photocurrent and the redox potentials of the different metallated porphyrins. They rationalized this by the observation that ionization potentials of the solid dyes were relatively insensitive to the type of metal atom present. A better correlation between the differing

competitive luminescence rates for each porphyrin and the quantum yield for charge injection was found.

Minami *et al.* studied the photoelectrochemistry of metallated monomeric, dimeric and trimeric porphyrins attached together by ester linkages in dimethylformamide solutions at SnO_2 electrodes.[61] Together with the usual H_2Q dependence a small variation in the photocurrent with aggregate type was seen but left unexplained. A fairly good correlation between the intersystem crossing yield and photocurrent suggested to them that the charge injection took place from the triplet state.

Matsumura *et al.* reported anodic photocurrents for ZnO and TiO_2 sensitized by xanthene and by a series of metalated porphyrin dyes in aqueous solution.[62] Xanthene dye exhibited photocurrent quantum yields of ~28% whereas porphyrins gave only about 0.1 to 2.3%. Fluorescence of the xanthene dyes was totally quenched whereas the porphyrins exhibited some fluorescence. Correlation was found between the excited state redox potential of the porphyrin and the photocurrent quantum yield. By these results the authors concluded that a higher barrier to electron injection existed for the porphyrin than for the xanthene dyes causing deactivation by fluorescence to compete with electron injection. This also explained the redox potential dependence. If the barrier for electron injection from xanthene was sufficiently low, its excited state would overlap completely with the conduction band. The higher barrier in the porphyrin case would mean that overlap would be partial and dependent on the redox potential of the individual porphyrin.

Miyasaka *et al.* measured anodic photocurrent for chlorophyll *a* and *b* LB films on highly doped SnO_2 in aqueous solution.[63] They reported the usual H_2Q dependence, a linear response with light level, a shift in the maximum photocurrent position of 60 mV/pH point and a hump-shaped

dependence of the size of the maximum photocurrent with pH centered at pH = 4. The photocurrent quantum yield was also found to increase with dilution of the chlorophyll in stearic acid with a peak quantum of yield of 16% at a dilution of 50%. This was attributed to the separation of dye molecules from one another reducing self quenching.

4.5.3 Summary of the Literature Findings

Three findings stand out:

1. Authors generally cited the effect of surface states and competitive deactivation routes.

2. Recombination or forward electron transfer via space charge tunneling was important for highly doped semiconductors.

3. The supersensitizer competes with back electron transfer in reduction of the oxidized dye.

4.6 Experimental Results

We shall discuss our results in relation to the energy level diagram shown in Figure 4.5. A photon absorbed by TTPa in its ground state (S_0) on the SnO_2 surface creates the excited singlet state S_1 of TTPa. S_1 then undergoes oxidation via one of three processes as shown in Fig. 4.5. The O_2/O_2^- acceptor level has been placed at +0.5 V vs. SHE as quoted for TiO_2.[64] The TU/TU^+ redox level of thiourea (TU) used as a supersensitizer has been estimated to be somewhat higher than the onset of dark anodic photocurrent since its value is not present in the literature. The oxidation potential of the TTPa monolayer is taken to be +1.2 V vs. SHE as quoted for free base tetraphenylporphine in DMSO.[65]

4.6.1 Deposition

The monolayer deposited as a Z layer on the SnO_2 substrate with an

Figure 4.5 An energy level diagram for the semiconductor-monolayer-electrolyte interface. Arrows indicate possible directions of electron travel. Energy levels are placed with respect to the standard hydrogen electrode.

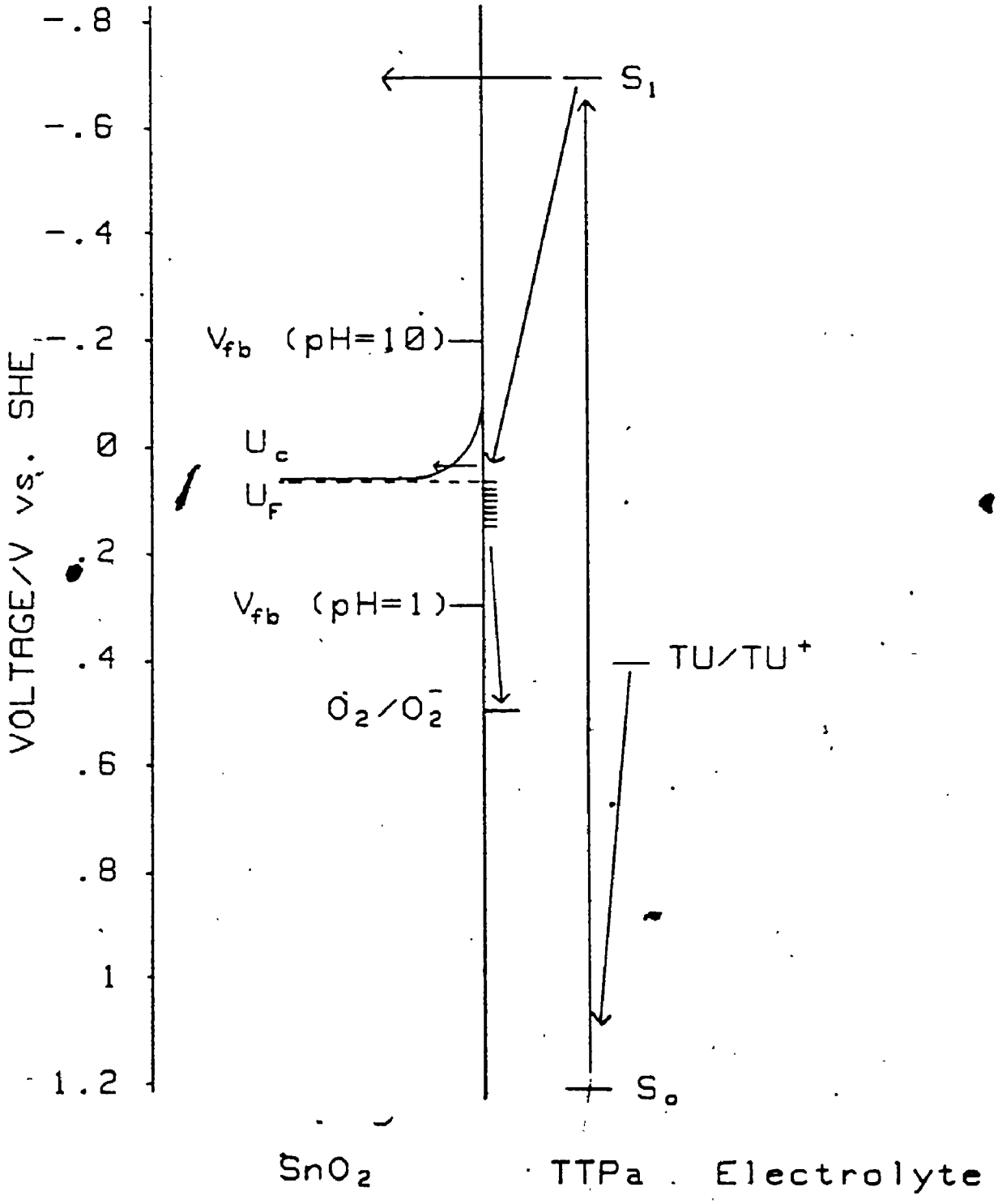
-.8
-.6
-.4
-.2
0
.2
.4
.6
.8
1
1.2
VOLTAGE/V vs. SHE
S1
Vfb (pH=10)
Uc
UF
Vfb (pH=1)
O2/O2-
TU/TU+
So
SnO2
TTPa
Electrolyte

average deposition ratio of 1.2 ± 0.1. The fact that the deposition ratio is greater than unity is probably due to surface roughness which would increase the actual surface area. It was difficult to obtain absorption spectra of these films due to interference patterns arising from the thinness of the SnO_2 layer. Instead photo-action spectra were utilized to determine the condition of the monolayer.

10:1 mixed monolayers with PC were also deposited onto the SnO_2 slides. The same deposition ratio as above was found in this case.

4.6.2 Photo-action Spectrum

The solid line in Figure 4.6 is the photovoltage action spectrum of the photoelectrochemical cell. While small changes were seen in the spectrum from sample to sample neither pH nor electrolyte composition were found to affect the action spectrum of any given sample. Thus the nature of the electrolyte does not appear to effect the porphyrin ring although deprotonation of the carboxylic acid cannot be excluded. It was shown in the first section of the thesis that this equilibrium affected the packing of the porphyrin monolayer at the air-water interface and that this in turn caused variations in the absorption spectra.[21] However, this effect might not be seen in the action spectrum since the low mobility of the molecules on the solid substrate would inhibit repacking.

The action spectrum is compared to two absorption spectra in Figure 4.6. The dashed line spectrum is taken from Figure 3.6 and is that of a porphyrin LB film deposited from unbuffered water onto a quartz slide. The Soret band is split into two peaks by the packing effect mentioned above. Two distinct packing arrangements exist in this film as discussed in the first section. The dotted line also taken from Figure 3.6 is the absorption spectrum of a mixed 1:1 DOPC/TTPa LB film

Figure 4.6 Comparison of the cell photo-action spectrum with absorption spectra. Action spectrum (——), absorption spectrum of a pure TTPa LB film deposited on quartz (- - -), absorption spectrum of a 1:1 DOPC/TTPa mixed LB film (···). subphase unbuffered water at = 20 ± 2°C

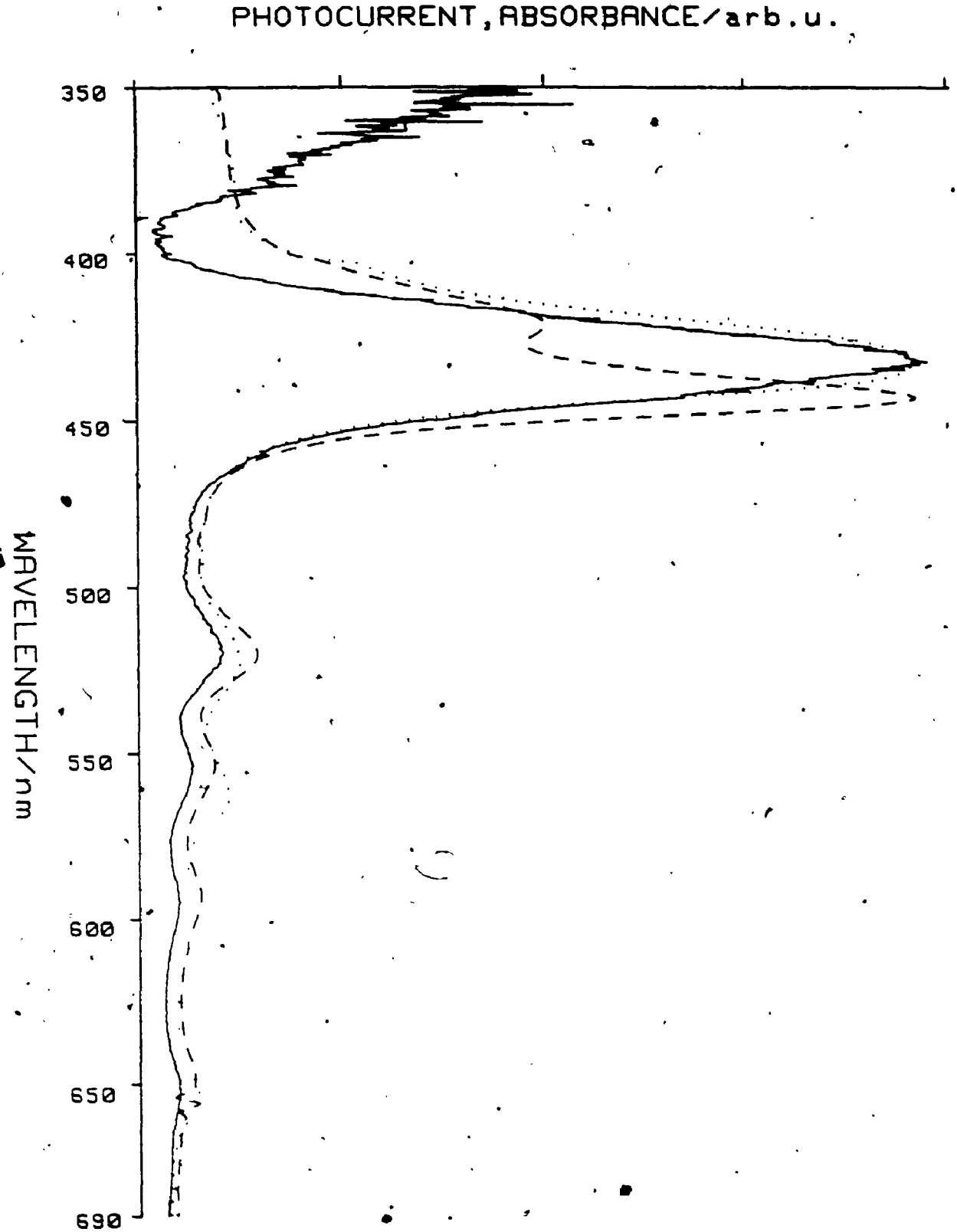
PHOTOCURRENT, ABSORBANCE/arb.u.
350
400
450
500
550
600
650
690
WAVELENGTH/nm

on quartz in which TTPa molecules are only partially blocked from one another by interposed DOPC molecules. In this case a range of interactions may be supposed to exist causing the Soret band to represent an envelope of lines each shifted slightly from the other. The action spectrum seems to contain such a distribution rather than two distinct subpopulations. It is therefore proposed that this is caused by substrate surface roughness. Valleys in the substrate would cause the oriented chromophores to interact closely while peaks would pull them apart. Surface roughness is confirmed by SEM although not of the scale required to explain the observed effect fully.

4.6.3 Current-voltage curves

A series of current-voltage plots are shown in Figure 4.7 for a cell containing only supporting electrolyte. Bubbling of oxygen through the electrolyte increases both the dark and light response of the cell in the cathodic direction. Bubbling with nitrogen reduces both the dark and light cathodic response.

Addition of thiourea introduces dark anodic current and a very small anodic photocurrent. On addition of both thiourea and Na_2SO_3, added to scavenge adsorbed oxygen from the electrode surface, a substantial anodic photocurrent is seen (see Figure 4.8). Addition of only Na_2SO_3 with the supporting electrolyte produces an anodic response at anodic bias for some samples. Those samples not producing an anodic response upon addition of Na_2SO_3 also did not do so on addition of TU with Na_2SO_3.

4.6.4 Dependence of the Photocurrent on pH

Figure 4.9 shows current-voltage plots at high and low pH for the cell with and without Na_2SO_3 and TU. A reduction in the pH enhances both

Figure 4.7 Current-voltage plots for the cell under conditions of oxygen and nitrogen bubbling. Horizontal axis is applied cell voltage. Vertical axis is cell current. L_2 and D_2 are light and dark responses respectively for nitrogen bubbling conditions. L_1 and D_1 are light and dark responses for no bubbling. L_3 and D_3 are light and dark responses respectively for oxygen bubbling. Electrolyte composition: 0.5M NaCl

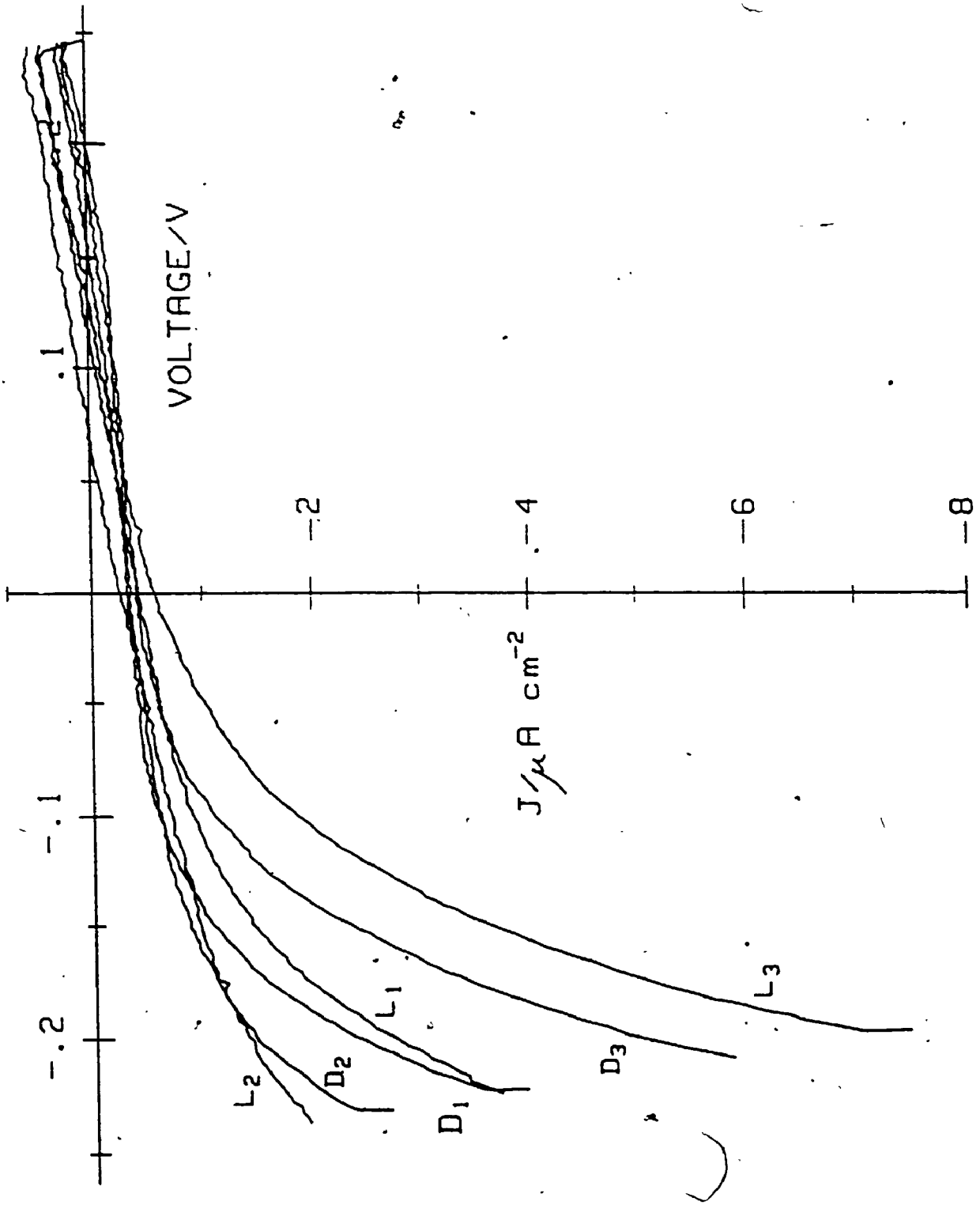
VOLTAGE/V
.1
-.1
-.2
-2
-4
-6
-8
J/μA cm⁻²
L2
D2
L1
D1
D3
L3

Figure 4.8 Current voltage plots for two electrolyte compositions. L_1 and D_1 are the light and dark responses respectively for electrolyte composition: 0.25 M KH_2PO_4, 0.5 M NaCl, 1 M TU, 0.1 M Na_2SO_3. L_2 and D_2 are the light and dark responses respectively for electrolyte composition: 0.25 M KH_2PO_4, 0.5 M NaCl. The pH of both electrolytes is 1.5.

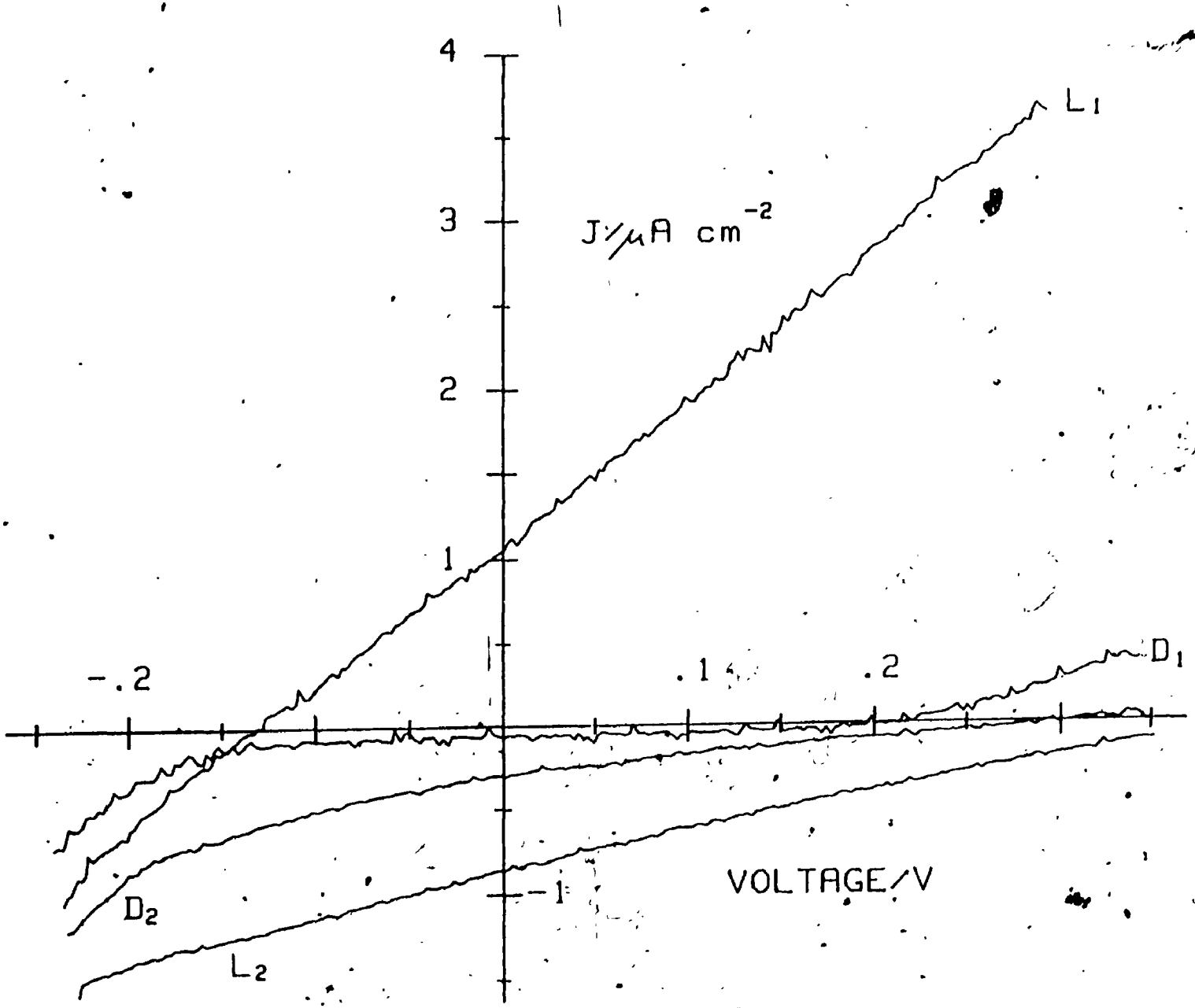
4
3
2
1
-1
-.2
.1
.2
J/μA cm⁻²
VOLTAGE/V
L1
D1
D2
L2

Figure 4.9 Current-voltage plots under high and low pH conditions. Electrolyte composition: 0.25 M KH_2PO_4, 0.5 M NaCl, 1 M TU, 0.1 M Na_2SO_3. L_2 and D_2 are the light and dark responses respectively at pH = 8.2. L_1 and D_1 are the light and dark responses at pH = 2.1

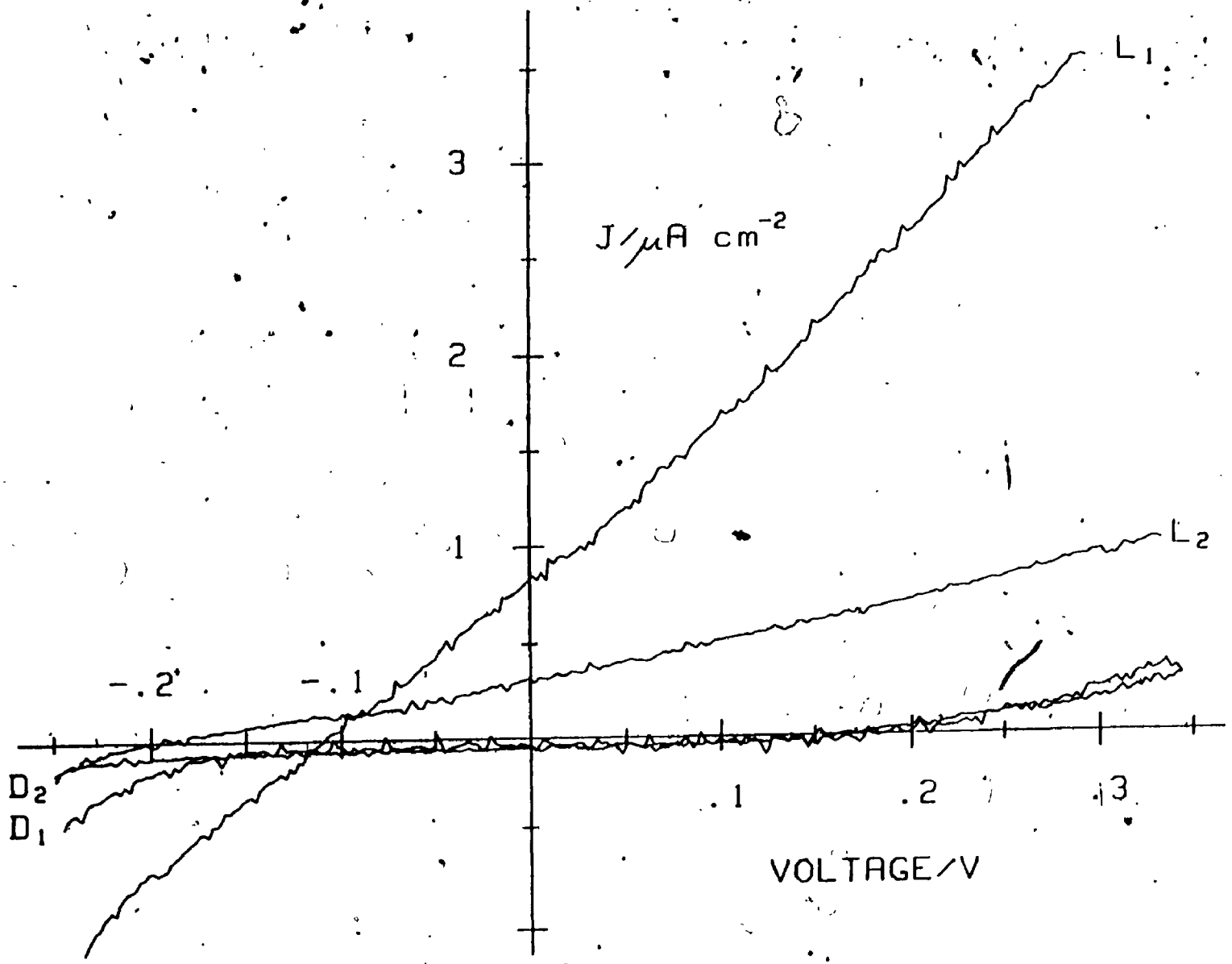
L1
L2
3
2
1
J/μA cm⁻²
-.2
-.1
.1
.2
.3
D2
D1
VOLTAGE/V

the anodic and cathodic photocurrent. The rather complicated pH dependence of the anodic case can be explained in terms of conflicting anodic and cathodic currents. Figure 4.10 compares the pH dependence of the light response for addition of only supporting electrolyte, addition of Na_2SO_3, and then addition of TU. The Na_2SO_3 case can be seen to be the addition of a pH independent anodic current plus a pH dependent cathodic current. Addition of TU adds a third pH dependent anodic current so that the light response with all four components in solution is the superposition of at least three currents. Very similar pH dependence is seen for the anodic photocurrent produced by replacing Na_2SO_3 with N_2 bubbling (see Figure 4.11).

4.6.5 Mott-Schottky Plots

A series of Mott-Schottky plots is shown in Figure 4.12. Plots taken on blank electrodes indicate a slightly lower reciprocal capacitance than those bearing a LB film. This may be due to a blockage of the surface by the film. However, the in-phase impedance of 52 ± 8 Ω impedance was the same for both types of electrode showing no trend to higher impedance for samples bearing an LB film. The donor density of the SnO_2 is 10^{20} cm^{-3} as determined by the slope of the plots. The flatband potential at pH = 7.0 is 0 ± 0.1 V vs. SHE and varies by 54 mV/pH as shown in Figure 4.13. These flat band potentials were obtained from the Mott-Schottky plots by a linear least squares extrapolation from the data points closest to zero reciprocal capacitance. Flatband potentials for the blank slide and the one bearing a film were the same.

It is expected that a single monolayer should not affect the impedance appreciably. Spaces in the packing of the chromophores would be sufficiently large to allow electrolyte to pass through the film.

Figure 4.10 Plots of light response vs. pH under various electrolyte conditions. (a) 0.25 M KH_2PO_4, 0.5 M NaCl, 1 M TU, 0.1 M Na_2SO_3, electrode potential: +0.25 V w.r.t. Ag/AgCl (b) 0.25 M KH_2PO_4, 0.5 M NaCl, 0.1 M Na_2SO_3, electrode potential: +0.25 V w.r.t. Ag/AgCl (c) 0.25 M KH_2PO_4, 0.5 M NaCl, electrode potential: -0.25 V w.r.t. Ag/AgCl

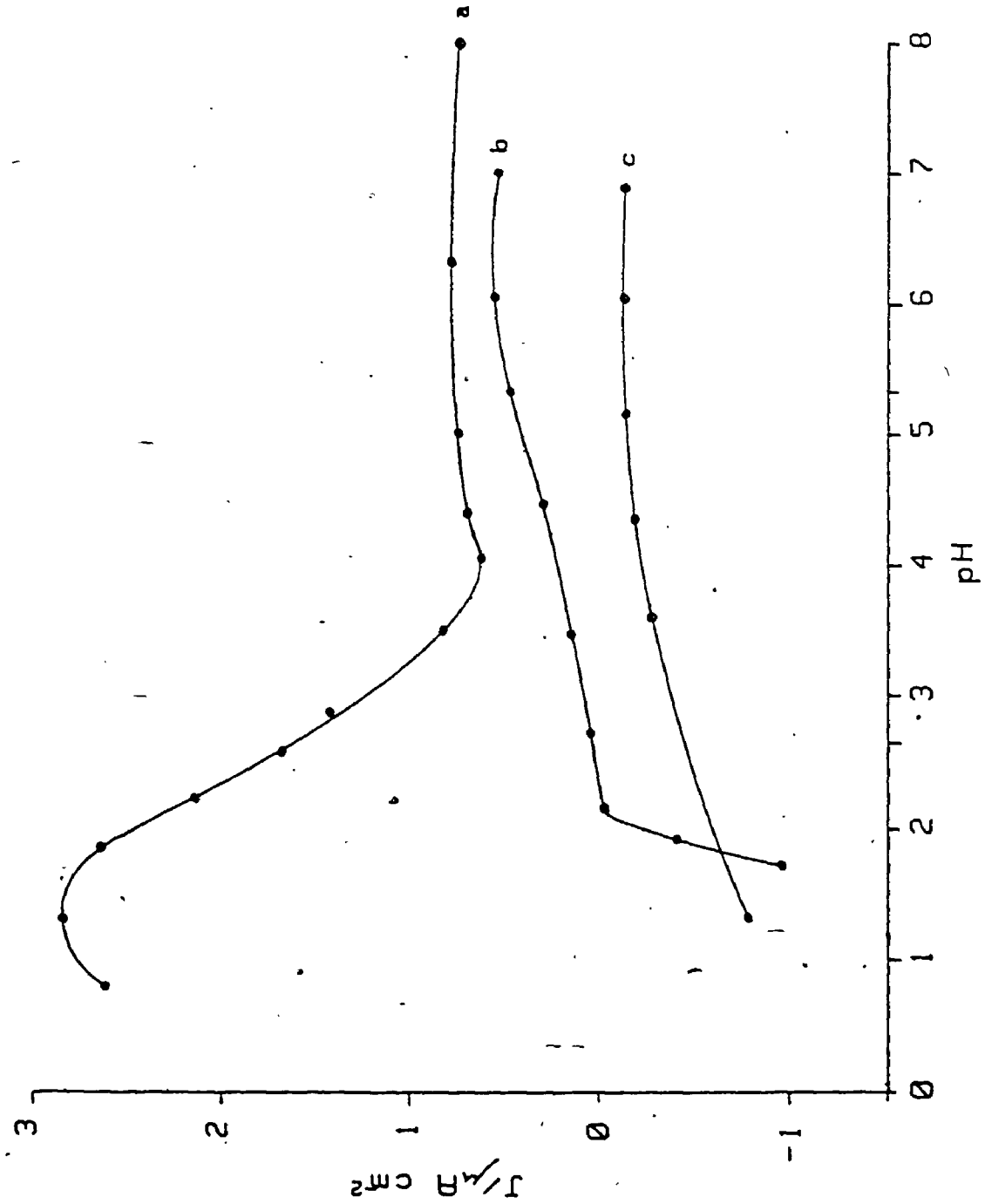
a
b
c
3
2
1
0
-1
0
1
2
3
4
5
6
7
8
pH
J/μA cm²

Figure 4.11 (a) light response as in Fig. 22a. (b) 0.25 M KH_2PO_4, 0.5 M NaCl, 1 M TU, vigorous nitrogen bubble (c) light response for a blank electrode: Current multiplied by a factor of ten. Electrolyte conditions: 0.25 M KH_2PO_4, 0.25 M NaCl, 1 M TU, 0.1 M Na_2SO_3 Electrode potential for all cases: +0.25 V w.r.t. Ag/AgCl

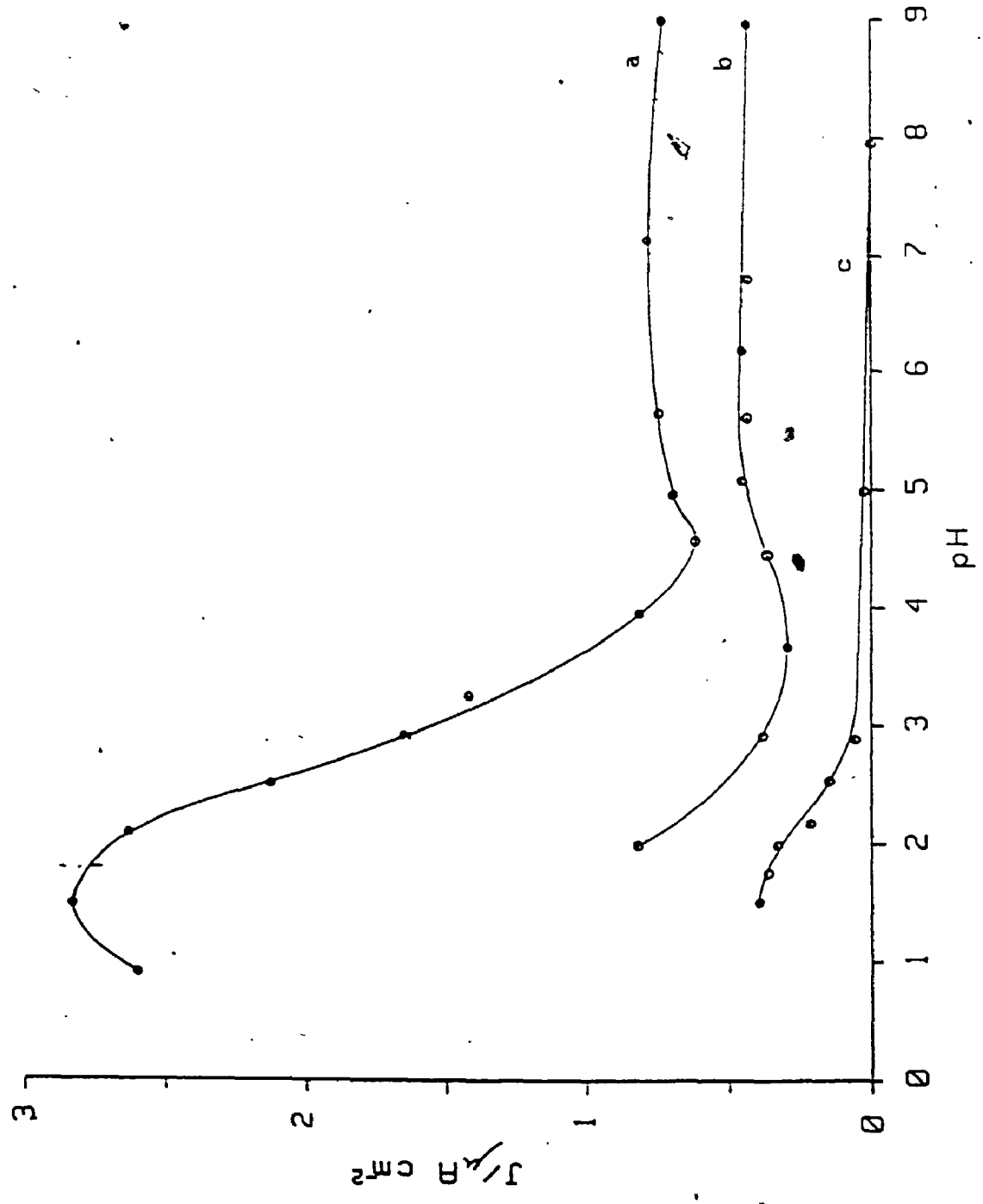
a
b
c
pH
0
1
2
3
4
5
6
7
8
9
1
2
3

Figure 4.12 Mott-Schottky plots under various pH conditions. The vertical axis is the inverse square of the capacitance of the cell. The horizontal axis is applied cell voltage with respect to the Ag/AgCl electrode. Electrolyte composition: 1 M $NaNO_3$, .25 M KH_2PO_4 (a) pH = 9.85, (b) pH = 7.76, (c) pH = 5.16, (d) pH = 4.38, (e) pH = 2.99, (f) pH = 2.17 (g) pH = 9.05, (h) pH = 7.00, (i) pH = 6.20, (j) pH = 2.16. x's are the data points for a blank SnO_2 electrode. O's are the data points for a SnO_2 electrode bearing a single monolayer.

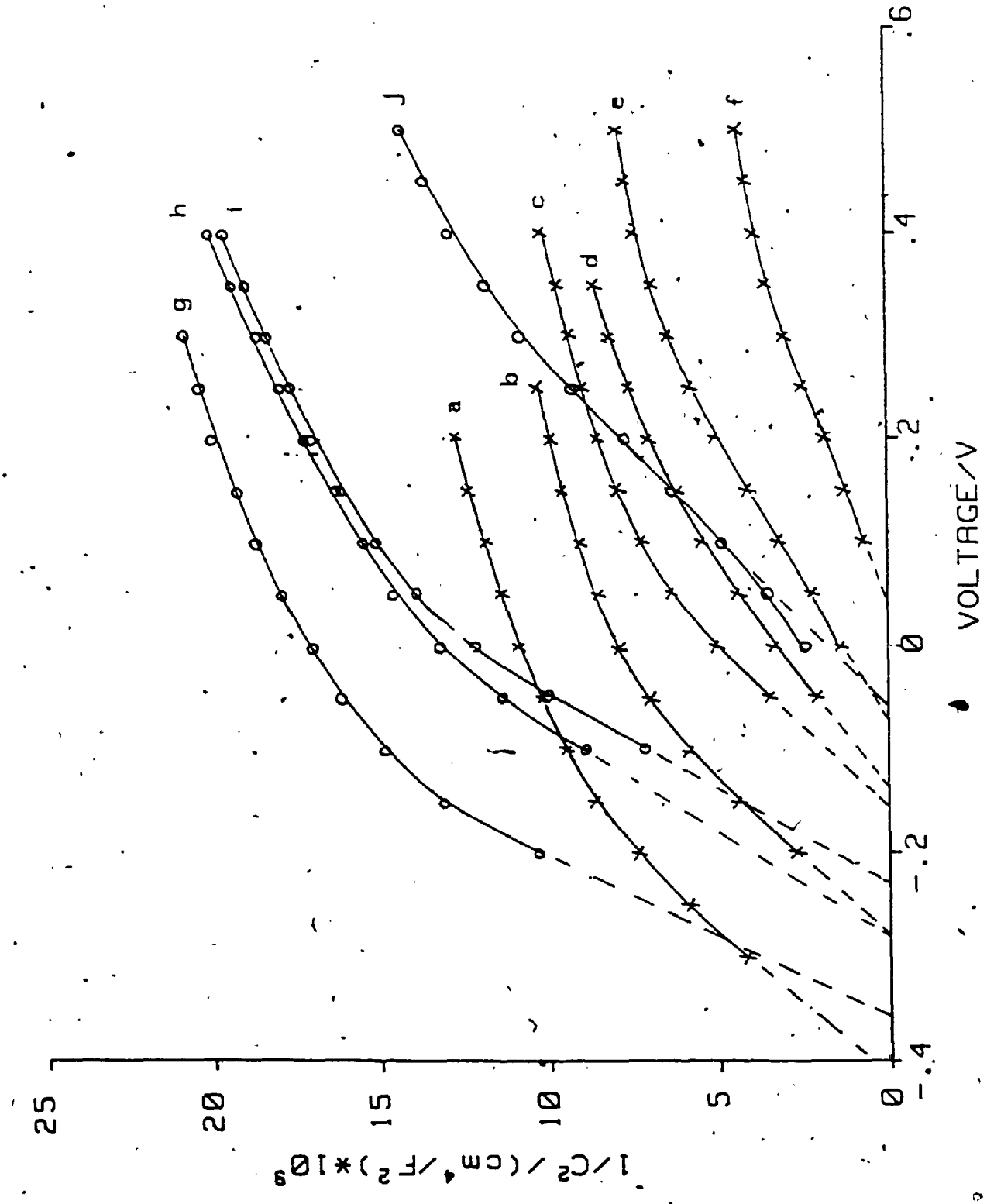
1/C² /(cm⁴/F²)*10⁹
25
20
15
10
5
0
-.4
-.2
0
.2
.4
.6
VOLTAGE/V
a
b
c
d
e
f
g
h
i
J

Figure 4.13 Variation of flatband potential as determined by Mott-Schottky plots with pH. Flatband potentials measured with respect to the Ag/AgCl electrode. x's are the data points for a blank SnO_2 electrode. O's are the data points for a SnO_2 electrode bearing a single monolayer.

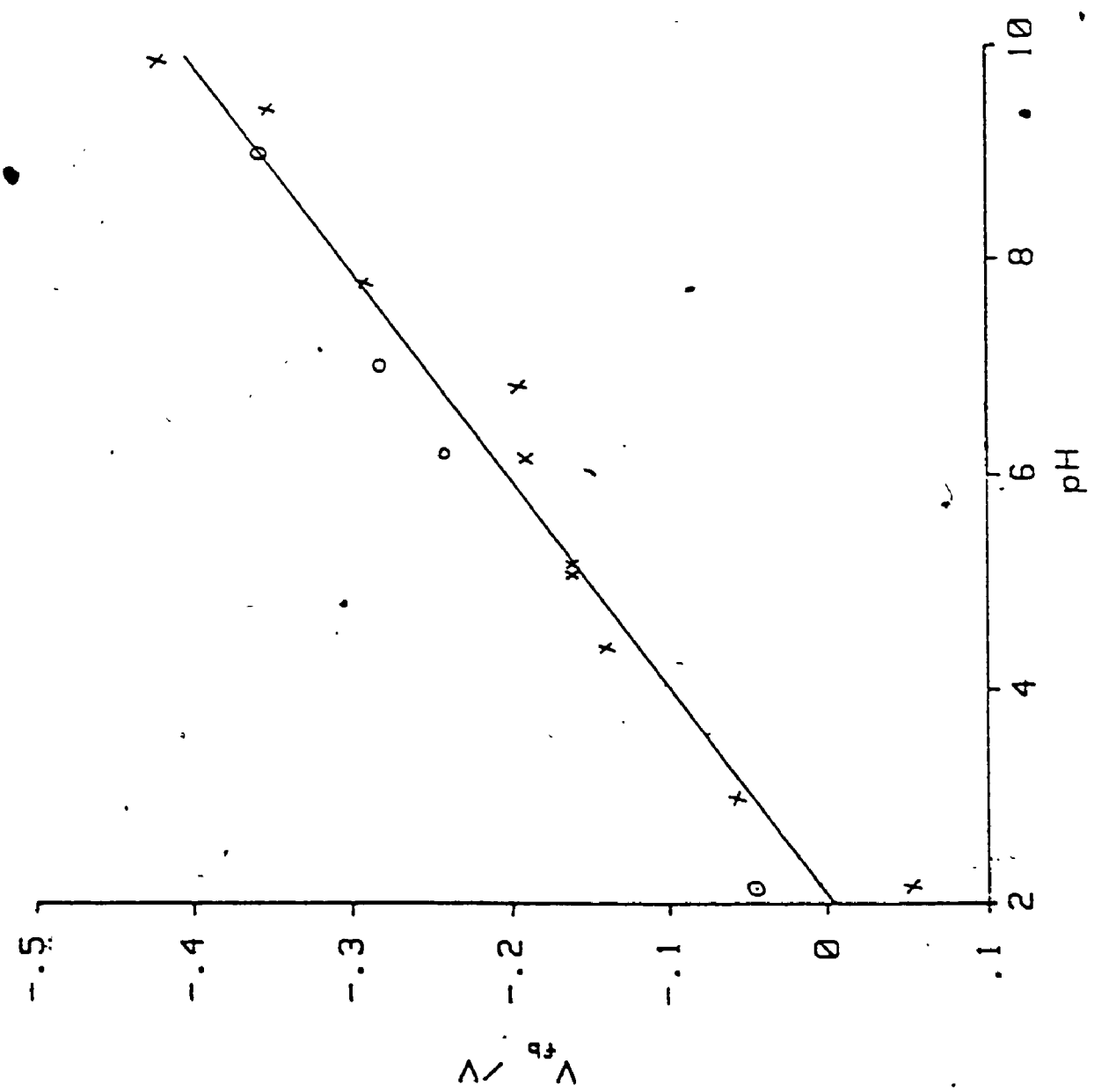
-.5
-.4
-.3
-.2
-.1
0
.1
2
4
6
8
10
pH
V_{fb} /V

This is supported by the fact that dark current-voltage plots of the SnO_2 substrate are identical to those for the substrate bearing the film. Protons from the bulk solution can therefore pass through the film and determine the Helmholtz potential via the equilibria[66]

$$SnOH \rightleftharpoons SnO^- + H^+ \quad (4.46)$$

$$Sn^{2+} + OH^- \rightleftharpoons SnOH^+ \quad (4.47)$$

Since the space charge capacitance is approximately the same size as the expected Helmholtz capacitance it cannot be assumed to dominate. This case has been worked out by De Gryse *et al.*[67] The Helmholtz capacitance is assumed to be independent of the applied potential and only affects the placement of the observed flatband potential. Following their calculations an uncertainty of 0.1 V is placed on the assignment of the flatband potential.

A second non-ideality can be seen in the curvature of the plots which may be due to non-uniform doping of the semiconductor with depth. This would cause the apparent donor density to change with space charge width and hence with applied voltage.

4.6.6 Dependence of the Photocurrent on Irradiance

Figure 4.14 shows the dependence of anodic photocurrent on irradiance for conditions of high and low solution pH. Clearly both are sublinear. The dependence was found to be invariant with respect to TU concentration.

4.6.7 Dependence of the Photocurrent on Thiourea Concentration

Figure 4.15 shows the dependence of photocurrent on TU concentration for conditions of high and low pH. At high pH the photocurrent response is virtually unaffected by the addition of TU.

Figure 4.14 Variation of anodic photocurrent with incident light irradiance for two electrolyte pH conditions. O's are the light intensity data points for pH = 8.91. x's are the light intensity data points for pH = 1.89. electrolyte conditions: 0.25 M KH_2PO_4, 0.5 M NaCl, 0.25 M Na_2SO_3, 1 M TU. Electrode potential: +0.25 w.r.t. Ag/AgCl

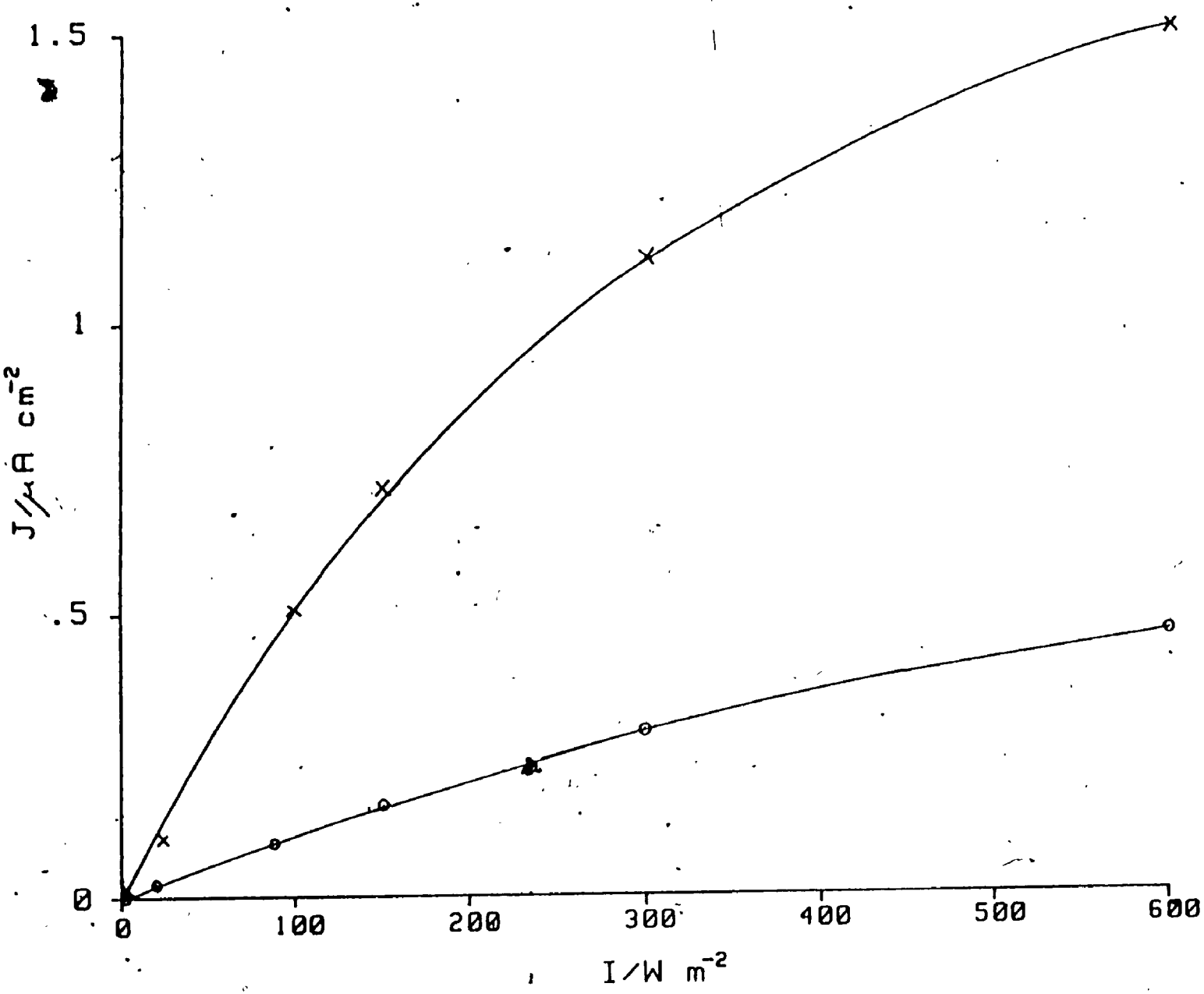
1.5
1
.5
0
J/μA cm⁻²
0
100
200
300
400
500
600
I/W m⁻²

Figure 4.15 Plots of light response of the cell vs. TU concentration at high and low pH. Electrolyte composition: 0.25 M KH_2PO_4, 0.5 M NaCl, 0.25 M Na_2SO_3. x's are the response for pH = 2.1. O's are the response for pH = 8.2.

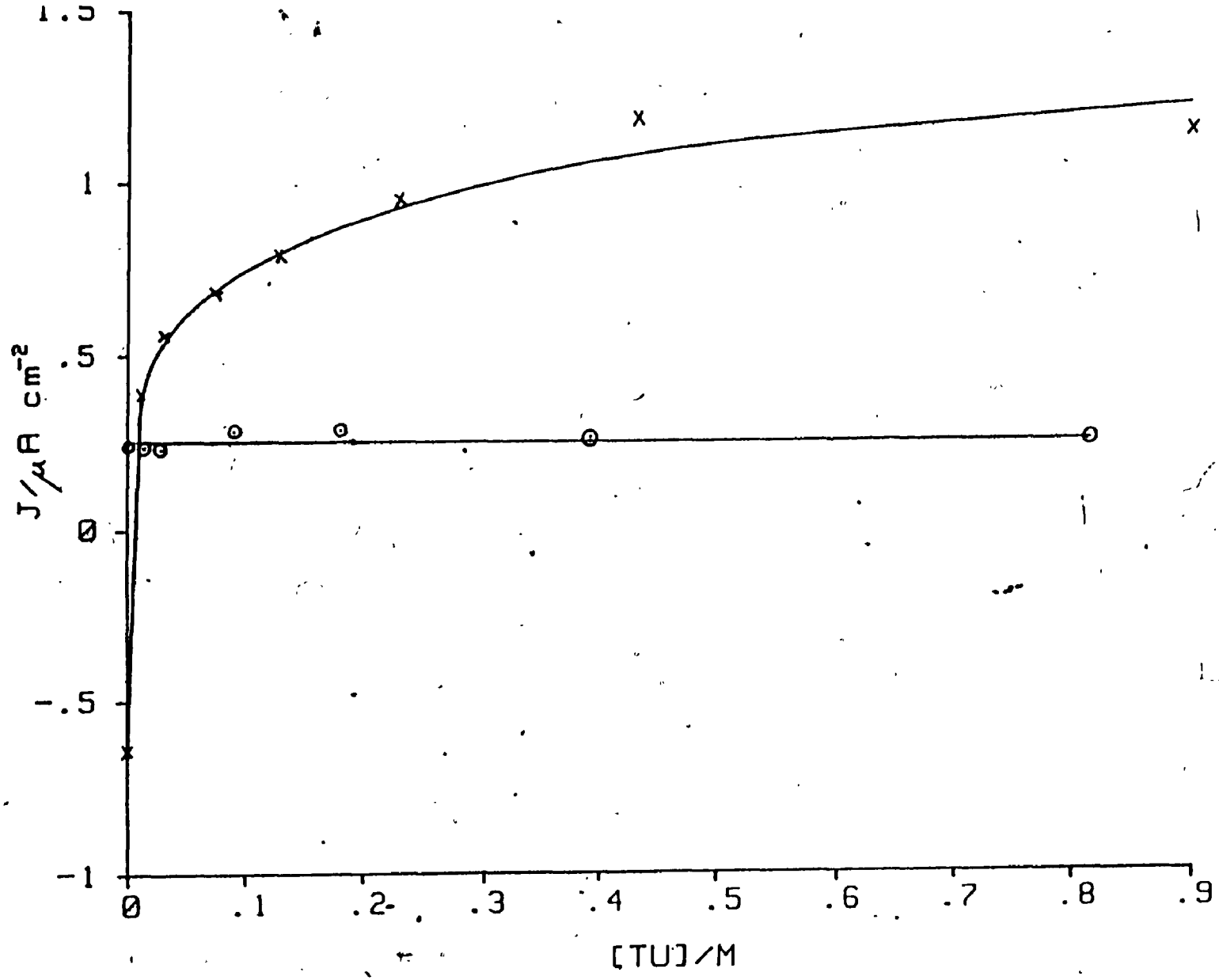
1.5
1
.5
0
-.5
-1
J/μA cm⁻²
0
.1
.2
.3
.4
.5
.6
.7
.8
.9
[TU]/M

Those samples that display anodic response at high pH do not increase their response on addition of TU. Those samples not displaying a high pH response in the absence of TU do not begin to do so on addition of TU. At low pH the photocurrent is highly dependent upon TU concentration usually beginning at a cathodic photocurrent response with no TU present and increasing to a larger anodic photoresponse for TU concentrations approaching unity.

4.6.8 Photocurrent Quantum Yield

The anodic photocurrent quantum yield for the cell under conditions of low pH with TU, Na_2SO_3, NaCl and KH_2PO_4 present was 10% ± 3%. The photocurrent quantum yield for the cell under identical conditions with a 10:1 mixed monolayer of DOPC and TTPa was roughly the same. Since the current was a factor of ten less than that of the pure monolayer, measurement under monochromatic light conditions was impossible. The current under white light conditions was therefore measured for a series of samples and compared to that of the pure monolayer samples under similar conditions.

4.6.9 Photocurrent Onset Voltages

Figure 4.16 compares photo-onset voltages of anodic and cathodic photocurrents with the flatband potential and oxygen acceptor level respectively. The anodic photocurrent onset potential follows the pH variation of the flatband potential except at extreme pH while the cathodic photocurrent onset potential matches that of the literature value for the placement of adsorbed oxygen.[64]

4.6.10 Fluorescence quenching

The fluorescence lifetimes of three 10:1, DOPC/TTPa mixed LB films deposited on SnO_2 were measured. It proved impossible to obtain

Figure 4.16 Onset of photocurrent vs pH for two electrolyte conditions. x's: 0.25 M KH_2PO_4, 0.5 M NaCl, 0.25 M Na_2SO_3, 1 M TU. O's: 0.25 M KH_2PO_4, 0.5 M NaCl. (a) redox level for adsorbed oxygen, (b) flatband potential of the semiconductor

Voltage measured w.r.t. Ag/AgCl

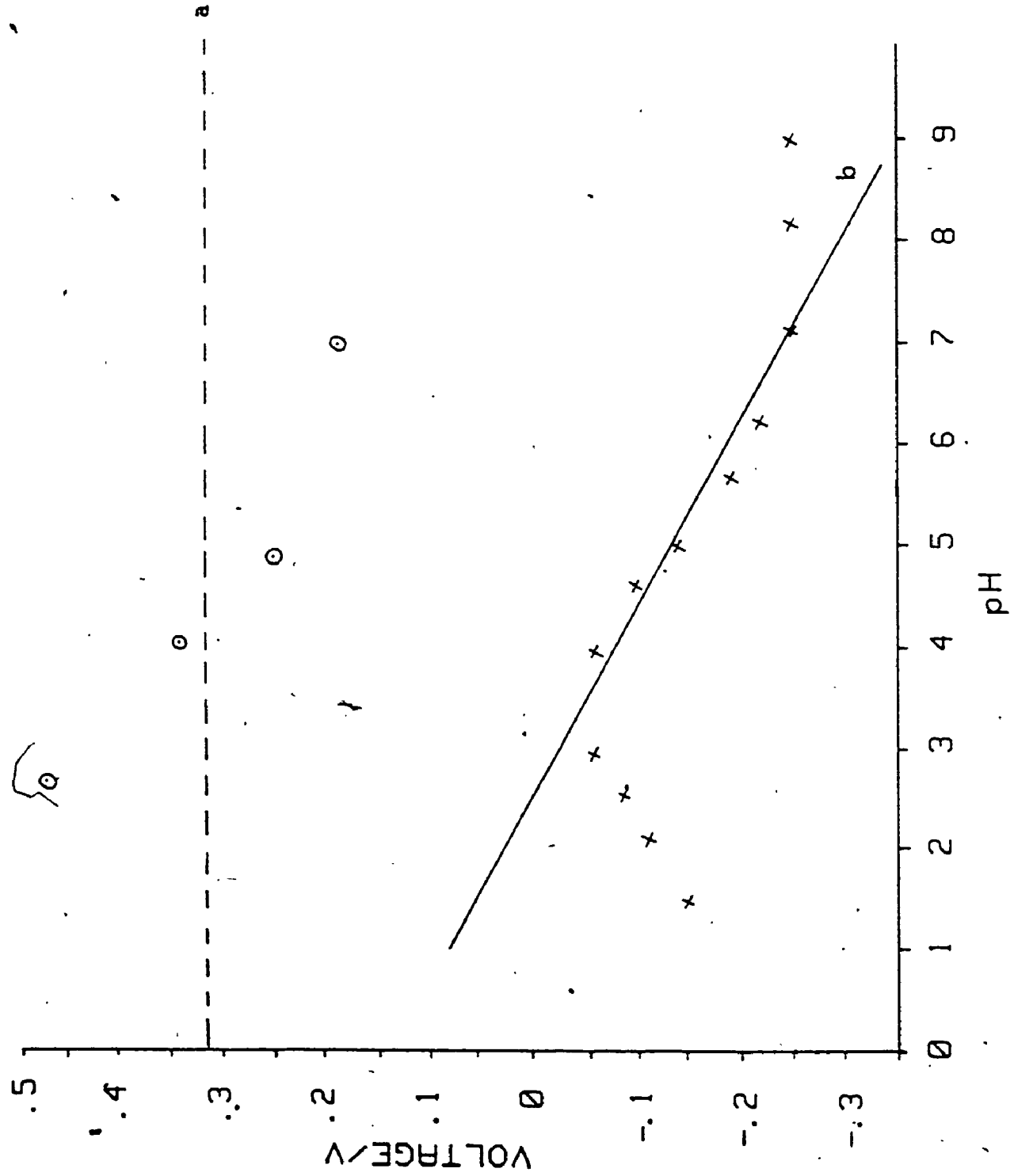
a
b
VOLTAGE/V
pH
.5
.4
.3
.2
.1
0
-.1
-.2
-.3
0
1
2
3
4
5
6
7
8
9

reproducible results for the decay components probably because of the heterogeneity of the surface. All profiles were multicomponent with the longest lifetime being 6 ns. Therefore while some quenching of the film fluorescence is present it is not complete. The lifetimes were compared to those of the same film deposited on a quartz slide which gave a lifetime of 10.5 ns.

4.7 Discussion of the Results

With only supporting electrolyte present the current-voltage plot resembles that of a rectifying Schottky barrier and may be fitted by the modified Shockley equation given by equation 4.36 ie. plot of ln current should be linear with applied voltage as shown in Figure 4.17 for a blank slide. No difference in dark current-voltage dependence between blank slides and slides bearing a single monolayer was observed. Addition of TU introduces an anodic dark current component which must be due to space charge tunneling since the onset potential is well below the flatband potential. The oxygen and nitrogen bubbling experiments indicate that oxygen must act as an electron acceptor both for electrons emitted from the excited state of the dye and from the conduction band of the semiconductor, as evidenced by the enhanced dark current on oxygen bubbling. Since addition of TU alone produced no anodic photocurrent, oxygen must be acting as a preferential electron acceptor over the conduction band. Bubbling with nitrogen produced a very small anodic photocurrent at anodic voltages and reduced the cathodic photocurrent at cathodic voltage. Addition of Na_2SO_3 produced this same effect much more strongly. This seems to indicate that the oxygen which is acting to capture the excited state electron must be adsorbed to the surface of the semiconductor, since bubbling with nitrogen displaces the

Figure 4.17 Plot of the natural logarithm of the dark current response against applied cell voltage for a blank SnO_2 slide. Voltage measured with respect to zero surface barrier for the pH of this solution. Electrolyte conditions: 0.5 M NaCl, pH = 7.65

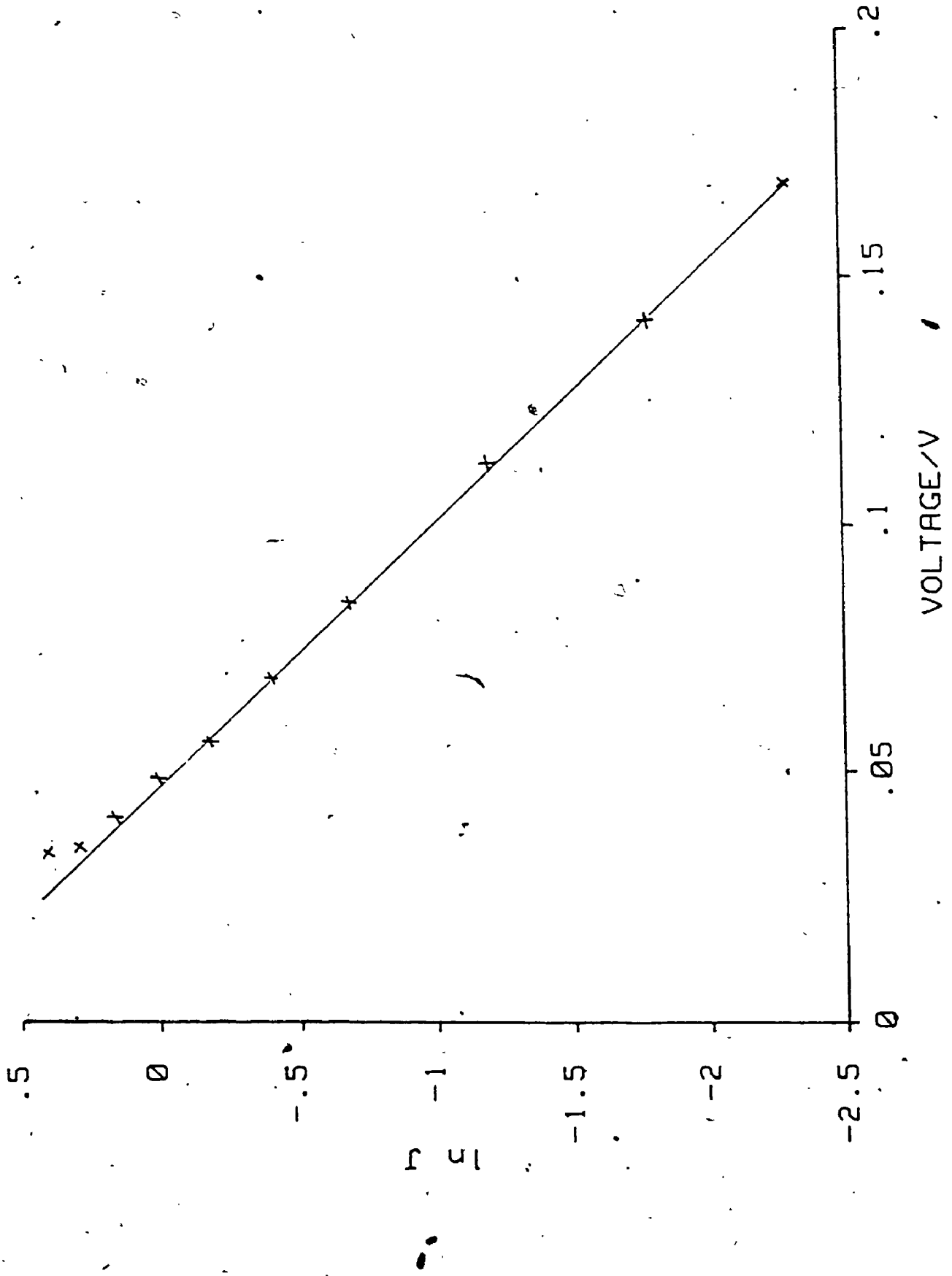
.2
.15
.1
.05
0
VOLTAGE/V
-.5
0
-.5
-1
-1.5
-2
-2.5
ln J

oxygen from solution and only weakly from the surface while Na_2SO_3 is capable of reacting with surface adsorbed oxygen strongly.[54]

The similarity of the pH dependence of the anodic photocurrent under conditions of nitrogen bubbling or addition of Na_2SO_3 seems to indicate that the Na_2SO_3 is acting as an oxygen scavenger only and that this effect is not particularly pH dependent since one would not expect the oxygen displacement ability of N_2 to be pH dependent. Concentrations of species thought to be active scavengers of oxygen have been shown to be present in substantial amounts throughout the pH range tested.[68] Interpretation of the anodic response as the superposition of three currents suggests that only some of the oxygen is scavenged from the surface allowing electron injection into the semiconductor. Those electrons that are injected into the bulk may follow either of two paths; one which is pH sensitive and one which is not.

An injection scheme that has been put forth by Memming[69] to explain low photocurrent quantum yields for heavily doped semiconductors is that of direct injection followed by recombination via back electron tunneling through the space charge layer. This predicts the opposite pH effect on anodic photocurrent to that which is observed for our system since at higher pH back electron transfer should be inhibited due to a thicker space charge layer. It therefore appears that pH must be affecting the initial electron injection step as well as the back tunneling rate.

Two mechanisms have been suggested in the literature that include a pH dependent electron injection step. The first, which was referred to in the literature review[53] predicts a logarithmic dependence with pH based on an increasing Helmholtz potential at low pH. Our results cannot be fit to this type of dependence. Rather they resemble sigmoidal

functions. A second mechanism which predicts this type of dependence was proposed by Clark and Sutin.[70] They proposed that if the distribution of the oxidation potentials of the excited state overlapped incompletely with the surface conduction band edge, the degree of overlap and hence the probability of isoenergetic electron transfer would be controlled by the position of the band edge. Since this is pH controlled, it predicts that the anodic photocurrent should increase at low pH. This does not seem likely for our system since the oxidation potential of the first excited singlet state of the dye is well above the surface conduction band edge at any pH.

A mechanism similar to that proposed by Frippiat *et al.* may be operating in which some of the electrons are injected directly into the bulk and others are captured by unoccupied surface states at the Fermi level. Indeed surface states probably mediate the electron capture by adsorbed oxygen as well since the pH dependences of both these currents are similar.

The pH dependence of photocurrent due to capture by surface states may either arise from the pH dependence of the tunneling probability from the surface into the bulk or the pH dependence of the population of trapping states at the Fermi level. The voltage dependence of the photocurrent suggests the later. As the voltage is made more anodic a greater number of surface states are emptied and become available to trap the electrons. The increasing slope of this dependence with reduction in pH agrees with this since the number of surface states at each energy level would increase with decreasing pH. If forward tunneling through the space charge barrier was rate limiting, the current should decrease with increasingly positive voltage due to the increasing thickness of the barrier at the Fermi level.

pH dependence of the surface state population has been proposed by a number of authors for ionic semiconductors.[71] The equilibria are generally of the type

$$M^{2+} + OH^- \rightleftharpoons M\text{–}OH^+ \qquad (4.48)$$

Here the metal cation M^{2+}, in our case Sn^{2+}, acts as the initial trap for photoinjected electrons.

The following electron injection scheme summarizes these conjectures:

$$S_o \xrightarrow{I_a} S_1 \qquad \text{Step 1}$$

$$S_1 \xrightarrow{k_r} S_o \qquad \text{Step 2}$$

$$S_1 \xrightarrow{k_b} S^+ + e_b^- \qquad \text{Step 3}$$

$$S_1 \xrightarrow{k_s} S^+ + e_s^- \qquad \text{Step 4}$$

$$e_s^- \xrightarrow{k_e} e_b^- \qquad \text{Step 5}$$

$$S^+ + e_s^- \xrightarrow{k_r'} S_o \qquad \text{Step 6}$$

$$TU + S^+ \xrightarrow{k_t} TU^+ + S_o \qquad \text{Step 7}$$

$$O_2 + e_s^- \xrightarrow{k_o} O_2^- \qquad \text{Step 8}$$

$$e_b^- + S^+ \xrightarrow{k_c} S_o \qquad \text{Step 9}$$

In this scheme an electron injected into the semiconductor bulk may

either be injected directly (Step 3) or trapped by a surface state at the Fermi level creating an oxidized dye, reduced surface state intermediate pair as proposed by Fromhertz (Step 4). If the surface state is in the proximity of adsorbed oxygen, it will reduce it (Step 8). The oxidized dye is then reduced by an electron from the conduction band producing cathodic photocurrent.(Step 9). If the reduced surface state is not in the proximity of adsorbed oxygen it may either recombine with the oxidized dye molecule (Step 6) or tunnel through the space charge layer into the semiconductor bulk if the oxidized dye is reduced by a TU molecule (Steps 5,7). Steps 6 and 7 compete in reduction of the oxidized dye.

We associate Step 3 with the pH independent part of the anodic photoresponse and Step 4 with the pH dependent part which arises from trapping by Sn^{2+} atomic surface states. Regions where the Sn^{2+} surface concentration is high will favor this step. Such heterogeneity of response was observed by Frippiat *et al.*[54] and might also explain the occasional absence of the pH independent part of the anodic photoresponse for some samples.

This model also explains the difference between the TU dependence of the photocurrent at high and low pH. At high pH we propose that direct electron injection predominates. The space charge layer is relatively thick due to the high surface barrier at this pH. Therefore recombination of electrons with the oxidized dye via back tunneling is minimized. A small current should be seen even without the presence of TU and should remain relatively insensitive to it's presence. At low pH where trapping by surface states predominates supersensitization by TU (Step 7) competes with recombination in regions of the surface where adsorbed oxygen is absent. The current should therefore strongly depend

on the TU concentration.

The dependence observed on irradiance should be linear since the recombination process should be geminate. The sublinearity cannot be associated with nongeminate bimolecular recombination since such a mechanism would predict a dependence of the curvature of the TU dependence on light irradiance. Such a dependence is not found. Rather the curvature seems to be associated with the size of the photocurrent. This would suggest that the interface behaves as an imperfect junction in which back tunneling competes with forward electron transfer. The curvature at both pH levels supports the hypothesis that back electron tunneling is not the main pH dependent mechanism.

Applying the steady state approximation to S_1 and the intermediate state e_s^- in the scheme postulated yields the following expression for photocurrent q_{ss} due to surface state trapping.

$$q_{ss} = \frac{\phi_s [TU]\ I_a}{k_t [TU] + k_r'} \tag{4.49}$$

The total current q_t at low pH will be the sum of the three currents

$$q_t = q_{step3} + q_{step5} + q_{step9} \tag{4.50}$$

The direct injection current q_{step3} and the cathodic current due to oxygen q_{step9} are independent of the TU concentration and are subsumed into a single current q_2. The TU dependence should be as follows:

$$q(TU) \propto \frac{(I_a \phi_s / k_r')[TU]}{(k_t / k_r')[TU] + 1} + q_2 \tag{4.51}$$

The TU dependence at low pH may be fitted using the ratio $k_t/k_r' = 30$ and $q_2 = -680\ nA/cm^2$ however a better fit is obtained by the addition of.

a term directly proportional to TU concentration as shown in Figure 4.18. This suggests that an additional mechanism may be playing a part in the low pH anodic photocurrent such as photoreduction of the excited dye by TU followed by electron injection from the reduced dye as suggested by Chandrasekaran *et al.* for sensitization at lightly doped SnO_2.

A further confirmation of the surface state effect was obtained by studying the pH dependence of the intrinsic photocurrent produced by a blank slide. Its dependence is shown in Figure 4.11c. Intrinsic photocurrent generated by subbandgap radiation is produced by excitation of electrons from semiconductor surface states at the Fermi level into the conduction band. The size of this current will be proportional to the density of surface states at the Fermi level. Therefore while this current contributes negligibly to the total sensitized current, it provides an indicator for the density of surface states at any pH level. The similarity of its pH dependence to that of the dye sensitized current confirms that the low pH current arises primarily from trapping of the excited dye electron by surface states.

The electrolyte which included TU, Na_2SO_3, KH_2PO_4, and NaCl was observed to turn yellow at low pH. This effect probably arises from some complexation between the Na_2SO_3 and TU since the presence of both is required for the color change. It probably is not involved in the photoelectrochemistry for two reasons. The first is that a similar pH dependence of the anodic photocurrent was observed when Na_2SO_3 addition was replaced with vigorous nitrogen bubbling (see Figure 4.11). The second is that absorption spectra of the electrolyte indicate that the rise in absorbance of the solution producing the yellow color takes place approximately two pH units lower than that at which the anodic

Figure 4.18 The low pH dependence of the light response of the cell vs. TU concentration fitted to the following expression.

$$\frac{[TU] \times 558}{[TU] \times 120 + 1} + [TU] \times 3.24 - 2.1$$

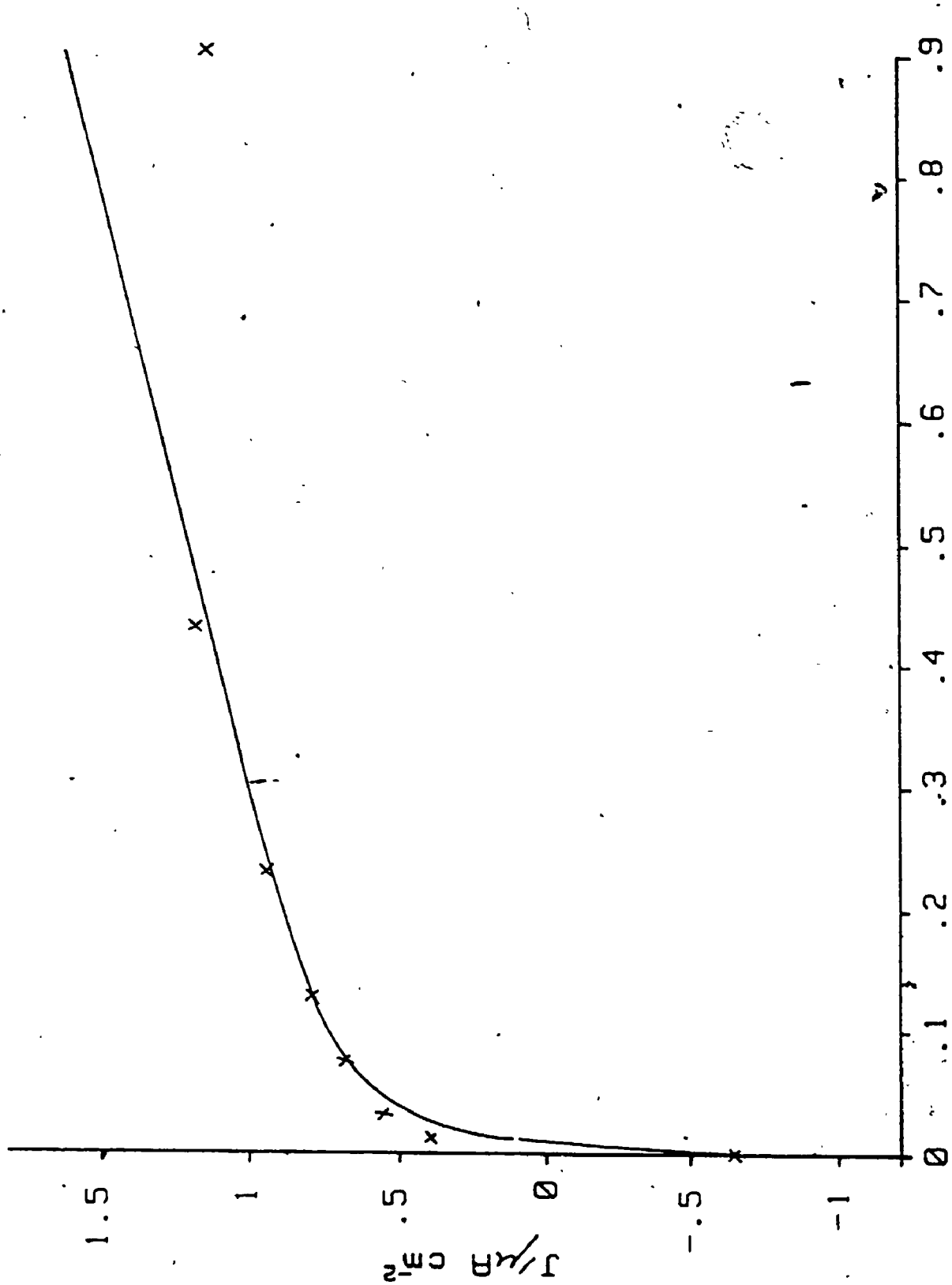
1.5
1
.5
0
-.5
-1
J/μB cm⁻²
0
.1
.2
.3
.4
.5
.6
.7
.8
.9
[TU]/M

photocurrent rises sharply.

Photocurrent onset voltages for anodic current agree with the Mott-Schottky plots in placement of the flatband potential and confirm that the current is due to eventual injection of electrons into the conduction band. Cathodic photocurrent onset agrees with the reduction potential assignment of +0.5 V w.r.t. SHE for adsorbed oxygen which is much lower than that of oxygen in solution. The reason for the pH dependence of the cathodic onset potential is unclear here, since it is not certain whether the O_2/O_2^- redox level should shift with pH.

Evidence for a substantial barrier to electron injection is provided by the similarity of the action and absorption spectra. The well defined action spectrum indicates that all the electron injection must be taking place from the S_1 zero vibrational level. Injection from higher nonthermalized levels would introduce distortions into the spectrum since the electron injection probability would vary with electronic energy. Direct photoinjection of the electron into the conduction band from the ground state is also precluded since this would involve an entirely different absorption process and spectrum. We thus conclude that the electron injection is therefore slower than the thermalization rate.

A second interesting observation regarding the action spectrum is that both monomeric and aggregate type TTPa molecules appear to take part in the photoelectron injection as evidenced by the fact that the 430 nm peak extends to include both types. This is supported by the fact that the quantum yield of photocurrent does not increase with dilution. If only the longer lived monomeric specie were active, the quantum yield would increase with dilution as this specie became more predominant in the LB film. It is reasonable that the aggregate specie

as well as the monomeric specie would be involved in photoelectron transfer since the fluorescence lifetime of the aggregate state is not vastly different from that of the monomeric state. By contrast Miyasaka *et al.*[63] observed a large increase in the quantum yield for chlorophyll a on dilution. The fluorescence lifetime of chlorophyll monolayers is much more sensitive to dilution than that of TTPa monolayers, presumably due to the much larger overlap of the absorption and fluorescence spectra for chlorophyll monolayers than for TTPa monolayers. Also the lifetime of the aggregate chlorophyll specie is orders of magnitude shorter than the monomeric specie lifetime. It is therefore more likely that a competitive deactivation route would differentiate between chlorophyll species than between TTPa species.

The electron injection rate constant for the monomeric specie can be determined by

$$k_{et} = 1/\tau_1 - 1/\tau_2$$

where τ_1 is the fluorescence lifetime of 6 ns of the monomeric form on the SnO_2 and τ_2 is the fluorescence lifetime of 10.5 ns of the monomeric form on quartz. Here we have assumed that all the fluorescence quenching of the dye on the SnO_2 as compared to quartz is due to electron injection. The electron injection rate constant obtained in this way is $7 \times 10^7\ s^{-1}$. The fluorescence quantum yield for TTPa in benzonitrile has been estimated by Schmidt *et al.* to be ~10%.[72] If we adopt this result for our system then a maximum photocurrent quantum yield of 7% is expected if only monomeric species are involved in photoinjection. This is inconsistent with our results and is therefore further confirmation that aggregate species must be involved in photoinjection.

Clearly the rate constant for the aggregate species photoinjection

must be higher than that for the monomeric specie since such a rate would not compete with the higher rate of deactivation due to fluorescence observed for the aggregate species. The aggregate species must therefore be interacting more closely with the SnO_2 surface than the monomeric specie. This might arise from a difference in the orientation of the chromophores with respect to the surface.

CHAPTER 5 CONCLUSIONS AND SUGGESTIONS FOR FURTHER RESEARCH

5.1 Summary of Observations

5.1.1 Photophysical Studies

1. 50:1 DOPC/TTPa LB_t films deposited on quartz exhibited absorption spectra, and steady state and time resolved fluorescence characteristics similar to those of dilute TTPa dissolved in methylene chloride.

2. LB films composed of pure TTPa exhibited red shifted aggregate type spectra and quenched lifetime profiles.

5.1.2 Photoelectrochemical Studies

1. The photo-action spectrum matched the absorption spectrum for a TTPa LB film deposited onto quartz.

2. Oxygen bubbling increased the cathodic photocurrent whereas nitrogen bubbling decreased it.

3. Addition of TU and Na_2SO_3 induced anodic photocurrent.

4. Mott-Schottky plots indicated an increase in the flatband potential of 54 mV per pH unit.

5. No difference between the current-voltage plots or in-phase impedance values with or without the LB film was observed.

6. pH dependence of the photocurrent indicated a superposition of two pH dependent currents, one anodic and one cathodic, plus an anodic pH independent current.

7. The quantum yield for anodic photocurrent under optimum conditions was ~10%.

8. The photocurrent dependence on irradiance was sublinear.

9. The TU concentration dependence was large for low pH and negligible for high pH.

5.2. Conclusions

5.2.1 Photophysical Studies

It was found that TTPa aggregation in LB films can be reduced by dilution in DOPC. The resulting monomeric TTPa fluoresced with a reproducible lifetime of 10.7 ±0.2 ns which was offered as a standard. The reduced aggregation was also apparent in the absorption and fluorescence spectra as a blue shift away from the earlier reported aggregate spectrum toward that of TTPa in methylene chloride.

5.2.2 Photoelectrochemical Studies

TTPa.LB films deposited onto SnO_2 semiconductor slides were found to produce either cathodic photocurrent, corresponding to photoelectron injection into solution or anodic photocurrent corresponding to injection into the semiconductor, depending on the electrolyte conditions. Comparison of photo-action spectra with absorption spectra indicate that the observed photocurrent arises from light interacting with the dye monolayer. Differences in this spectrum with the absorption spectra of LB films of TTPa deposited on quartz slides were attributed to heterogeneity of the semiconductor surface. The action spectrum indicated that both aggregate and monomeric type TTPa species were involved in photocurrent production.

Mott-Schottky plots as well current-voltage plots indicated that the LB film only partially blocked the surface allowing ions to pass in between the dye molecule interstitial sites.

Adsorbed oxygen was found to act as an electron acceptor for the dye excited state electron mediating cathodic photocurrent. In the absence of oxygen, anodic photocurrent was observed and was postulated to arise from both direct injection of photoelectrons from the dye film.

into the conduction band of the semiconductor and also trapping of the excited electron by surface states. The surface state population was postulated to depend on the solution pH increasing at low pH. The thiourea concentration dependence gave evidence for the existence of competition between recombination of a surface state oxidized dye pair and rereduction of the oxidized dye by the thiourea.

5.3. Suggestions for further research

Preliminary studies of the fluorescence lifetime distribution of the standard system have already been performed. These could be extended to include a range of DOPC/TTPa mixing ratios at various temperatures. which might shed some light on the question of whether the quenching seen is diffusional or static. In connection with this the fluorescence photobleaching recovery technique might be helpful in indicating the degree of diffusional freedom experienced by the dye molecules in the LB film environment. Preliminary experiments here have indicated the existence of a wide range of mixing ratio dependent diffusion coefficients for these films.

Further experimentation needs to be carried out to determine the exact mechanism of charge injection at the TTPa semiconductor interface. One experiment would be to vary the distance of the attached chromophore from the surface. This might be done by synthesizing a series of surface active porphyrins in which the chromophore is linked to the hydrophilic group by alkane chains of varying length. Presumably an exponential fall-off in photocurrent with distance would be seen if the injection process is via a tunneling mechanism. Variation of the redox potential of the supersensitizer might help to pin down the dynamics of the low pH supersensitization process. Variation of the surface character by controlled etching might also be helpful.

Experiments have indicated that it is possible to deposit LB films of porphyrin-quinone compounds linked by an amide linkage. Here the quinone is thought to be the hydrophylic portion of the molecule. Deposition of the monolayer on to a semiconductor would sandwich the quinone between the porphyrin and the semiconductor producing an intermediate photoelectron acceptor site. It would be interesting to compare the fluorescence quenching data from studies of these molecules in solution with photocurrent quantum yield for electrodes modified by the attachment of these same molecules. The presence of such an acceptor might profoundly increase the quantum yield of photoelectron injection.

REFERENCES

1. Bolton, J.R. *Solar Energy* 1983, 31, #5, 483-502.
2. Bolton, J.R. *Ann. Rev. Energy* 1979, 4, 353-401.
3. see for example Okuda, K.; Okamoto, H.; Hamakawa, Y. *Jpn. J. Appl. Phys*, 1983, 22, 605-607.
4. Calvin, M. *J. Theoret. Biol.* 1961, 2, pp.258-287
5. Bolton, J.R. In *Inorganic Chemistry: Toward the 21st Century*, ACS Symposium Series #211; Chisholm, M.H. ed.; American Chemical Society: Washington, D.C., 1983, 1-19.
6. Bolton, J.R.; Connoly, J.S. In *Photoinduced Electron Transfer*; Fox, M.A.;Chanon, M. eds.; Elsevier Science Publishers, 1988, (in press).
7. Little, R.G.; Anton, J.A.; Loach, P.A.; Ibers, J.A. *J. Heterocycl. Chem.* 1975, 12, 343-349.
8. James, D.R.; Ware, W.R. *Chem. Phys. Lett.* 1986, 126, 7-11.
9. (a) James, D.R.; Liu, Y-S.; de Mayo, P.; Ware, W.R., *Chem. Phys. Lett.* 1985, 120, 460-465. (b) James, D.R.; Ware, W.R. *Chem. Phys. Lett.* 1986, 126, 7-11.
10. Turro, N. J. *Modern Molecular Photochemistry*; Benjamin/Cummings: London, 1978, p.174.
11. Cundall, R.B. In *Time-Resolved Fluorescence Spectroscopy in Biochemistry and Biology*; Cundall, R.B.; Dale, R.E., eds.; Plenum Press: New York, 1983, 59-83.
12. (a) Shapiro, S.L.; Kollman, V.H.; Campillo, A.J. *FEBS* Lett. *1975,* 54, 358-362. (b) Beddard, G.S.; Porter, G.; Tredwell, C.J., *Nature* 1975, 258, 166-168.
13. Ware, W.R. In *Time-Resolved Fluorescence Spectroscopy in Biochemistry and Biology*; Cundall, R.B.; Dale, R.E., Ed.; Plenum

Press; New York, 1983; pp. 23-57.

14. O'Connor, D.V.; Philips, D. *Time-correlated Single Photon Counting*; Academic Press: London, 1984, pp. 36-54.

15. Goddard, E.D. *Monolayers*; American Chemical Society: Washington, D.C., 1975, p. 139.

16. Blodgett, K.B.; Langmuir, I. *Phys. Rev.* 1937, *51*, 964-982.

17. Adamson, A.W. *Physical Chemistry of Surfaces*; Wiley-Interscience: New York, 1976, p. 183

18. Picard, G.; Munger, G.; Leblanc, R.M.; LeSage, R.; Sharma, D.; Siemiarczuk, A.; Bolton, J.R. *Chem. Phys.* Lett. 1986, 129, 41-47.

19. Agrawal, M.L.; Chauvet, J.P.; Patterson, L.K. *J. Phys.Chem.* 1985, 89, 2979.

20. Chauvet, J.P.; Agrawal, M.L.; Hug, G.L.; Patterson, L.K. *Thin Solid Films* 1985, 133, 227-234.

21. Bardwell, J.A.; Bolton, J.R. *Photochem. Photobiol.* 1984, 39, 735-746.

22. Bohorquez, M.; Patterson, L.K. *J. Phys. Chem.* 1988, 92, 1835-1839.

23. Birks, J.B.; Dyson, D.J.; Munro, I.H. *Proc. R. Soc. London*, A 1963, 275, 575-588.

24. Ducharme, D.; Salesse, C.; Leblanc, R.M. *Thin Solid Films* 1985, 132, 83-90.

25. Kuhn, H. *Pure Appl. Chem.* 1979, 51, #2, 341-352.

26. Stanberry, B.J.; Gouterman, M.; Burgess, M. *J. Phys. Chem.* 1985, 89, 4950-4956.

27. Kuhn, H. *J. Chem. Phys* 1970, 53, #1, 101-108.

28. Bardwell, J.A. Ph.D. Thesis, The University of Werstern Ontario, 1983, pp. 63-73; *Dissert. Abstr. B* 1983, 44(10), 3091.

29. Dare-Edwards, P.M.; Goodenough, J.B.; Hamnet, A.; Seddon, K.R.; Wright, D.R. *Faraday Discusions of the Chemical Society* 1980, #70, 285-298.

30. Tributsch, H.; Gerischer, H. *Ber. Bunsenges Phys. Chem.* 1969, 73, 251-260.

31. Memming, F.S.; Bringmann, U. *J. Electroanal. Chem.* 1979, 100, 307-318.

32. McTigue, P.; Farrell, J. *J. Electroanal. Chem.* 1982, 37, p.139

33. Ioffe, A.F. *Physics of Semiconductors*; Academic Press: New York 1960, p.125

34. Bockris, J.O'M.; Reddy, A.K.N. *Modern Electrochemistry*; Plenum Publishing Co.: New York, 1977, pp.813-816.

35. Morrison, S.R. *Electrochemistry at Semiconductor and Oxidized Metal Electrodes*; Plenum Press: New York, 1980, p.96.

36. Bolton, J.R.; Archer, M.D. *Photocoversion of Solar Energy* Section C.5.6; John Wiley & Sons. to be published

37. ref. 34. pp. 623-639.

38. Bulkowski, J.E. *Report* 1983 from *Energy Res. Abstr.* 1984, 9,#22, Abstr. #45717.

39. ref. 35 p.41.

40. Sears, F.W.; Zemansky, M.W.; Young, H.D. *University Physics* 6th ed.; Addison-Wesley: Reading, Mass., 1982, p.516.

41. Blok, L.; De Bruyn, P.L. *J. Coll. Interf. Sci.* 1970, 32, #3 518-526.

42. Gerischer, H. *Top. Appl. Phys.* 1977, 31. 115-172.

43. Marcus, R.A. *J. Chem. Phys.* 1965, 43, 679-701.

44. Gerischer, H. *Z. Phys. Chem. N.F.* 1961, 27, 48-79.

45. Albery, W.J. *Electrode Kinetics*; Clarendon Press, Oxford,

1975, 116-117.

46. Memming, R.; Schroppel, F.; Bringmann, U. *J. Electroanal. Chem.* 1979, 100, 307-318.

47. Schultz, J.W.; Vetter, K.J. *Electrochim. Acta* 1973, 18, 889-896.

48. Honda, K.; Fujishima, A.; Watanabe, T. In *Surface Electrochemistry: Advanced Methods and Concepts* Takamura, T.; Kozawa, A. eds. pp.141-177.

49. Memming, R. *Progress in Surface Chemistry* 1984, 17, 7-74.

50. Honda, K.; Nakao, M.; Itoh, K.; Watanabe, T. *Ber. Bunsenges. Phys. Chem.* 1985, 89, 134-138.

51. Gerischer, H.; Michel-Beyerle, M.E.; Rebentrost, F.; Tributsch, H. *Electrochemica Acta* 1968, 13, 1509-1515.

52. Miyasaka, T.; Watanabe, T.; Fujishima, A.; Honda, K. *J. Am. Chem. Soc.* 1978, 100, 6657-6665.

53. Watanabe, T.; Fiujishima, A.; Tatsuoki, O.; Honda, K. *Bull. Chem. Soc. Jpn.* 1976, 49, 8-11.

54. Frippiat, A.; Kirsch-De Mesmaeker, A. *J. Electrochem. Soc.* 1987 134, 66-71.

55. Fromhertz, P.; Arden, W. *J. Am. Chem. Soc.* 1980, 102, 6211-6218.

56. Fromhertz, P.; Arden, W., *J. Electrochem. Soc.* 1980, 127, 370-378.

57. Bulkowski, J.E.; Bull, R.A.; Sauerbrunn, S.R. In *Photoeffects at Semiconductor-Electrolyte Interfaces*; Nozik, A. ed.; ACS Symp. Ser. 146, American Chemical Society: Washington, D.C., 1981, pp. 279-293.

58. Chandrasekan, K.; Giannotti, C.; Monserrat, J.; Otruba, J.P.; Whitten, D.G. *J. Am. Chem. Soc.* 1982, 104, 6200-6206.

59. Umezawa, Y.; Yamamura, T.; *J. Electroanal. Chem.* 1979, 95, 113-116.

60. Breddels, P.A.; Blasse, G. *J. Chem. Soc. Faraday Trans.* 2, 1984, 80, 1055-1065.

61. Ninami, N.; Ichimura, K. *J. Electroanal. Chem.* 1984, 165, 181-194.

62. Matsumura, M.; Mitsuda, K.; Yoshizawa, N.; Tsubomura, H. *Bull. Chem. Soc. Jpn.* 1981, 54, 692-695.

63. Miyasaka, T.; Watanabe, T.; Fujishima, A; Honda, K. *J. Am. Chem. Soc.* 1978, 100, 6657-6665.

64. Sprunken, H.R.; Schumaker, R.; Schindler, R.N. *Ber. Bunsenges Phys. Chem.* 1980, 84, 1040-1045.

65. Davis, D.G. In *The Porphyrins*; David Dolphin ed.; Acedemic Press: New York, 1978 p.143.

66. Memming, R.; Mollers, F. *Ber. Bunsenges Phys. Chem.* 1972, 76, #6, 469-475.

67. De Gryse, R.; Gomes, W.P.; Cardon, F.; Vennik, J. *J. Electrochem. Soc.* 1975, 122, 711-712.

68. Guthrie, J.P., private communication

69. ref. 49 p.55

70. Clark, W.D.K.; Sutin, N. *J. Am. Chem. Soc.* 1977, 99, 4676-4682.

71. ref. 35 p.158

72. Schmidt, J.A.; McIntosh, A.R.; Weedon, A.C.; Bolton, J.R.; Connoly, J.S.; Hurley, K.J.; Wasielewski, M.R. *J. Am. Chem. Soc.* 1988, 110, 1733-1740.